AN ABSTRACT OF THE THESIS OF

William E. Gallahan III for the degree of Doctor of Philosophy in Oceanography presented on October 7, 1996. Title: Geochronology and Geochemistry of Low Temperature Hydrothermal Alteration in Oceanic Crust: An Investigation of Celadonite in the Troodos Ophiolite, Cyprus.

Abstract approved: Redacted for privacy

Robert A. Duncan

Celadonite, a low-temperature hydrothermal alteration mineral, sampled from drill cores and outcrops within the extrusive units of the Troodos ophiolite, Cyprus has been studied with geochronological and geochemical methods to provide new constraints on the timing and extent of chemical exchange between seawater and oceanic crust. Potassium-argon age determinations of 54 celadonite samples yield ages ranging from 90.9 $\pm$ 1.0 to 49.8 $\pm$ 0.5. The oldest age is in close agreement with the estimated 91-92 Ma crystallization age of Troodos igneous rocks. The youngest age indicates that low temperature chemical exchange continued for at least 40 m.y. after crustal formation. This represents a 100 percent increase over previous estimates based on radiometric dating of secondary alteration minerals from Troodos. Extrapolation of these new data from Troodos, to contemporary *in situ* oceanic crust, partially resolves a discrepancy between geochronologic data from DSDP/ODP samples and geophysical data of heat flow and seismic wave velocities.

Major element compositions of Troodos celadonites are consistent with those analyzed from DSDP/ODP cores. They are defined by mixing between three components: pure celadonite, nontronite, and saponite. Fluorine and chlorine within Troodos celadonites demonstrate very different geochemical affinities. Both elements

demonstrate concentration maxima in some samples in which octahedrally coordinated cations sum to approximately 4. However, approximately 5 percent of all samples have at least 1.0 percent fluorine, with the highest having 4.8 percent. No sample contains greater than 0.25 percent chlorine. These data suggest that celadonite precipitation may act as a significant sink for fluorine and that it may fractionate halide elements.

Rare earth element (REE) concentrations were measured for 27 celadonites and the REE patterns of 24 samples mimic those of Troodos lava compositions. REE mineral/fluid partition coefficients were calculated using hypothetical fluids determined from a "single pass" dissolution/dilution model. These partition coefficients indicate that celadonite may act as a significant sink for REE in hydrothermal solutions. Three celadonites yielded anomalous REE concentrations and patterns that could be reproduced only from a different, light REE enriched source.

Alkali element concentrations and ratios indicate that celadonite is similar to other smectites and fractionates these elements. The Cs/Rb signatures of the celadonites are significantly higher than from those found along a mixing path between Troodos glasses and seawater for appropriate water/rock ratios.

Geochronology and Geochemistry of Low Temperature Hydrothermal Alteration in Oceanic Crust: An Investigation of Celadonite in the Troodos Ophiolite, Cyprus

by

William E. Gallahan III

A THESIS

submitted to

Oregon State University

in partial fulfillment of

the requirements for the

degree of

Doctor of Philosophy

Presented October 7, 1996

Commencement June 1997

Doctor of Philosophy thesis of William E. Gallahan III presented on October 7, 1996

APPROVED:

Redacted for privacy

Major Professor, representing Oceanography

Redacted for privacy

Dean of the College of Oceanic and Atmospheric Sciences

Redacted for privacy

Dean of Graduate School

I understand that my thesis will become part of the permanent collection of Oregon State University libraries. My signature below authorizes release of my thesis to any reader upon request.

Redacted for privacy

William E. Gallahan III, Author

ACKNOWLEDGMENT

The completion of this thesis marks the culmination of an educational experience that began in 1984. I have been aided, both academically and spiritually, during this long journey by many individuals, all of whom deserve recognition. Within this venue, I wish to acknowledge specific individuals who have had the greatest influence on my development as a student and, as a person.

My Ph.D. advisor, Robert Duncan, has provided continuous guidance, helpful suggestions, and overall support during my tenure as a doctoral student. He helped me to find an intellectual niche during my research and to focus my interest on certain areas. In addition, he provided a friendly ear during discouraging times of employment searches. Finally, he has demonstrated almost infinite patience in the time taken to complete this thesis. To him, I extend my deepest gratitude.

Roger Nielsen and David Graham have both provided friendship during trying times. They have each provided stimulating company and conversation regarding many facets of life. Much thanks are extended to them for helping me to remain sane, during insane times.

Robert McConnell, my undergraduate major advisor, sparked my fervor in geology. His encouragement prompted my initial interest in graduate studies and research. In addition, Bob has provided a friendship unmatched in mutual interests and viewpoints. Truly, I have found a kindred spirit during my academic journey.

Kathy Gillis provided profound insight to the geology and processes evidenced in the Troodos ophiolite. She provided an intellectual sounding board for ideas and observations. I thank her for being my expert guide to Troodos.

I wish to extend my thanks to my graduate committee members, John Dilles, John Chen, Gary Klinkhammer, and Stephen Giovannoni for their constructive timely reviews of my thesis.

Finally, this study would not have been possible without the financial support provided by the Office of Naval Research through a grant to Robert Duncan. My gratitude is extended to the Program Manager, Randy Jacobson, for his acknowledgement of the value of academic research and his continuing financial support during my Ph.D. studies.

TABLE OF CONTENTS

TABLE OF CONTENTS (Continued)

TABLE OF CONTENTS (Continued)

LIST OF FIGURES

LIST OF FIGURES (continued)

LIST OF TABLES

GEOCHRONOLOGY AND GEOCHEMISTRY OF LOW TEMPERATURE HYDROTHERMAL ALTERATION IN OCEANIC CRUST: AN INVESTIGATION OF CELADONITE IN THE TROODOS OPHIOLITE, CYPRUS

1

INTRODUCTION

1.1 Background

The discovery of hydrothermal vents at the Galapagos Spreading Center marked the first direct observation of thermally driven fluid convection through the oceanic crust [Corliss et al., 1979]. Prior to this discovery, indirect evidence of hydrothermal fluid circulation had long been noted by marine geologists and geophysicists. Such evidence included: 1. Large compositional changes of crustal material relative to unaltered crust [e.g. Hart, 1970; Humphris and Thompson, 1978], 2. Anomalously low measurements of conductive heat flow from relatively young oceanic crust [Lister, 1972; Williams et al., 1974; Wolery and Sleep, 1976], and 3. Variation in measured P-wave velocities as a function of crustal age [Christensen and Salisbury, 1972; Houtz and Ewing, 1976].

These observations had two common characteristics. First, and perhaps most importantly, the noted characteristics were not geographically constrained. Rather, they were observed, to varying degrees, at all sites that had been sampled/tested within the world's oceans. Consequently, they could be assumed to result from a process that is pervasive throughout the world oceans. Second, the observed evidence could be attributed to the alteration of, and associated secondary mineral precipitation in, oceanic crustal material. This alteration would result not only in compositional change but also a decrease in porosity and permeability of the crustal material [Honnorez, 1981]. Subsequent discoveries of hydrothermal vents in a variety of tectonic settings [Edmond

et al., 1979; Malahoff et al., 1982; Horbie et al., 1986] confirmed that thermally driven circulation of seawater-derived fluids and the resultant physicochemical changes are ubiquitous characteristics throughout the world ocean crust.

The acknowledged pervasiveness of oceanic hydrothermal circulation has prompted wide-ranging efforts to understand the duration and magnitude of the associated physicochemical effects [e.g. Anderson and Skilbeck, 1981; Honnorez, 1981; Staudigel et al., 1981; Thompson, 1983; Alt and Honnorez, 1984; Seyfried et al., 1986, Vanko, 1986; Gillis and Robinson; 1990; Klinkhammer et al., 1994]. Many studies have focused on the chemical and isotopic signatures of vent fluids and altered oceanic crust. These have repeatedly demonstrated that significant chemical exchange occurs between oceanic crust and seawater-derived fluids [e.g. Hart and Staudigel, 1979; Alt and Honnorez, 1984; Staudigel et al., 1995]. Such studies have led to the current paradigm of the oceanic crust as a significant chemical buffer for components in seawater and as a medium for recycling elements through earth's geochemical reservoirs [e.g. Thompson, 1983; Von Damm, 1985; Staudigel et al., 1995].

The working model of the oceanic crust as a chemical buffer to seawater has prompted a proliferation of geochemical modeling [e.g. Sleep and Wolery, 1976; Von Damm, 1985; Morton and Sleep, 1985]. Modeling of the fluid-rock chemical exchange reactions of oceanic hydrothermal systems have, historically, been based upon high temperature vent fluid chemistries and bulk rock analyses [e.g. Edmond et al., 1979]. Such models have proven effective in constraining the effects of high temperature water-rock reactions. However, recent modeling has shown that these reactions may represent a relatively small amount of the total chemical exchange between seawater and crustal material [Morton and Sleep, 1985; Mottl and Wheat, 1992; Stein and Stein, 1994]. Current estimates indicate that over 75% of lithospheric heat loss within the ocean basins occurs within the ridge flank, rather than the ridge crest/rift, environments.

Consequently, water-rock reactions within these environments may represent the vast majority of hydrothermally driven chemical exchange within the oceans.

Geochemical modeling of water-rock exchange in low temperature environments has proven difficult to constrain for several reasons. First, unlike high temperature "smokers" at mid-ocean ridges, low temperature hydrothermal circulation is a diffuse process. Visible effluent, which is relatively easy to measure and sample at high temperature vents, is difficult (if not impossible) to discern in low temperature environments. Thus, fluid compositions must be inferred from mineral compositions, isotopic studies, and mixing of endmember seawater and host rock compositions.

Second, in order to assess the total chemical exchange capacity of oceanic crust, fluxes must be integrated over appropriate time frames. Estimates for the duration of circulation of low temperature hydrothermal fluids have varied tremendously since 1979. Estimates based on heat flow measurements range from 6 m.y. at ODP Hole 504B [Fisher et al., 1994] to 70 m.y. in parts of the Atlantic [Anderson and Skilbeck, 1981], depending on variables such as sedimentation, spreading rates, crustal structure, and permeability. Stein and Stein [1994] have shown by numerical heat flow modeling that advection of heat from the ocean crust by seawater is primarily controlled by the age of the crust. They suggest that the "sealing age", defined as the age of oceanic crust that no longer contains sufficient thermal energy to drive hydrothermal circulation, for all oceanic crust is 65 ± 10 m.y. The results of these geophysical studies lie in contrast to results from geochronologic studies of secondary alteration minerals. Hydrothermally deposited vein minerals from several DSDP/ODP sites have yielded radiometric ages up to only 20 m.y. after crustal formation [e.g. Richardson et al., 1980; Duncan et al., 1984; Staudigel and Hart, 1985; Hart and Staudigel, 1986; Peterson et al., 1986]. While each of these methods have provided valuable information regarding ocean crustal

aging, they have been of limited value in constraining a mean timescale for the global ocean floor.

Third, alteration zones within oceanic crust are often superimposed, which result in reactions between low temperature hydrothermal fluids and previously altered material [Alt and Honnorez, 1984; Gillis and Robinson, 1990]. These reactions are recorded in cross-cutting relationships of secondary minerals. In addition, the alteration of crustal material in low temperature environments is nonpervasive and heterogeneous [e.g. Alt et al., 1985; 1986; Gillis, 1986]. The occurrence of multi-stage alteration, along with heterogeneous low temperature conditions, provides for uncertain modeling between two endmember components consisting of "fresh" crustal material and seawater. Yet, with all the complications, stratigraphic/structural boundaries marking terminal reaction zones in oceanic crust are usually sharp and record distinct conditions in which the fluid-rock exchange has occured [Gillis and Robinson, 1990].

1.2 Low Temperature Alteration Studies from *In Situ* Ocean Crust

It is clear that adequately constrained models for geochemical mass-balance in low temperature environments are dependent upon detailed understanding of the fluid circulation, circulation longevity, and chemistry of alteration minerals. To this end, results from the Deep Sea Drilling Project (DSDP) and Ocean Drilling Project (ODP) have provided valuable insight to these processes. Drillcores, coupled with geophysical measurements, recovered from various worldwide sites have allowed for significant progress in understanding alteration within the upper 1 km of the oceanic crust. Important results from these sites may be summarized as follows:

1. The uppermost crust (0 to 100's meters) commonly displays intense, pervasive alteration at low temperatures and large lateral and vertical variation in the degree of

alteration [Shipboard Scientific Crew, Legs 51 and 53, 1979a; 1979b]. This alteration "facies" is chemically characterized by gains in K_2O, Fe_2O_3, H_2O, CO_2, Rb, Ba and depletions in SiO_2 and Sr. The abundances of other major components such as CaO, MgO, Na_2O, TiO_2, and Al_2O_3 show relatively small variations, both positive and negative, relative to fresh crustal material [e.g. Honnorez, 1981; Alt and Honnorez, 1984]. Based on O and Sr isotopes, the region is considered to be isothermal and representative of alteration with ambient seawater [e.g. Hart and Staudigel, 1979; Staudigel et al., 1995].

2. Stratigraphically underlying the pervasive alteration zone commonly occurs a region of significantly less alteration. It is characterized by variable alteration with fresh volcanic glass occasionally preserved. Alteration is primarily focused in areas of high permeability such as flow margins, interpillow voids, and breccia margins with less permeable regions (flow interiors) experiencing little alteration. Chemical characteristics of this alteration "facies" includes gains of Na_2O, K_2O, MgO, H_2O, Rb, Ba, and loss of SiO_2, CaO, and Sr [Honnorez et al., 1983; Alt and Emmerman, 1985; Alt et al., 1986]. This alteration zone extends to the lithologic transition zone between extrusive flows and sheeted dikes where alteration conditions change from low to high temperature. The region is considered to be a low temperature region, with temperatures less than 100°C [Hart and Staudigel, 1979; Alt et al., 1985].

3. Geophysical measurements have shown that the extrusive sequence within the oceanic crust is nearly isothermal [Alt et al., 1986]. This contrasts with measurements of bulk permeability that indicate roughly exponential decrease with depth, revealing the likely result of an increase in massive flow units relative to pillow units [Anderson et al., 1985; Becker, 1985]. In addition, heat flow measurements have revealed a correlation between topography and heat flow. High crustal heat flow has been shown to occur over topographic highs with corresponding low heat flows in topographic depressions

[Shipboard Scientific Crew, Leg 145, Hole 504B]. These geophysical data have been combined into a numerical model which simulates the geometry, along with other characteristics, of low temperature hydrothermal circulation [Fisher et al., 1994].

4. Geochronologic studies of limited numbers of alteration minerals, coupled with geophysical models of off-axis hydrothermal circulation, have provided the basis for a conceptual model of low temperature hydrothermal circulation and mineral precipitation [Fehn and Cathles, 1979; 1986; Peterson et al., 1986]. This model has been used to suggest that low temperature hydrothermal circulation decreases upward with age of the oceanic crust. Thus, sealing of the oceanic crust by precipitation of alteration minerals should be evident in relative ages of these minerals sampled from a large crustal section.

1.3 Low Temperature Alteration Studies from Ophiolites

Although studies of DSDP/ODP drillcore samples and their associated geophysical settings have advanced our understanding of low temperature oceanic hydrothermal systems, they have lacked a high degree of spatial continuity. That is to say, very few DSDP/ODP sites have multiple holes sufficient to provide a three dimensional view of circulation geometry and overall alteration. This deficiency has been addressed by studies of alteration in ophiolite (relict oceanic crust) suites [e.g. Coish, 1977; Spooner et al., 1977; Stern and Elthon, 1979; Stern et al. 1984; Alabaster et al., 1985; Gillis and Robinson, 1990; Bickle and Teagle, 1992; Booij et al., 1995]. Results from these investigations have provided valuable comparisons and contrasts with results from DSDP/ODP samples. For example, the Semail, Sarmiento, Del Puerto, and Troodos ophiolites all retain their original patterns of low temperature hydrothermal alteration [e.g. Gass and Smewing, 1973; Stern et al., 1976; Stern and Elthon, 1979; Elthon et al., 1984; Alabaster et al., 1985; Gillis and Robinson, 1985;

1990]. These patterns are in general agreement with those seen in DSDP/ODP cores. However, most of these suites do not contain the same mineral assemblages within the low temperature zones as those found in DSDP/ODP samples. Typically, the extrusive sequences within most ophiolites contain alteration mineral assemblages indicative of higher temperature environments.

The observed discrepancies between alteration mineral assemblages in extrusive units of most ophiolites and those in DSDP/ODP cores have been explained through a variety of mechanisms. For example, Alabaster et al. [1985] invoked closure of extrusive units to seawater exchange by overlying sediments to explain the higher temperature mineral assemblage in the Semail ophiolite. The hypothesized 10-20 m sediment layer nessary for closure, however, is at odds with results from numerical modeling of oceanic hydrothermal systems that indicate open circulation is possible through $\geq$ 100 m of sediment [Fisher et al., 1994]. Another explanation invoked to explain the alteration mineral assemblages in ophiolites has been higher thermal gradients. Stern and Elthon [1979] suggested that a continuous, steep thermal gradient occured during evolution of the Sarmiento ophiolite. In addition, large regional metamorphic zones were invoked to explain variations in the mineral assemblages within the suite. The hypothesized thermal gradient and regional metamorphic zones are, again, contrasted by subsequent work in numerical modeling and increased understanding as to the interdependences of sedimentation rate, permeability, cooling rate, and temperature [Alt et al., 1986; Gillis, 1987; Fisher et al., 1994].

Perhaps the most important result of alteration studies in ophiolites is that the low temperature mineral assemblages within the Troodos ophiolite are directly analogous with those defined from *in situ* crust [Gillis, 1987]. Within Troodos, Gillis mapped three distinct alteration zones within the extrusive units. These zones were designated, in stratigraphic order, the Seawater Zone (SWZ), the Low-Temperature

Zone (LTZ), and the Transition Zone (TZ). Each zone was characterized by chemical changes and mineral phases similar to the mapped zones in DSDP/ODP cores [Gillis and Robinson, 1988]. These are summarized as follows (Fig. 1.1):

1. SWZ Secondary mineralogy includes Fe-oxyhydroxides, K-feldspar, Al-saponite, analcime, and calcite. Bulk rock compositional changes include increased Fe_2O_3, K_2O, Ba, Sr, Rb, CO_2, and decreased SiO_2.

2. LTZ Secondary mineralogy includes Fe-oxyhydroxides, celadonite, Fe-saponite, zeolites, chalcedony, and calcite. Bulk rock compositional changes include increased K_2O, Ba, Rb, Na_2O and decreased CaO, SiO_2, and Sr.

3. TZ Secondary mineralogy includes saponite, chloritic smectite, albite, K-feldspar, laumontite, quartz, and alcime. Bulk rock compositional changes include increased Na_2O, MnO, and Zn, and decreased CaO and Sr.

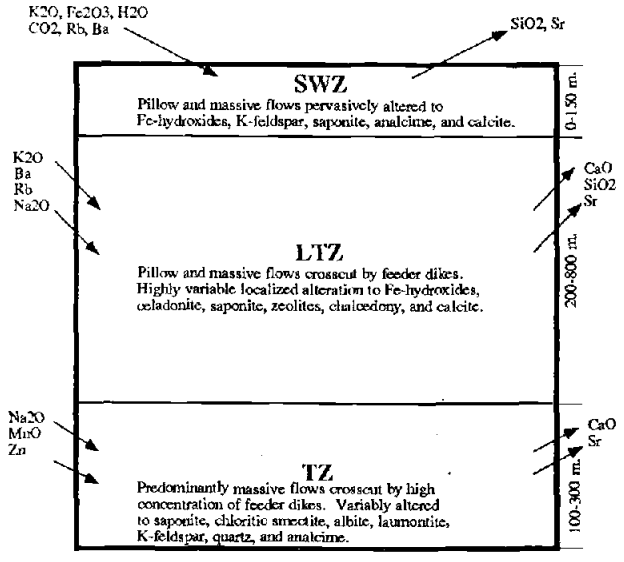

Figure 1.1 Schematic diagram of alteration zones and associated chemical changes in the upper 1 km of oceanic crust.

The results of the extensive work by Gillis [1987] provided a new venue for studying low temperature hydrothermal alteration in oceanic crust. Gillis clearly demonstrated that further study of the Troodos Ophiolite would yield additional information, not only applicable to this ancient hydrothermal system, but directly applicable to modern-day *in situ* oceanic crust.

1.4 Background of Troodos Ophiolite, Cyprus

Ancient ocean crustal rocks now exposed in the Troodos Mountains, Cyprus comprise perhaps the most intensively studied and well-characterized ophiolite in the world. This classic section marks the northwestern boundary of the circum-Arab ophiolite belt, a string of complexes along the northern margin of the Arabian plate that delineate the suture zone between the north moving Africa-Arabian plate and the Eurasian plate. Oceanic crust exposed within this region is of late Cretaceous (Cenomanian-Turonian) age [Tilton et al., 1981; Blome and Irwin, 1985; Mukasa and Ludden, 1987; Gallahan and Duncan, unpublished data] and is believed to represent seafloor formed within the ancient Tethys Ocean and subsequently uplifted during the Miocene-Pliocene during the continued closure of the Tethys Ocean [McCallum and Robertson, 1990; Robertson, 1990].

Compositions of Troodos lavas are distinct from mid-ocean ridge basalts and have arc-related chemical signatures [Miyashiro, 1973; Robinson et al., 1983; Schmincke et al., 1983; Moores et al., 1984; Cameron, 1985; Rautenshlein et al., 1985; Thy et al., 1985; Mehegan, 1988]. However, the exposed structure and stratigraphic relationships, including a complete section of oceanic lithosphere [Bott, 1971], are unambiguously associated with a spreading ridge environment [Moores and Vine, 1971; Varga and Moores, 1985; Allerton and Vine, 1987]. Within the massif, upper mantle

ultramafic rocks (layer 4) are successively overlain by intrusive rocks of frozen magma chambers and feeder dikes (layer 3), and massive, pillowed, and brecciated lavas (layer 2). The entire complex is capped by a Tethyan sedimentary sequence, including chalk, marl, chert, and limestone (layer 1).

Resulting from the excellent exposure and accessibility, the Troodos massif has proven the venue for the development of many models of formation and alteration of the oceanic crust [e.g. Moores and Vine, 1971; Gass and Smewing, 1973; Spooner and Fyfe, 1973; Miyashiro, 1973; Moores et al., 1984; Gillis and Robinson, 1990]. Moores et al. [1984] postulated a model for the synthesis of Troodos crust which incorporated a spreading ridge, above a north-dipping subduction zone, in a marginal region of the Tethys Ocean (Fig. 1.2). This model resolved the apparent discrepancies between lava compositions and exposed structures. In addition, it supports the tectonic model, based on gravity and seismic data, for uplift of the massif by underthrusting of continental crust (Africa-Arabian margin) from the south [Gass and Masson-Smith, 1963; Makris et al., 1983; McCallum and Robertson, 1990; Robertson, 1990].

Although the setting of Troodos has made petrologic and tectonic extrapolations to mid-ocean ridges debatable, numerous studies of crustal alteration processes have demonstrated comparable results between Troodos and in situ ocean crust. The relatively pristine nature of the massif, with no emplacement-related metamorphic overprint, has preserved secondary submarine alteration phases to a greater degree than within other ophiolites.

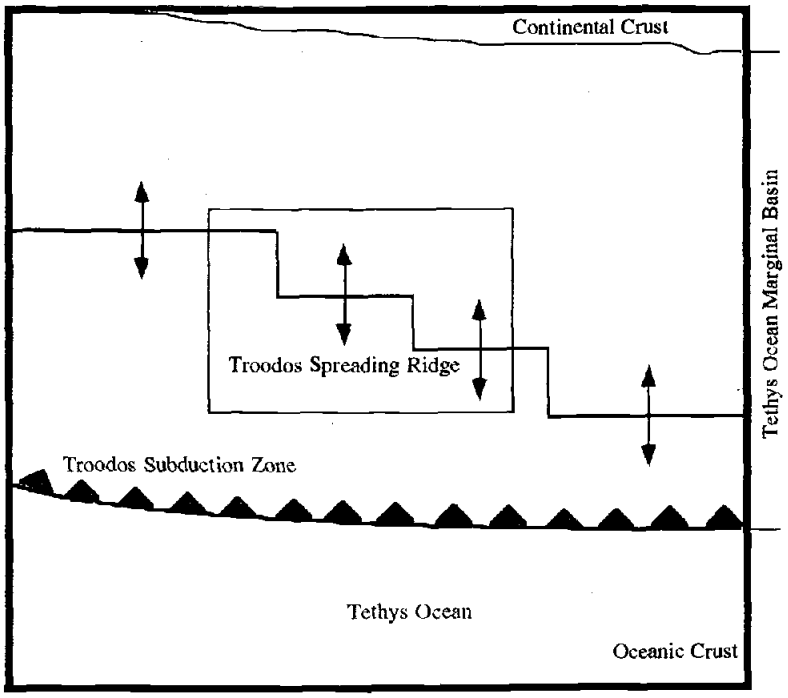

Figure 1.2 Schematic diagram of the tectonic setting of ancient Troodos oceanic crust.

1.5 Celadonite as a Hydrothermal Phase in Troodos

Low temperature hydrothermal alteration phases within the oceanic crust commonly include phyllosilicates, zeolites, calcite and chalcedony. These phases combine to form the terminal fracture-filling assemblage [e.g. Alt and Honnorez, 1984; Alt et al., 1986]. Of the terminal assemblage, the phyllosilicates are of special importance due to their chemical composition and structural complexity. They are commonly rich in alkali elements and have crystallographic sites that may accommodate most elements on the periodic table. In addition, they may take the form of one, or multiple, dioctahedral and trioctahedral clays and/or micas, that are physically or structurally mixed. The particular phyllosilicate phases that precipitate are determined

primarily by physicochemical conditions such as temperature, oxidation potential, and available chemical components [e.g. Wise and Eugster, 1964; Kastner and Gieskes, 1976; Seyfried et al., 1979; Alt and Honnorez, 1984; Gillis and Robinson, 1990]. As a result of their chemical and structural complexity, the importance of phyllosilicates on mass balance calculations of seawater-crust chemical exchange is poorly constrained. This is in spite of the fact that they may be important sinks for many important tracers of igneous and hydrothermal processes.

Within the Troodos ophiolite, the predominant low temperature alteration phase is celadonite, a K- and Fe^{3+}-rich dioctahedral mica. It has been studied, peripherally, as part of the extensive field mapping and analyses accomplished by Gillis (see Staudigel et al., 1986; Gillis, 1987; Gillis and Robinson, 1990). The phase is ubiquitous throughout the LTZ of the massif, typically associated with areas of relatively high permeability, including interpillow voids, flow margins, and interstitial breccias. It is identified in the field by a characteristic blue-green color. The structure and composition of celadonite indicate very high fO_2, high concentrations of SiO_2, low pH, and temperatures $\leq 40^{o}C$ [Kastner and Gieskes, 1976]. Such conditions are a common result of the interaction of cold, oxygenated seawater with igneous glass [Seyfried et al., 1979]. Consequently, the phase acts as an excellent indicator of low temperature hydrothermal circulation.

Another important aspect of celadonite is its suitability as a geochronometer. By comparing radiometric ages of celadonites with those determined for the host rocks, any differences may be interpreted as the duration of hydrothermal circulation. The structure and composition (K-rich, Ar-retentive mica) of celadonite have proven an effective combination for reliable K/Ar age determinations (see Duncan et al., 1984; Peterson et al., 1986; Staudigel et al., 1986). Within the Troodos ophiolite, limited numbers of celadonites from a small geographic area have previously yielded K/Ar ages ranging

from ~87 Ma to ~77 Ma [Staudigel et al., 1986]. Comparison of these ages with the 91-92 Ma age of Troodos crust [Mukasa and Ludden, 1987] indicates that low temperature hydrothermal circulation may have continued for up to 15 m.y. after crustal formation. Similar estimates for low temperature hydrothermal circulation have been derived from celadonite samples from DSDP/ODP cores [e.g. Duncan et al., 1984; Peterson et al., 1986]. Consequently, many researchers have developed the hypothesis that closure to low temperature hydrothermal circulation occurs within 15 m.y. post-crustal formation.

1.6 Thesis Objectives

This thesis was undertaken to: 1) test the hypothesized "15 m.y. limit" to low temperature hydrothermal circulation in the upper oceanic crust, 2) evaluate the model for preferred upward sealing of the oceanic crust, and 3) assess the effects of celadonite precipitation as a sink/source for components within seawater and mobilized from host crust. To this end, celadonite samples were collected from geographically, stratigraphically, and lithologically diverse regions within the extrusive units of the Troodos Ophiolite, Cyprus. In addition, samples of celadonite were collected from International Crustal Research Drilling Group (ICRDG) drillcores, housed in the Cyprus Geological Survey repository (Nicosia). The combination of outcrop and drillcore samples provided unambiguous 3-dimensional relationships of the samples. The samples were chemically and isotopically analyzed to determine K/Ar ages, along with major, minor, and trace element compositions. The objectives of this thesis were to: 1) assess any stratigraphic and/or lithologic K/Ar age correlations, and 2) determine any unusual chemical signatures associated with celadonite. The acknowledged analogue of Troodos with *in situ* crust allows for extrapolation of the results to contemporary seafloor hydrothermal processes.

2

SPATIAL AND TEMPORAL VARIABILITY IN CRYSTALLIZATION OF CELADONITES WITHIN THE TROODOS OPHIOLITE, CYPRUS: IMPLICATIONS FOR LOW-TEMPERATURE ALTERATION OF THE OCEANIC CRUST

William E. Gallahan and Robert A. Duncan

Published in *Journal of Geophysical Research*, volume 99, pages 3147-3161, 1994.

2.1 Abstract

Celadonite, a low-temperature (<40°C) hydrothermal alteration mineral, is a predominant fracture and void-filling phase within the volcanic rocks of the Troodos ophiolite. The combined chemical and structural properties of celadonite (i.e., high K_2O and Ar retentive), along with its common occurrence, provide a valuable tracer for studying the temporal and spatial variability of low-temperature hydrothermal fluid circulation and alteration within this ancient oceanic crust. Some 54 new K/Ar age determinations of celadonites from various geographic and stratigraphic locations within the extrusive rocks of Troodos yield crystallization ages ranging from 90.9 $\pm$ 1.0 to 49.8 $\pm$ 0.5 Ma, with the oldest in close agreement with the estimated 91-92 Ma crystallization age of Troodos igneous rocks. The youngest age indicates that low-temperature water/rock chemical exchange continued for at least 40 m.y. after crustal formation. This represents a 100% increase over previous estimates, based on limited numbers of K/Ar dates of celadonite, of the duration of low temperature mineral precipitation in Troodos. Correlation between celadonite ages and field relationships suggest the following: (1) There is no apparent relationship between celadonite crystallization and stratigraphic depth. (2) Celadonite crystallization occurs homogeneously on an outcrop scale, with adjacent samples from a single flow unit yielding equivalent K/Ar ages. (3) Flow units with relatively high primary permeabilities, e.g., pillows and breccias, yield celadonites with younger K/Ar ages. (4) Celadonite precipitation at distinct locations occurred rapidly, with little or no age difference between rim and core sections of single large deposits. The above correlations suggest that low-temperature hydrothermal fluid circulation and secondary mineral precipitation are controlled by the local alteration conditions, such as intrinsic permeability, degree of fracturing, and water/rock ratios, and are independent of time

and space. Integration of these local heterogeneities over the entire extrusive sequence suggests that the upper oceanic crust undergoes relatively homogeneous closure to hydrothermal fluid circulation. No evidence is found to support a progressive upward sealing of the oceanic crust.

2.2 Introduction

Evidence for hydrothermal fluid circulation within the oceanic crust had been noted by marine geologists and geophysicists [e.g., Hart, 1970; Lister, 1972; Christensen and Salisbury, 1972; Houtz and Ewing, 1976] long before the first hydrothermal vents were discovered along the Galapagos Spreading Ridge [Corliss et al., 1979]. In particular, many chemical and physical changes which correlated with age of the crust and/or distance from ridge axis were attributed to the progression from high- to lower-temperature alteration environments as the oceanic crust moved away from axial regions. These changes, primarily limited to the uppermost sequence of pillowed and massive flows, included an increase in the measured seismic wave velocities [Houtz and Ewing, 1976], increased conductive heat flow relative to convective transport [Anderson and Hobart, 1976], and large compositional variation relative to "zero age" crust [e.g., Hart, 1970; Andrews, 1977; Donnelly et al., 1979; Alt and Honnorez, 1984; Alt et al., 1986]. Subsequent discoveries of hydrothermal activity in a variety of tectonic settings, [e.g., Corliss et al., 1979; Malahoff et al., 1982; Horbie et al., 1986] revealed that hydrothermal fluid circulation is an intrinsic characteristic of the world ocean. In addition, analyses of the vent fluids revealed the magnitude of fluid/rock interaction and the significance of the oceanic crust as an elemental sink/source for chemical cycling within the oceans [e.g., Edmond et al., 1979].

It is now generally accepted that the evolutionary changes in oceanic crust are due to the progressive precipitation of low-temperature (<50°C) alteration minerals within veins and vugs of the fractured host rock [Honnorez, 1981]. These secondary minerals, the result of chemical exchange between heated "seawater" and the fractured host rock, continue to crystallize for millions of years following crustal accretion [e.g., Staudigel et al., 1986]. Variations in the ages of formation and chemical compositions of low-temperature vein-filling minerals provide data for understanding chemical exchange/flux mechanisms, fluid circulation geometry, and evolution of fluid compositions with temperature and time.

Low-temperature alteration phases within the oceanic crust include phyllosilicates (micas and/or clays), zeolites, calcite, and quartz (chalcedony), together forming the terminal fracture-filling mineral assemblage. Of these phases, the phyllosilicates are typically the most abundant, depending on local alteration conditions [Alt and Honnorez, 1984; Alt et al., 1986; Gillis and Robinson, 1988, 1990]. In addition, the phyllosilicates are sites of important chemical reactions, particularly alkali and Mg fixation, associated with low-temperature chemical equilibria between heated seawater and basaltic rocks that compose the oceanic crust. However, the effects of these reactions on mass balance calculations of seawater-crust chemical exchange are poorly constrained due to a lack of knowledge regarding the duration of low-temperature fluid circulation within oceanic crust. As a result, any new data regarding the mechanisms and time frame for precipitation of phyllosilicates will affect our assessment of the physical, as well as chemical, evolution of the oceanic crust.

Another important aspect of phyllosilicate precipitation within altered oceanic crust is the ability of some minerals to act as reliable geochronometers of low-temperature hydrothermal fluid circulation [Peterson et al., 1986; Staudigel et al., 1986]. Differences between radiometric ages of these secondary minerals and the age of crustal

material may be assumed to represent the time required to effectively seal fractures to fluid circulation. Celadonite, a K-rich, Ar-retentive mica, from the low-temperature alteration zone (LTZ) of the Troodos ophiolite, has proven to be particularly valuable in this respect. Previous K/Ar age determinations of these celadonites, along with samples from Deep Sea Drilling Project (DSDP) sites 417 and 597, have yielded ages of crystallization up to 15-20 m.y. younger than the crustal material [Duncan et al., 1984; Peterson et al., 1986; Staudigel et al., 1986]. Among these data, the 13 Ma and 19 Ma celadonite ages from Site 597 (28.6 Ma crust with a half spreading rate of 55.4 km/m.y.) are of particular significance. By combining these ages and spreading rate, Petersen et al. [1986] calculated that low-temperature hydrothermal circulation was active at least 550 km off ridge crest and possibly to a distance of ~1000 km off axis. Clearly, these vein-filling minerals act as important "tracers" of long-term physical and chemical processes which occur in the off-axis, low-temperature regions of oceanic crust.

Despite the relative importance of secondary phyllosilicates to understanding long-term changes within the upper oceanic crust, their compositional variations and precipitation mechanisms are poorly understood. For example, analyses of phyllosilicates from various seafloor and Ocean Drilling Program (ODP) sites indicate that compositional variations may be explained by mixing between three components, celadonite (a K, Mg, Fe^{3+} mica), saponite (a Na, Mg trioctahedral smectite), and nontronite (a K, Fe^{3+} dioctahedral smectite) [Seyfried et al., 1978; Andrews, 1980; Bohlke et al., 1980; Humphris et al., 1981; Alt and Honnorez, 1984; Alt et al., 1986; Gillis and Robinson, 1990]. However, the actual relationships between these components, whether they represent physical mixtures, mixed layering, or progressive lower-temperature chemical exchange with a preexisting higher-temperature phase, such as chlorite, remains unresolved. New data regarding the spatial and temporal variability

of these phyllosilicates can provide enormous insight into the changes in alteration conditions with time.

In this paper, we present the results of a combined field, geochronological, and geochemical study of low-temperature secondary phyllosilicates (hereafter referred to collectively as celadonite) from a variety of geographic and stratigraphic positions within the Troodos ophiolite, Cyprus. Complementary studies which map and compare alteration zones and secondary mineral assemblages within this ancient oceanic crustal section with those recovered in DSDP/ODP cores from modern in situ crust [Gillis and Robinson, 1988; 1990] allowed us to interpret our data in the context of present-day hydrothermal and crustal evolution processes. Our goals are to identify spatial and temporal variations in celadonite formation and composition and to infer from these any related changes in hydrothermal fluid conditions and circulation geometry which affect the overall evolution of the ocean crust.

2.3 Previous Studies

2.3.1 Troodos Ophiolite

The Troodos massif in Cyprus is perhaps the most intensively studied and well-characterized ophiolite in the world. It marks the northwestern boundary of the circum-Arab ophiolite belt, a string of complexes along the northern margin of the Arabian plate that delineate the suture zone between the north moving Africa-Arabian plate and the Eurasian plate. Oceanic crust exposed within this region is of late Cretaceous (Cenomanian-Turonian) age [Tilton et al., 1981; Blome and Irwin, 1985; Mukasa and Ludden, 1987] and is believed to represent seafloor formed within the ancient Tethys

Ocean and subsequently uplifted during the Miocene-Pliocene during the continued closure of the Tethys Ocean [McCallum and Robertson, 1990; Robertson, 1990].

Compositions of Troodos lavas are distinct from mid-ocean ridge basalts, containing arc-related chemical signatures [Miyashiro, 1973; Robinson et al., 1983; Schmincke et al., 1983; Moores et al., 1984; Cameron, 1985; Rautenshlein et al., 1985; Thy et al., 1985; Mehegan, 1988]. However, the exposed structure and stratigraphic relationships, including a complete section of oceanic lithosphere [Bott, 1971], are unambiguously associated with a spreading ridge environment [Moores and Vine, 1971; Varga and Moores, 1985; Allerton and Vine, 1987]. Within the massif, upper mantle ultramafic rocks (layer 4) are successively overlain by intrusive rocks of frozen magma chambers and feeder dikes (layer 3), and massive, pillowed, and brecciated lavas (layer 2) (Figure 2.1). The entire complex is capped by a Tethyan sedimentary sequence, including chalks, marls, cherts, and limestones (layer 1).

Moores et al. [1984] postulated a model for the synthesis of Troodos crust which incorporated a spreading ridge, above a north dipping subduction zone, in a marginal region of the Tethys Ocean. This model resolved the apparent discrepancies between lava compositions and exposed structures. In addition, it supports the tectonic model, based on gravity and seismic data, for uplift of the massif by underthrusting of continental crust (Africa-Arabian margin) from the south [Gass and Masson-Smith, 1963; Makris et al., 1983; McCallum and Robertson, 1990; Robertson, 1990].

Although the setting of Troodos has made petrologic and tectonic extrapolations to mid-ocean ridges argumentative, numerous studies of crustal alteration processes have demonstrated comparable results between Troodos and in situ crust. The relatively pristine nature of the massif, with no emplacement-related metamorphic overprint, has preserved secondary alteration mineral phases which are representative of the submarine environment. From the focused axial high-temperature regions [Chapman and Spooner,

1977; Spooner et al., 1977; Constantinou, 1980; Malpas et al., 1987; Schiffman and Smith, 1988; Richards et al., 1989] to the dispersed low-temperature hydrothermal assemblages [Gillis and Robinson, 1988, 1990] in Troodos, all secondary alteration can be correlated with phases/zones found in DSDP/ODP cores. Of particular significance, the extensive study of low-temperature alteration by Gillis [1987] demonstrated correlations between five mineral assemblage zones and factors such as the degree of sedimentation, permeability, temperature, and direction/patterns of hydrothermal fluid flow. Subsequent comparison of these results with DSDP/ODP cores demonstrated that the alteration zones were similar and more systematic than previously recognized [Gillis and Robinson, 1988]. Such studies have provided the context for examining evolutionary processes in contemporary oceanic crust by further study of Troodos.

2.3.2 Celadonite Chemistry and Occurrence

Celadonite is typically turquoise to dark green, is microscopically acicular (massive macroscopically), and occurs as a replacement for interstitial glass in pillows, olivine phenocrysts in flows (although typically not associated with iddingsite), and pervasive phases within the groundmass/matrix of submarine lavas. In addition, it is the predominant fracture, void, and vug-filling phase. The relative abundance of the phase lends itself to studying temporal and spatial geochemical variability in low-temperature hydrothermal reactions. Within the Troodos ophiolite, it is distributed throughout most of the LTZ [Gillis, 1987; Gillis and Robinson; 1990].

Chemical compositions of celadonite may be defined as "mixtures" of three end-member components: pure celadonite $KMgFe^{3+}Si_4O_{10}(OH)_2$, nontronite $(K_x{\cdot}nH_2O)Fe^{3+}{}_2(Si_{4-x}Al_x)(OH)_2$, and saponite $(Na_x{\cdot}nH_2O)(Fe^{2+},Mg)_3(Si_{4-x}Al_x)(OH)_2$. Explanations for the above chemical and structural variations have conflicting

implications for the evolution of alteration conditions. One explanation suggests progressive dissolution and precipitation of saponite to celadonite [Donnelly et al., 1979; Stakes and Scheidegger, 1981] in a manner similar to the diagenetic mechanism for Fe-smectite to glauconite conversion [Buatier et al., 1989]. Such a mechanism would imply evolution from a reducing Fe^{2+} environment (relatively low water/rock ratio) to a more oxidizing Fe^{3+} environment with a high water/rock ratio. This would be consistent with the formation of high-temperature, low f_{O2} phases in proximal, near-ridge environments, followed by chemical/structural phase reequilibration with age and distance from the spreading axis. Another explanation for the observed trends is a progression from celadonite-nontronite to saponite through sequential precipitation [Alt and Honnorez, 1984; Alt et al., 1986]. This is consistent with progressively lower water/rock ratios as secondary minerals fill fractures and vugs within the oceanic crust. Such a mechanism would result in zoned fractures and vugs containing physical mixtures of the phases. While there are ample petrographic and geochemical data from DSDP/ODP which support either interpretation, results of this study suggest partial to complete reequilibration of a preexisting phase is the predominant mechanism in Troodos celadonites.

2.4 Field Area, Sampling Methods, and Analyses

Sampling of celadonites from the Troodos ophiolite followed two basic strategies. First, field sampling was concentrated within the LTZ, defined and mapped by Gillis [1987], along the northern margin of the complex (see Figure 2.1). The area was chosen in order to maximize collection from a variety of stratigraphic and geographic locations within this well characterized region. Second, drill cores from holes CY-1A and CY-2 of the Cyprus Crustal Study Project (CCSP) were studied and

sampled. These cores provided unequivocal stratigraphic relationships for assessing chemical/age variations with depth.

Methods employed in celadonite analyses included thin section petrography, electron microprobe analysis, atomic absorption flame spectrophotometry, and noble gas mass spectrometry. Chemical analyses of 132 celadonites were obtained with a Cameca SX-50 electron microprobe at Oregon State University. Beam conditions were set at 30 nA current and 20 keV accelerating bias. Major elements were counted for 10 s on peak with the minor elements Mn, F, and Cl being counted for 20 s. Background counts were taken on each side of elemental peaks for one half the peak counting time. In order to minimize volatization and resulting loss of alkalis, a partially defocused beam (diameter of 5 μm) was used, with Na, K, and Ca being the first elements analyzed. Because of the inherent difficulties in microprobe analysis of soft, hydrous phases (i.e. polishing problems and volatization), the reproducibility of our data was difficult to assess. Data validity was determined by calculating structural formulas based upon the chemical analyses. If the formulas were stoichiometric for the celadonite-nontronite-saponite composition/structural space, then analyses were considered acceptable. Approximately 10% of the analyzed points yielded nonstoichiometric formulas or extremely low oxide totals (<75%). These points were eliminated from the data set

Ages of 54 celadonites were determined using the K/Ar method [Dalrymple and Lanphere, 1969]. Samples were gently crushed and sieved to 100-200 mm grain size. Representative homogeneous splits for K determination and Ar isotope analysis were separated using a binocular microscope. Potassium analyses were obtained by atomic absorption flame spectrophotometry (AAS) at the University of Oregon. Comparative analyses of U.S. Geological Survey (USGS) standards RGM-1, AMH-1, and W-2 reproduced the K contents within 1% of accepted values. Ar analyses were determined on an Associated Electrical Industries MS-10S noble gas mass spectrometer at Oregon

State University. Samples were loaded in Mo crucibles in water-cooled furnace bottles, baked out in vacuo at <50°C for 12 hours to minimize fractionation of Ar isotopes from loosely bound sites, then fused by induction heating. Argon isotopes and ratios were determined by isotopic dilution of the fused sample by a known ^{38}Ar spike, calibrated against the USGS biotite standard FCT-3. Five sweeps of the ^{36}Ar, ^{38}Ar, and ^{40}Ar mass peaks were obtained, and the peak heights were regressed against time to obtain initial ratios. The standard error on $^{40}Ar/^{38}Ar$ was typically <0.1% and for $^{38}Ar/^{36}Ar$ <1.5%.

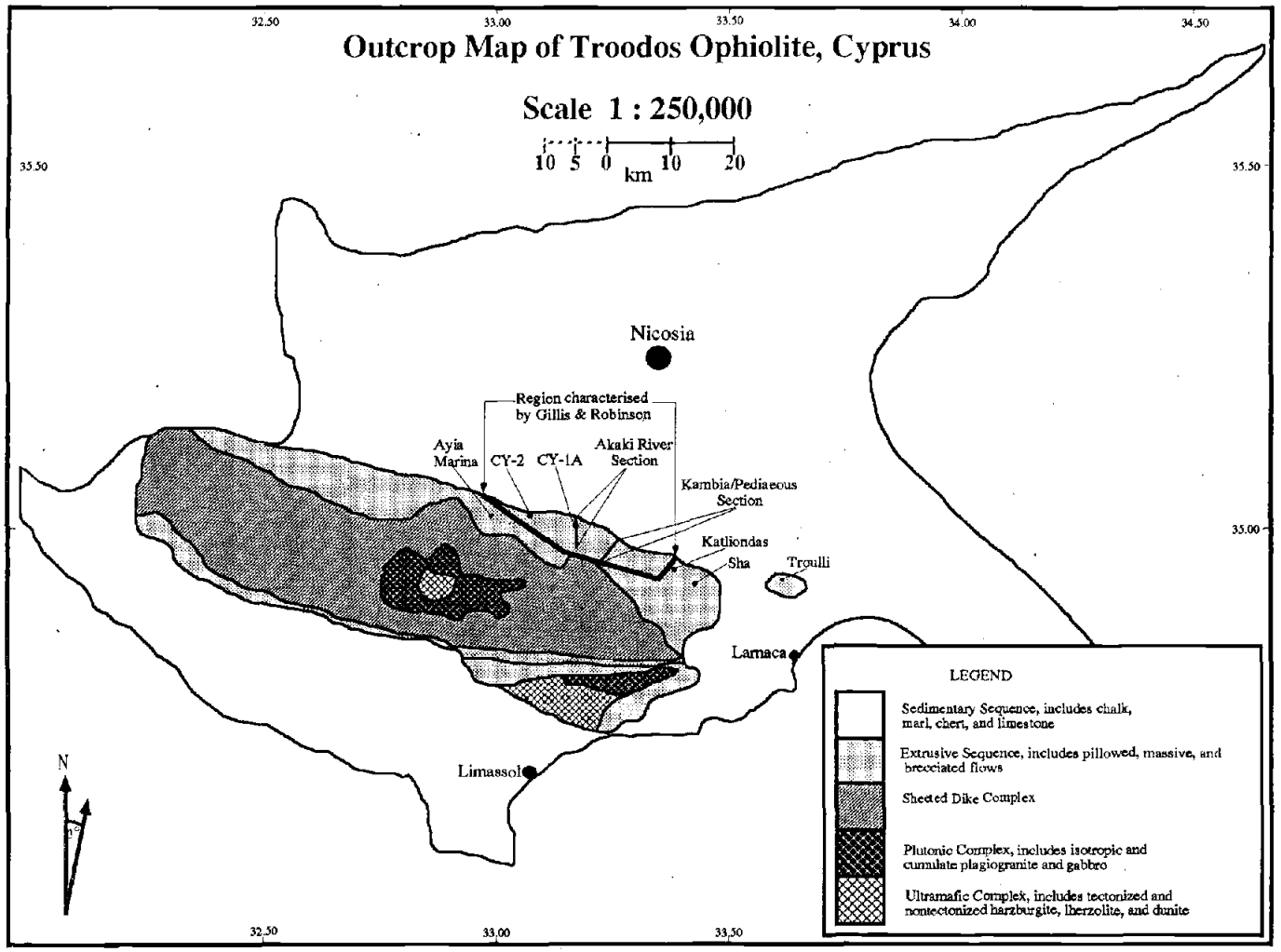

Figure 2.1 Outcrop map of the Troodos ophiolite showing concentric exposure of classical oceanic lithosphere stratigraphy. Areas sampled for celadonite are annotated in the extrusive unit of the map.

2.5 Results

2.5.1 Field and Core Sampling

Approximately 150 celadonite samples were collected from the CCSP drill cores and from the stratigraphic/geographic locations indicated in Figure 2.1. Outcrop samples ranged from veined celadonite (micrometer to millimeter scale) within meter-sized crustal rocks to monomineralic (centimeter size) deposits within fractures and interstitial pillow spaces. The largest sample, a subspherical mass approximately 10 cm in diameter, was collected intact in order to assess any difference in ages determined from analyses of varying sections of the sample. Based on outcrop relationships, the following generalizations can be made: (1) there is a higher density of macroscopic celadonite deposits in areas of massive flows and dikes, relative to pillow and breccia units; (2) within the massive units, celadonite occurs along flow margins and in fractures separating relatively fresh flow interiors; and (3) along flow margins, whether pillow, massive flow, or dike, celadonite is commonly intermixed with variably palagonitized-to-fresh glass. Drill core samples were typically 1/4 or 1/2 core sections, approximately 5 to 10 cm long, containing vein (same scale as outcrop samples) and occasional massive celadonite. Massive samples typically occur at flow margins and within voids.

2.5.2 Petrographic Analyses

Fourteen polished thin sections of celadonite-filled veins and vugs from core CY-2 were examined under plain and cross-polarized light. The samples spanned the core interval from 117.85 to 211.80 m. In all sections, celadonite is the predominant (>70%) void-filling phase. Minor amounts of intermixed chalcedony and cross-cutting

calcite occur in six of the sections. Staining from iron oxyhydroxides(?) is present in three sections. Optically, no zoning of celadonite in veins or vugs was detected.

2.5.3 Microprobe Analyses

Major and minor element abundances were determined for samples from four intervals within core CY-2 in order to compare chemical compositions of Troodos celadonites with those analyzed from DSDP/ODP drillcores. Table 2.1 lists representative full analyses of multiple samples from each interval. Because of coupled substitutions and charge balancing constraints within a three-component system, direct comparison between full analyses of Troodos samples and DSDP/ODP celadonites is difficult. In Figure 2.2, the molar proportions of potassium, iron, and magnesium from 132 data points are plotted on a ternary diagram and compared with the compositions of DSDP/ODP samples. The result indicates that Troodos celadonites fall well within the compositional space defined by samples from in situ ocean crust, suggesting that no post crystallization compositional changes have occurred during tectonism. In addition, two distinct mixing trends can be distinguished, between the celadonite and nontronite end-members and the celadonite and saponite components. It is important to note that most of the Troodos samples cluster near "pure celadonite" and on the trend between celadonite and nontronite.

Table 2.1. Representative electron microprobe analyses of celadonites from ICRDG core CY-2.

	Interval, m								
	135.45	135.45	123.30	123.30	199.60	199.60	199.60	119.00	119.00
SiO_2	52.98	51.69	52.87	51.67	51.95	50.17	51.61	53.05	55.50
TiO_2	0.11	0.17	0.15	0.12	0.20	0.23	0.23	0.03	0.00
Al_2O_3	4.71	4.39	3.98	3.92	3.39	8.57	5.14	3.22	2.80
Fe_2O_3	19.47	20.03	21.95	21.39	19.72	17.93	17.74	26.34	22.99
MgO	4.59	4.56	4.62	4.60	5.14	5.06	7.75	3.49	4.60
CaO	0.19	0.21	0.29	0.47	0.18	0.52	0.59	0.37	0.14
MnO	0.02	0.11	0.09	0.12	0.13	0.11	0.11	0.11	0.06
Na_2O	0.22	0.18	0.17	0.06	0.21	0.94	0.60	0.35	0.17
K_2O	7.52	7.16	7.83	7.10	8.61	4.87	5.80	6.27	8.66
F	0.52	0.17	2.67	2.25	0.58	0.32	0.06	0.05	0.03
Cl	0.03	0.04	0.05	0.05	0.03	0.04	0.01	0.01	0.01
OH	3.80	3.89	2.82	2.91	3.70	3.86	4.04	4.10	4.20
Total	94.16	92.60	97.49	94.66	93.84	92.62	93.68	97.39	99.16
Cation Totals for Different Coordination Sites on the Basis of 22 Oxygen Atoms									
Σ $(Si,Al)^{iv}$	8.00	8.00	8.00	8.00	8.00	8.00	8.00	8.00	8.00
Σ $(Al,Fe,Mg,Mn,Ti)^{vi}$	3.87	3.91	3.88	3.90	3.85	4.35	4.21	3.90	3.81
Σ $(Na,K,Ca)^{viii}$	1.51	1.47	1.56	1.45	1.74	1.28	1.36	1.32	1.64
Cation Total	13.38	13.38	13.44	13.35	13.59	13.63	13.57	13.22	13.45

Percent hydroxide calculated by balancing the analyzed cation oxide percentages and anions to 22 oxygen atoms.

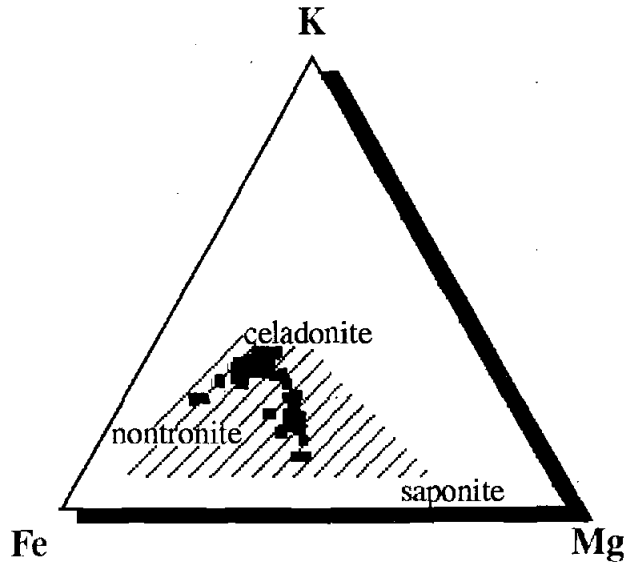

Figure 2.2 Comparison of ternary phyllosilicate compositions and mixing trends of Troodos celadonites (solid squares) with analyses of DSDP/ODP drill core samples (shaded region). DSDP/ODP data are from holes 396B [Bohlke et al., 1980], 417A&D [Alt and Honnorez, 1984], 504B [Alt et al., 1986], and 597B&C [Peterson et al., 1986].

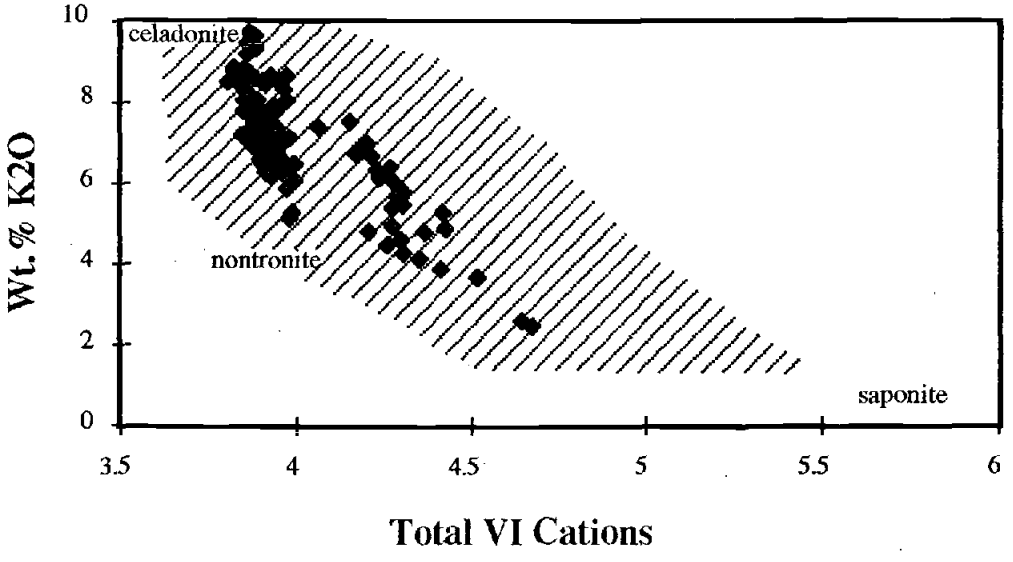

Figure 2.3 Correlation of potassium content (wt % K_2O) with phyllosilicate structure for Troodos celadonites (solid diamonds), compared with trends defined by analyses of DSDP/ODP samples (shaded region).

Another important measure of the chemical, as well as structural, variation in the Troodos celadonites is the correlation of potassium with octahedrally coordinated (VI) cations. As the pure celadonite component of the sample increases, there should be a concomitant increase in K_2O and decrease in VI cations. Figure 2.3 shows the K_2O versus VI cations relationship for the same data included in Figure 2.2. Again, the same trends and distribution of data are apparent. These trends can also be discerned by the MgO content of the phases (Figure 2.4) with trioctahedral saponite having the highest wt % MgO, followed by dioctahedral celadonite with moderate MgO contents and nontronite. Underscoring the relative low abundance of saponite component in these celadonitic micas/clays is the result that only 26 of 132 data points contain VI cation totals greater than 4, with none greater than 4.7. End-member saponite contains 5.5 to 6.0 octahedrally coordinated cations.

Chemical/structural variation of celadonites as a function of stratigraphic position was examined by subdividing analyses based upon the core interval (Figure 2.5). Several observations can be made from Figure 2.5. First, samples from the stratigraphically highest three intervals plot within the dioctahedral field (one point excepted) and define the steep-trending, celadonite-nontronite mixing line. Second, with the exception of one data point, all of the trioctahedral data points are from the lowest interval (199.60 m) and define a mixing trend between saponite and celadonite-nontronite. Finally, samples from 199.60 m demonstrate the largest variation in composition, ranging from the highest percentage of saponite to "pure celadonite" and trending toward the nontronite component.

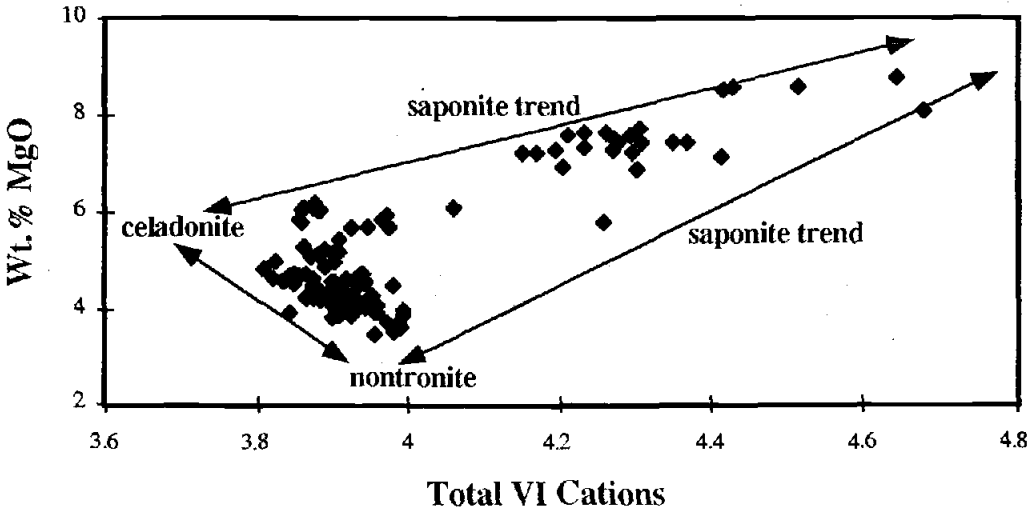

Figure 2.4 Variation of magnesium content (wt % MgO) of Troodos celadonites with phyllosilicate structure. Arrows denote mixing trends of the ternary phyllosilicates.

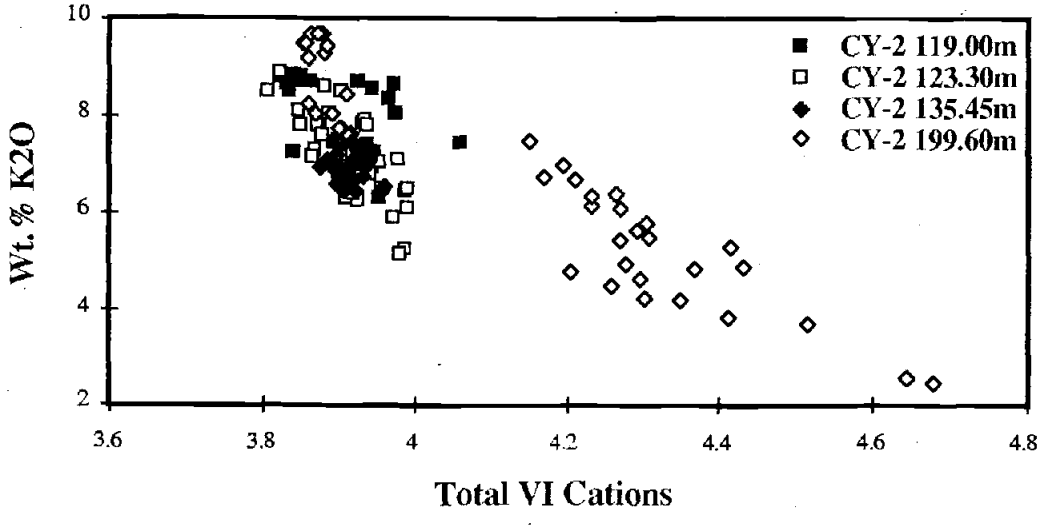

Figure 2.5 Variation of celadonite chemistry and structure with depth of sample intervalfrom CCSP drill core CY-2

Although zoning within veins and vugs was not optically detected during petrographic analysis, a test for chemical/structural variation was performed by microprobe traverses across two separate celadonite-filled veins. The veins were selected based on the criteria: (1) they were of similar size (~135 μm); (2) neither contained intermixed chalcedony or vein calcite; and (3) neither had visual iron staining. Traverses were accomplished in 5-μm (beam diameter) steps for 25 points, bracketed by 5-μm margins to avoid fluorescence of host material. The results of the two traverses (Figure 2.6) reveal definite chemical heterogeneity within both veins. More importantly, however, is that the mixing of the different end-member components does not result in a structurally heterogeneous vein sample. Each vein contains either a dioctahedral or a trioctahedral phase. This characteristic constrains the possible formation mechanisms for the celadonite, and it allows for the sampling of bulk vein material for geochronologic analyses.

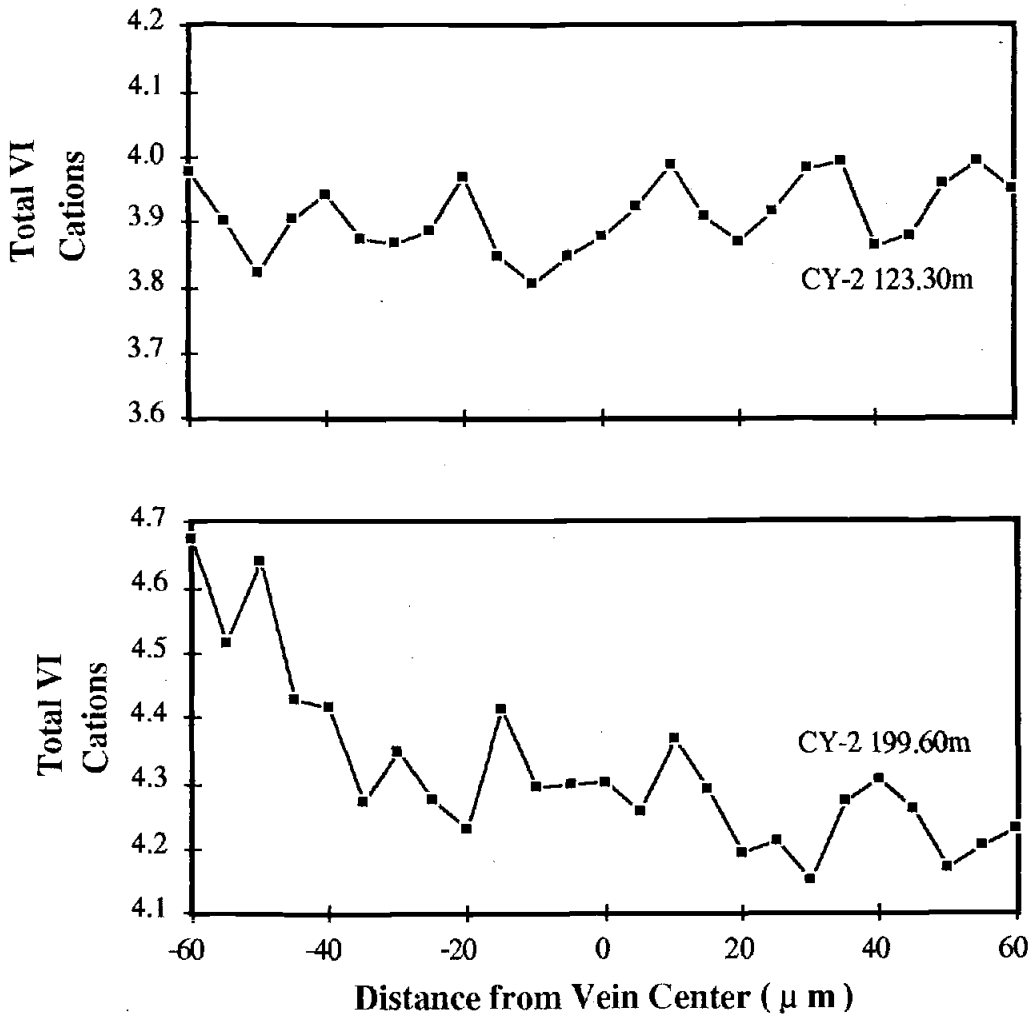

Figure 2.6 Plot of microprobe traverses of two celadonite-filled veins showing structural/chemical variability within each vein.

2.5.4 K/Ar Ages

Table 2.2 lists 54 new K/Ar age determinations of celadonite from geographic/stratigraphic locations (illustrated in Figure 2.7) within the upper crustal section of the Troodos ophiolite. Dates range from 90.9 + 1.0 to 49.8 + 0.5 Ma, with the oldest in close agreement with the estimated 91-92 Ma crystallization age of Troodos igneous rocks [Blome and Irwin, 1985; Mukasa and Ludden, 1987]. The youngest ages indicate that celadonite precipitation continued at least into the middle Eocene, yielding a minimum estimate for the duration of low-temperature hydrothermal fluid/rock interaction of 40 m.y. This represents a >100% increase over previous estimates, based on limited numbers of K/Ar and Rb/Sr age determinations of celadonite, of the duration of low-temperature mineral precipitation in Troodos [Staudigel et al., 1986].

Samples from two field areas with well-characterized volcanic stratigraphies, Akaki Canyon and Pediaeos/Kambia [see Gillis, 1987; Gillis and Robinson, 1988, 1990], and from the CCSP drill cores CY-1A and CY-2 were used to assess possible stratigraphic control on the ages of celadonite precipitation. Figures 2.7a, 2.7b, and 2.7c show the K/Ar ages of celadonites plotted against relative position in the various stratigraphic sections measured from the top of lava sections. No systematic pattern is apparent for the distribution of ages on a crustal scale. However, analyses of adjacent samples from individual flow units yield approximately equivalent ages of crystallization. For example, samples CY-90-12K, CY-90-40K, and CY-90-41K from the base of flow unit "K" [Schminke et al., 1983] in the Akaki Canyon area all yield ages of crystallization between 78.9 and 80.0 Ma. Other examples include samples CY-90-34L and CY-90-36L, samples CY-92-36, CY-92-37, and CY-92-38, and samples CY-1A (13.90 m) and CY-90-9C.

Table 2.2 Analytical results of 54 K/Ar age determinations of celadonites from various stratigraphic/geographic locations within Troodos

CCSP Core	Depth, m	K, %	^{40}Ar Radiogenic, x 10^{-5} cm^3/g	^{40}Ar Radiogenic, %	Age, Ma (+/- 1σ)
CY-1A	13.90	4.22	1.5164	77.1	90.2 ± 0.9
	46.00	3.36	1.0154	62.7	76.2 ± 0.9
	49.90	3.38	1.0931	72.2	81.4 ± 1.0
	50.40	3.41	0.9823	60.3	72.7 ± 0.8
	64.50	4.36	1.3947	76.5	80.5 ± 0.9
	66.80	7.06	2.2365	88.2	79.8 ± 0.8
	92.90	6.70	2.1430	92.0	80.5 ± 0.8
	132.90	6.87	2.3246	83.0	85.1 ± 0.9
	134.70	6.53	2.2649	91.4	87.2 ± 0.9
	135.70	4.65	1.5037	80.4	81.4 ± 0.8
	202.00	6.73	1.9810	79.9	74.2 ± 0.8
CY-2	117.85	6.74	2.3317	84.7	86.9 ± 0.9
	123.30	6.66	2.2138	76.8	83.6 ± 0.9
	135.45	5.07	1.8069	70.4	89.5 ± 0.9
	163.65	4.31	1.3794	26.7	80.6 ± 0.9
	165.20	6.82	2.1660	58.5	80.0 ± 0.8
	192.10	6.23	2.0799	80.2	84.0 ± 0.9
	195.80	5.98	1.9780	80.6	83.2 ± 0.9
	196.30	6.94	2.3843	83.7	86.3 ± 0.9
	199.60	6.19	1.9437	80.9	79.1 ± 0.8
	199.80	6.12	2.0089	82.6	82.6 ± 0.9
	211.80	5.98	1.8561	65.5	78.2 ± 0.8
	212.20	6.25	1.9983	90.2	80.5 ± 0.8

Geographic Area	Sample	K, %	^{40}Ar Radiogenic, x 10^{-5} cm^3/g	^{40}Ar Radiogenic, %	Age, Ma
Mitsero Graben					
Akaki Canyon	CY-90-9C	4.17	1.5094	65.1	90.9 ± 1.0
	CY-90-10E	3.37	1.0935	68.0	81.7 ± 0.9
	CY-90-12K	4.13	1.2932	74.8	78.9 ± 1.0
	CY-90-34L	4.31	1.3037	84.3	76.2 ± 0.8
	CY-90-36L	5.29	1.5367	80.0	73.3 ± 0.8
	CY-90-40K	7.18	2.2805	88.8	80.0 ± 0.8
	CY-90-41K	7.82	2.4633	87.8	79.3 ± 0.8
	CY-90-43I	6.40	1.9372	88.4	76.3 ± 0.8
	CY-90-45G	4.23	1.1247	83.2	67.2 ± 0.7
	CY-92-1G	5.73	1.8125	75.1	79.6 ± 0.8
Ayia Marina	CY-92-35	7.11	2.0633	76.2	73.2 ± 0.8
	CY-92-36	6.37	1.6148	78.0	64.1 ± 0.7
	CY-92-37	6.78	1.7523	77.1	65.3 ± 0.7
	CY-92-38	6.08	1.6080	64.3	66.8 ± 0.8

Table 2.2 (continued)

Larnaca Graben					
Pediaeous/	CY-90-3	6.88	1.4858	75.2	54.8 ± 0.6
Kambia	CY-90-4a	7.49	2.1348	84.7	71.9 ± 0.7
	CY-90-5a	7.12	2.2650	82.6	80.1 ± 0.8
	CY-90-5b	5.67	1.7221	82.5	76.5 ± 0.8
	CY-90-6	7.13	1.9911	75.0	71.2 ± 0.7
	CY-90-7	6.81	2.1190	76.7	78.4 ± 0.8
	CY-90-8a	7.69	1.9738	91.5	64.9 ± 0.7
	CY-90-8b	7.61	2.3908	83.2	79.1 ± 0.8
	CY-90-26	3.97	1.0594	44.4	67.4 ± 0.7
	CY-90-27	6.47	1.2684	52.1	49.8 ± 0.5
	CY-90-28	5.15	1.7074	83.1	83.4 ± 0.9
	CY-90-29	6.36	1.6447	75.5	65.4 ± 0.7
	CY-90-33	8.07	1.9222	86.1	60.5 ± 0.6
	CY-92-2	7.81	1.8394	84.5	59.6 ± 0.6
Kataliondas	CY-92-48	4.17	1.3649	82.9	82.4 ± 0.9
Sha	CY-90-14	5.13	1.2511	64.1	61.5 ± 0.7
Troulli	CY-90-23	4.44	1.1859	68.5	67.5 ± 0.7

Analyses are subdivided based upon sample locations within specified graben structures. All ages are calculated using the following decay abundance constants: $\lambda(^{40}K) = 0.581 \times 10^{-10}\ yr^{-1}$; $\lambda(^{40}K_{\beta}) = 4.962 \times 10^{-10}\ yr^{-1}$; $^{40}K/K = 1.167 \times 10^{-4}$ mol/mol.

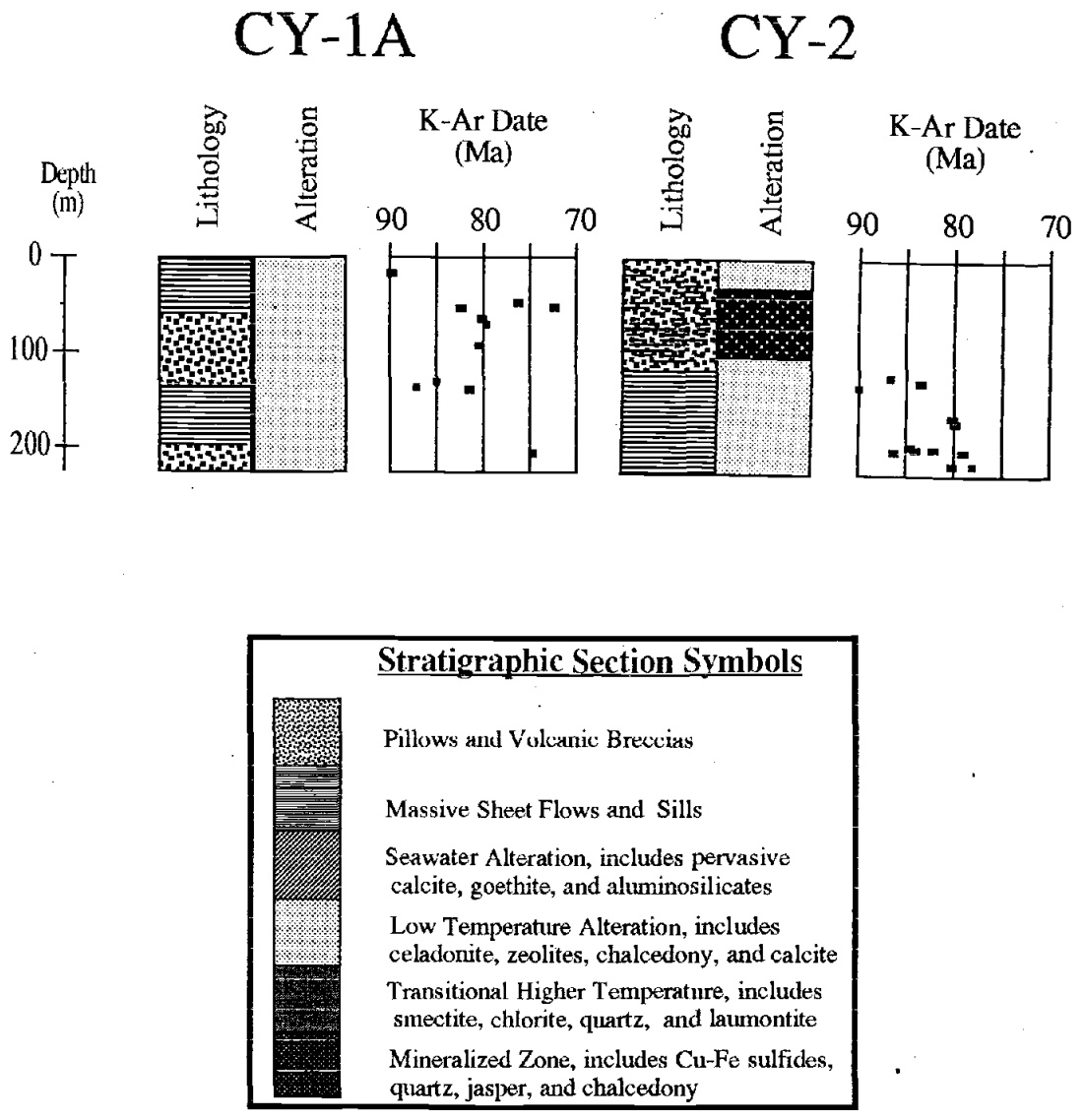

Figure 2.7 Stratigraphic sections with lithologic types, type of alteration, and relative location and K/Ar ages of celadonites determined for stratigraphic section CCSP cores CY-1A, CY-2, Akaki River canyon and Kambia/Pediaeos area. Stratigraphic sections are after Gillis and Robinson [1990].

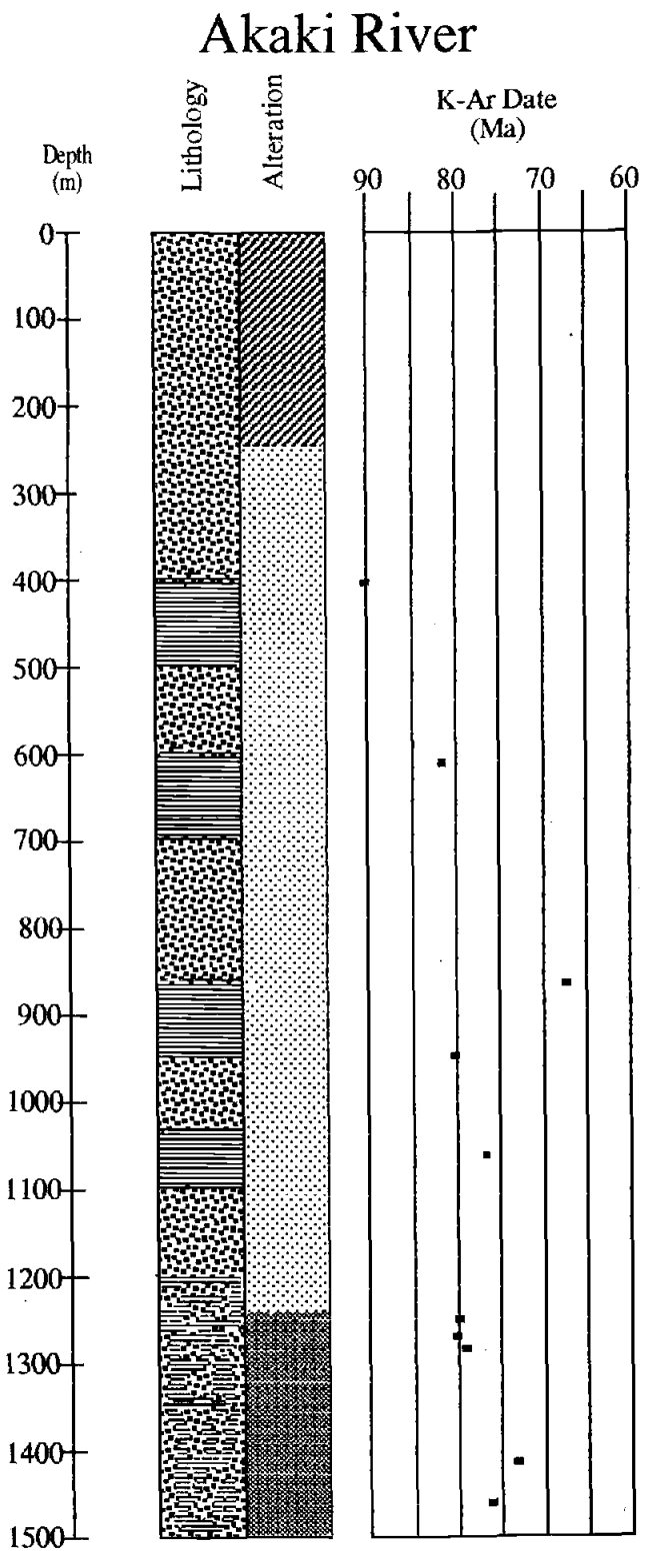

Figure 2.7 Continued

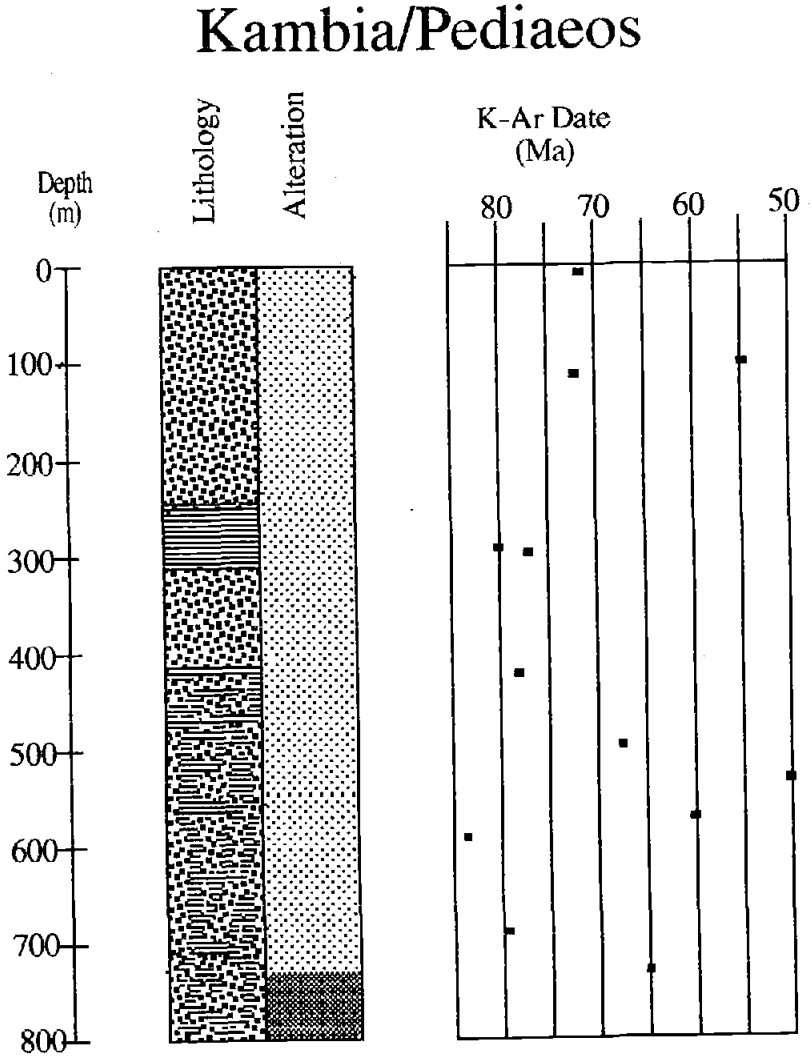

Figure 2.7 Continued

The effect of sample heterogeneity on celadonite K/Ar ages was determined by analyzing separate splits of the perimeter and core areas of CY-90-6 (large sample previously described). Analyses yielded K values of 7.04 and 7.24 for the core and perimeter, respectively. When combined with the measured Ar isotopic ratios of the splits, crystallization ages of 70.5 $\pm$ 0.7 Ma for the core and 72.0 $\pm$ 0.7 Ma for the perimeter were calculated. The weighted average for the two samples is listed in Table 2. The small variability in K values and K/Ar ages between the two splits suggests that the chemical heterogeneity noted in microprobe traverses (Figure 2.6) is integrated within macroscopic splits and has little, if any, effect on calculated ages. Further evidence for integrating microscopic heterogeneity in macroscopic celadonite splits is seen in a comparison of the average percent K_2O value (7.13 $\pm$ 1.03) from the 25 data points in the microprobe traverse (CY-2 123.30 m) with the AAS analysis (8.02% K_2O) of a whole vein split. The whole vein percent K_2O value falls within the 1σ confidence interval of the average microprobe value.

2.5.5 *Validity of Dates*

The age determinations listed in Table 2.2 are considered to be reliable measurements of celadonite crystallization/precipitation, and not an artifact of preferential Ar loss, based on several points of evidence: (1) The Staudigel et al. [1986] study revealed that K/Ar ages of four celadonites from Troodos were concordant with Rb/Sr isochron ages determined from the same samples. (2) Age determinations of two adjacent samples (CY-90-12K and CY-90-41K) with very different K concentrations yielded equivalent ages, within analytical precision. (3) Two separate age determinations of the same sample (CY-90-14) yielded equivalent ages (60.7 $\pm$ 0.8 Ma and 62.2 + 0.7 Ma) within analytical precision. (4) Peterson et al. [1986] demonstrated

that celadonitic clays with as little as 2.7% K remain Ar retentive and yield reliable crystallization ages. (In Table 2 the lowest sample percent K is 3.36.) (5) There is close agreement between the oldest celadonite ages and the Troodos crustal age [Mukasa and Ludden, 1987]. Any regional metamorphism, or other event resulting in celadonite Ar loss, should be apparent in K/Ar ages throughout the entire suite. There is no evidence for such a loss, and thus we conclude that the data in Table 2 are crystallization ages.

2.6 Discussion

2.6.1 Controls on Celadonite Crystallization and Fluid Circulation

Correlations of field relationships with geochemical and geochronological data for Troodos celadonites provide important new constraints on the history of precipitation of the primary fracture-filling minerals. On a crustal scale, the ~40-m.y. range and the lack of stratigraphic correlation of celadonite K/Ar ages suggest that fluid circulation and secondary mineral precipitation have varied on small spatial scales (meter) within the upper extrusive suite (~1 km). The preferential occurrence of celadonite within distinct volcanic lithologies, as noted in the field areas, suggests that locally heterogeneous characteristics such as intrinsic permeability, degree of faulting/fracturing, water/rock ratios, and structure, play the predominant role on millimeter to meter scale alteration and fluid circulation. These factors have been noted previously in studies of DSDP/ODP samples [e.g., Alt and Honnorez, 1984], experimental work [Seyfried et al., 1978], and thermodynamic modeling [Zierenberg and Shanks, 1983]. We see no evidence for a systematic decrease in fluid circulation with stratigraphic position with time.

Evidence supporting localized control of alteration can be found in a compilation of whole rock $^{87}Sr/^{86}Sr$ values for samples from different stratigraphic levels within the extrusive suite of Troodos [Bickle and Teagle, 1992, Figure 4]. Strontium isotopic ratios range from ~0.7037 (fresh glass) to 0.7071 (90 Ma seawater, ~0.7073), with no correlation between isotopic composition and depth of sample. Bickle and Teagle [1992] argue that the wide range of values results from nonpervasive, kinetically limited fluid-solid exchange. This is consistent with the noted channeling of fluid around pillow margins, along flow margins and joint surfaces, and in veins [Gillis and Robinson, 1990], and with the preferential crystallization of celadonite at these margins.

Further support for localized control of celadonite precipitation is a comparison between adjacent samples from different flow units. The samples CY-90-12K, CY-90-40K, and CY-90-41K, as noted previously, all yield K/Ar ages of ~79-80 Ma. However, two samples from the Akaki flow unit "L" [Schmincke et al., 1983] immediately below, CY-90-34L and CY-90-36L, yield younger ages of crystallization (~73-76 Ma). In addition, a general correlation of host rock lithology and the radiometric ages of celadonite can be made. Samples collected from zones with relatively high primary (prepalagonitization) permeabilities, such as pillow and breccia units, yield distinctly younger K/Ar ages than relatively impermeable units. For example, the Kambia/Pediaeos region, an area of complex lithologic relationships and multiple volcanic centers, contains a high percentage of breccia units [Bednarz and Schmincke, 1987]. Celadonites from outcrops in this section yield the youngest K/Ar ages on Troodos, including four samples dated at <60 Ma (Table 2). The total age range of ~83-50 Ma suggests widely variable fluid flow and alteration conditions, consistent with the crosscutting relationships of the dikes, breccias, and flow units of this region. Other examples include the four samples from the Ayia Marina region, with K/Ar ages of 64-73 Ma, which were collected from intensely altered pillow lavas. These relatively

young celadonites can be compared with samples from drill cores CY-1A and CY-2 and from the massive units of the Akaki region (Table 2.2). These units yield samples with crystallization ages >73 Ma, one Akaki point excepted.

At the outcrop scale, the reproducibility and consistency of K/Ar ages (e.g., CY-90-14 and CY-90-6) within individual celadonite samples suggest that alteration conditions remained relatively constant during the time frame required for macroscopic celadonite to form. This may be explained either by rapid celadonite crystallization and closure of the void to further fluid contact or by relatively slow dissolution/precipitation overprinting of previous vein-filling phases. Sequential precipitation of different ternary phyllosilicates in response to changing alteration conditions, proposed by Alt and Honnorez [1984], to explain observed mixing trends (e.g., Figure 2.2) is not observed on a bulk sample scale. Geochemical and geochronological data from the above samples do not indicate the systematic heterogeneities which would result from sequential precipitation. This does not imply that sequential precipitation does not occur, rather that relatively rapid crystallization of celadonite within voids isolates that zone from further changes in alteration conditions.

2.6.2 Ternary Component Mixing Relationships

The mixing trends noted in Figure 2.2 are unequivocal evidence that all Troodos celadonites contain multiple components of the phyllosilicate ternary. Microprobe traverses of the two drillcore veins (Figure 2.6) further indicate microscopic heterogeneities due to mixing of the various components. However, as previously noted, no systematic variation in structure is seen which suggests that ternary mixing is limited by phase structures and/or local alteration conditions. In order to look more closely at component mixing within each vein, specific nontronite, celadonite, and

saponite components were defined on the basis of general compositional formulae. Component mole fractions (X) for each datum were calculated from the analyzed tetrahedrally coordinated Al (8-Si = Al^{iv}), K, and Na, as follows:

$$X_{saponite} = Na$$

$$X_{nontronite} = Al^{iv} - Na = K_{nontronite}$$

$$X_{celadonite} = K - K_{nontronite}$$

where all Na was assumed to be in saponite. Comparison between the two veins of component mixing in each (Figure 2.8) indicates distinctly different degrees of mixing, which suggests different precipitation mechanisms.

It is proposed that data from sample CY-2 123.30 m, containing >70% celadonite, with minor proportions of nontronite and almost no saponite, indicate physical mixtures of celadonite and nontronite as a result of relatively rapid crystallization. Geochemically, rapid crystallization and reequilibration within a void should approximate a closed system. Precipitation of celadonite-nontronite at a rate faster than chemical diffusion within the fluid should act as a chemical buffer and result in oscillatory chemical zoning, analogous to that found in mineral phases of igneous rocks. The systematic covariation between minima and maxima of the celadonite and nontronite components in Figure 8 supports this interpretation.

Mixing within CY-2 199.60 m is apparently more complex than in 123.30 m. Larger covariation of different pairs of components, and in some cases all three components simultaneously, is indicative of the broad mixing trend between saponite and the celadonite-nontronite join (Figures 2.3 and 2.4). It is probable that this greater variation in component mixing indicates the incomplete replacement either of celadonite-nontronite by saponite [Alt and Honnorez, 1984] or of saponite by celadonite-nontronite [Donnelly et al., 1979; Stakes and Scheidegger, 1981]. The direction of the reaction is indeterminate.

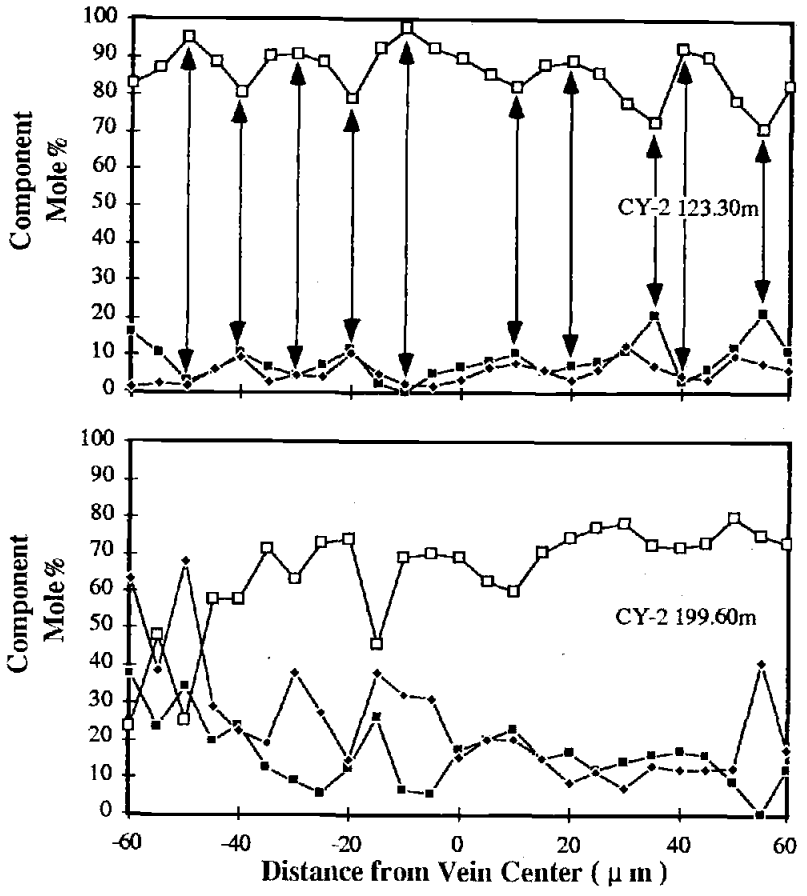

Figure 2.8 Molar percentages of phyllosilicate ternary components in each datum from the electron microprobe traverses in Figure 2.6. Open squares are pure celadonite, solid squares are nontronite, and solid diamonds are saponite. Arrows in top plot (sample CY-2 123.30 m) illustrate correlated minima and maxima of celadonite and nontronite components. Component mixing relations are more complex in bottom plot (sample CY-2 199.60 m).

Further evidence of an incomplete replacement reaction within CY-2 199.60 m is the chemical composition of vug-filling celadonites immediately adjacent to the analyzed vein (see Figure 2.4). These samples contain the highest percentage of celadonite components of the entire set. Similar vugs containing celadonite within 123.30 m, along with the other sampled intervals, did not demonstrate the extreme chemical variability seen in 199.60 m.

2.6.3 *Effects of Celadonite Composition on K/Ar Ages*

The possibility that two different precipitation mechanisms result in different chemical/structural compositions of the celadonitic material suggests that the K/Ar ages may have been affected by the chemistry (percent K) of the samples. Progressive K fixation, or loss, by replacement reactions may be revealed by systematic variations in K/Ar ages with percent K. However, the timescale of chemical replacement and minimum percent K level of Ar retention are the limiting factors in affecting K/Ar ages. A plot of K/Ar ages as a function of percent K for the samples in Table 2.2 (Figure 2.9) indicates no correlation between the calculated radiometric ages and celadonite K

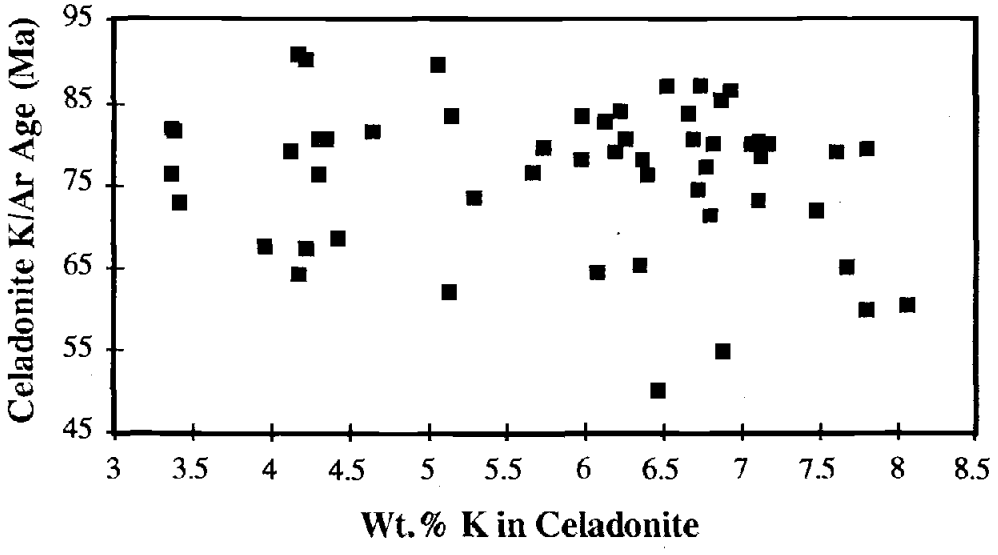

Figure 2.9 Plot of celadonite K/Ar ages versus potassium content (wt % K) of sample. No compositional dependence of radiometric ages is apparent.

2.7 Implications

2.7.1 Chemical Cycling Within the Oceans

Reactions between hydrothermal fluids and oceanic crust at various temperatures have been shown to be important for the cycling of elements within the oceans [e.g., Edmond et al., 1979; Honnorez, 1981]. In particular, low-temperature reactions which fix alkalis and Mg within the oceanic crust are important factors for calculating elemental sinks in overall chemical mass balances [Hart, 1970; Thompson, 1983; Staudigel and Hart, 1983]. In order to balance these elemental sinks, chemical fluxes must be integrated over appropriate time frames. Historically, estimates of the duration of low-temperature water/rock chemical exchange have varied tremendously, based on indirect or direct evidence. Heat flow and seismic velocity anomalies from old oceanic crust have been suggested as possible evidence for hydrothermal alteration continuing for up to 70 m.y. after crustal formation [Houtz and Ewing, 1976; Anderson et al., 1977]. However, prior to this study, radiometric dating of secondary minerals has yielded estimates for hydrothermal circulation up to ~20 m.y. after crustal accretion [e.g., Peterson et al., 1986; Staudigel et al., 1986]. Although the new 40-m.y. minimum estimate of alteration processes in Troodos greatly expands previous estimates, it is to be emphasized that low-temperature alteration is dependent upon many factors (e.g., sedimentation, spreading rates, crustal structure, and permeabilities). Variability of these factors will affect the duration of alteration processes at different locations. Given the established analogy of Troodos alteration processes to those within in situ crust, these results suggest that similar timescales for alteration may also occur within contemporary oceanic crust.

2.7.2 *Models of Low-Temperature Hydrothermal Circulation*

Historically, conceptual models of off-axis hydrothermal circulation have included thermally driven convection cells within the upper oceanic crust to explain fluid and mass transport [e.g., Fehn and Cathles, 1979, 1986]. These models, combined with the geophysical measurements above, have been used to suggest that low temperature hydrothermal circulation decreases upward with age of the oceanic crust [see Peterson et al., 1986]. However, the data and field observations of this study indicate that a general model of progressive upward sealing of the oceanic crust by secondary minerals is not appropriate for the geometry of low-temperature fluid convection. Based on these findings, we conclude that no particular geometry is favored for fluid circulation and that sealing of the upper crust by secondary minerals occurs throughout the extrusive section, dependent on permeability, thus forcing redirection of circulating fluids. In this manner, closure to hydrothermal fluids occurs in an overall homogeneous manner.

2.8 Conclusions

1. Based on K/Ar ages of celadonites from the Troodos ophiolite, a new estimate of >40 m.y. for the duration of low-temperature hydrothermal alteration within this ancient oceanic crust is proposed.

2. Apparent lack of correlation between stratigraphic position and crystallization ages of celadonite indicates that fracture sealing within the oceanic crust occurs in discrete areas, on a flow unit scale, independent of time or position.

3. Hydrothermal fluid paths and secondary mineral precipitation are determined by local conditions, such as permeability, degree of fracturing, faulting, and water/rock ratios.

4. Multiple precipitation mechanisms for the ternary phyllosilicates are likely in Troodos samples.

5. Mixing of ternary phyllosilicate components within individual samples is limited by alteration conditions and/or phase structures.

6. Celadonite is a valuable mineral for dating low-temperature alteration and yields consistent ages for a wide range of K content.

Acknowledgments. Gracious thanks are extended to C. Xenophontos and A. Panayioutou of the Cyprus Geological Survey Department for their geological and logistical support of our field program. Kathy Gillis has provided valuable insight to the overall alteration processes evidenced in Cyprus. Lew Hogan provided needed assistance in the noble gas isotope lab. Reviews by Keir Becker, Paul Robinson, and an anonymous reviewer provided constructive input which considerably enhanced the manuscript. This work was supported by Office of Naval Research grant N00014-90-J-1032 to R.A.D.

2.9 References

Allerton, S., and F.J. Vine, Spreading structure of the Troodos ophiolite Cyprus: Some paleomagnetic constraints, *Geology*, *15*, 593-597, 1987.

Alt, J.C., and J. Honnorez, Alteration of the upper oceanic crust, DSDP site 417: Mineralogy and chemistry, *Contrib. Mineral. Petrol.*, *87*, 149-169, 1984.

Alt, J.C., K. Muehlenbachs, and J. Honnorez, An oxygen profile through the upper kilometer of the oceanic crust, Deep Sea Drilling Project hole 504B, *J. Geophys. Res.*, *91*, 10,309-10,335, 1986.

Anderson, R.N., and M.A. Hobart, The relationship between heat flow, sediment thickness, and age in the eastern Pacific, *J. Geophys. Res.*, *81*, 2968-2989, 1976.

Anderson, R.N., M.G. Langseth, and J.G. Sclater, The mechanism of heat transfer through the floor of the Indian Ocean, *J. Geophys. Res.*, *82*, 3391-3409, 1977.

Andrews, A.J., Low temperature fluid alteration of oceanic layer 2 basalts, DSDP leg 37, *Can. J. Earth Sci.*, *14*, 911-926, 1977.

Andrews, A.J., Saponite and celadonite in layer 2 basalts, DSDP leg 37, *Contrib. Mineral. Petrol.*, *73*, 323-340, 1980.

Bednarz, U., and H.-U. Schmincke, Volcanology in the Pediaeos, Onouphrios, Kokkinovrysi and Mazovounos river system, in *Troodos '87: Ophiolites and Oceanic Lithosphere Symposium Field Excursion Guidebook*, pp. 260-285, Cyprus Geological Survey Department, Nicosia, 1987.

Bickle, M.J., and D.A.H. Teagle, Strontium alteration in the Troodos ophiolite: implications for fluid fluxes and geochemical transport in mid-ocean ridge hydrothermal systems, *Earth Planet. Sci Lett.*, *113*, 219-237, 1992.

Blome, C.D., and W.P. Irwin, Equivalent radiolarian ages from ophiolitic terranes of Cyprus and Oman, *Geology*, *13*, 401-404, 1985.

Bohlke, J.K., J. Honnorez, and M.B. Honnorez-Guerstein, Alteration of basalts from site 396B, DSDP: Petrographic and mineralogic studies, *Contrib. Mineral. Petrol.*, *73*, 341-364, 1980.

Bott, M.H.P., *The Interior of the Earth*, St. Martin's, New York, 1971.

Buatier, J., J. Honnorez, and G. Ehret, Fe-smectite-glauconite transition in the hydrothermal green clays from the Galapagos Spreading Center, *Clays Clay Miner.*, *37*, 532-541, 1989.

Cameron, W.E., Petrology and origin of primitive lavas from the Troodos ophiolite, Cyprus, *Contrib. Mineral. Petrol.*, *89*, 239-255, 1985.

Chapman, H.J., and E.T.C. Spooner, ^{87}Sr enrichment of ophiolitic sulphide deposits in Cyprus confirms ore formation by circulating seawater, *Earth Planet. Sci. Lett.*, *35*, 71-78, 1977.

Christensen, N.I., and M.H. Salisbury, Sea floor spreading, progressive alteration of layer 2 basalts, and associated changes in seismic velocities, *Earth Planet. Sci. Lett.*, *15*, 367-375, 1972.

Constantinou, G., Metallogenesis associated with the Troodos ophiolite, in *Ophiolites, Proceedings, International Ophiolite Symposium, Cyprus 1979*, edited by A. Panayiotou, pp. 663-673 Cyprus Geological Survey Department, Nicosia, 1980.

Corliss, J.B., et al., Submarine thermal springs on the Galapagos Rift, *Science*, *203*, 1073-1083, 1979.

Dalrymple, G.B., and M.A. Lanphere, *Potassium-Argon Dating*, W.H. Freeman, New York, 1969.

Donnelly, T.W., G. Thompson, and P.T. Robinson, Very-low-temperature hydrothermal alteration of the oceanic crust and the problem of fluxes of potassium and magnesium, in *Deep Sea Drilling Results in the Atlantic Ocean: Ocean Crust*, edited by M. Talwani, C.G. Harrison, and D.E. Hayes, AGU, pp. 369-382, Washington, D. C., 1979.

Duncan, R.A., C. Peterson, and K.F. Scheidegger, The duration of hydrothermal circulation in crust from age determinations on celadonite, *EOS Trans. AGU*, *65*, 1126, 1984.

Edmond, J.M., et al., Ridge crest hydrothermal activitiy and the balances of the major and minor elements in the oceans: The Galapagos data, *Earth Planet. Sci. Lett.*, *45*, 1-18, 1979.

Fehn, U., and L. Cathles, Hydrothermal convection at slow-spreading midocean ridges, *Tectonophysics*, *55*, 239-260, 1979.

Fehn, U., and L. Cathles, The influence of plate movement on the evolution of hydrothermal convection cells in the oceanic crust, *Tectonophysics*, *125*, 289-312, 1986.

Fisher, A.T., K. Becker, T.N. Narasimhan, M.G. Langseth, and M.J. Mottl, Passive, off-axis convection through the southern flank of the Costa Rica Rift, *J. Geophys. Res.*, *95*, 9343-9370, 1990.

Gass, I.G., and D. Masson-Smith, The geology and gravity anomalies of the Troodos Massif, Cyprus, *Philos. Trans. R. Soc. London, Ser. A, 255*, 417-467, 1963.

Gillis, K.M., Multistage alteration of the extrusive sequence, Troodos ophiolite, Cyprus, Ph.D. thesis, Dalhousie Univ., Halifax, Nova Scotia, 1987.

Gillis, K.M., and P.T. Robinson, Distribution of alteration zones in the upper oceanic crust, *Geology*, *16*, 262-266, 1988.

Gillis, K.M., and P.T. Robinson, Patterns and processes of alteration in the lavas and dykes of the Troodos ophiolite, Cyprus, *J. Geophys. Res.*, *95*, 21,523-21,548, 1990.

Hart, R.A., Chemical exchange between sea water and deep ocean basalts, *Earth Planet. Sci. Lett.*, *9*, 269-279, 1970.

Honnorez, J., The aging of the oceanic crust at low-temperatures, in *The Sea*, vol.7, *The Oceanic Lithosphere*, edited by E. Emiliani, pp. 525-588, Wiley-Interscience, New York, 1981.

Horbie, Y., K.-R. Kim, and H. Craig, Hydrothermal methane plumes in the Marianas back-arc spreading center, *Nature, 324*, 131, 1986.

Houtz, R., and J. Ewing, Upper crustal structure as a function of plate age, *J. Geophys. Res.*, *81*, 2490-2498, 1976.

Humphris, S., W.G. Melson, and R.N. Thompson, Basalt weathering on the East Pacific Rise and Galapagos Spreading Center, DSDP Leg 54, *Initial. Rep. Deep Sea Drill. Proj.*, *54*, 773-787, 1981.

Lister, C.R.B., On the thermal balance of a mid ocean ridge, *Geophys. J. R. Astro. Soc.*, *26*, 515-535, 1972.

Makris, J., et al., Seismic refraction profiles between Cyprus and Israel, *Geophys. J. R. Astron. Soc.*, *75*, 575-591, 1983.

Malahoff, A., G.M. McMurtry, J.C. Wiltshire, and H.-W. Yeh, Geology and chemistry of hydrothermal deposits from active submarine volcano Loihi, Hawaii, *Nature, 298*, 234-239, 1982.

Malpas, J.G., T. Calon, and C. Xenophontos, Plutonic rocks of the Troodos ophiolite, in *Troodos '87: Ophiolites and Oceanic Lithosphere Symposium Field Excursion Guidebook*, pp. 158-181, Cyprus Geological Survey Department, Nicosia, 1987.

McCallum, J.E., and A.H.F. Robertson, Pulsed uplift of the Troodos massif-Evidence from the Plio-Pleistocene Mesaoria basin, in *Troodos '87: Ophiolites and Oceanic Lithosphere Symposium Volume*, edited by E.M. Moores, pp. 217-229, Cyprus Geological Survey Department, Nicosia, 1990.

Mehegan, J.M., Temporal, spatial, and chemical evolution of the Troodos ophiolite lavas, Cyprus: Supra-subduction zone volcanism in the Tethys Sea, Ph.D. thesis, Dalhousie Univ., Halifax, Nova Scotia, 1988.

Miyashiro, A., The Troodos ophiolite was probably formed in an island arc, *Earth Planet. Sci. Lett.*, *19*, 218-224, 1973.

Moores, E.M., and F.J. Vine, The Troodos massif, Cyprus and other ophiolites as oceanic crust: Evaluation and implications, *Philos. Trans. R. Soc. London, Ser. A, 268*, 443-466, 1971.

Moores, E.M., P.T. Robinson, J. Malpas, and C. Xenophontos, A model for the origin of the Troodos Massif, Cyprus and other mid-east ophiolites, *Geology, 12*, 500-503, 1984.

Mukasa, S.B., and J.N. Ludden, Uranium-lead isotopic ages of plagiogranites from the Troodos ophiolite, Cyprus, and their tectonic significance, *Geology, 15*, 825-828, 1987.

Peterson, C., R. Duncan, and K.F. Scheidegger, Sequence and longevity of basalt alteration at Deep Sea Drilling Project site 597, *Initial Rep. Deep Sea Drill. Proj., 92*, 505-515, 1986.

Rautenschlein, M., et al., Isotopic and trace element composition of volcanic glasses from the Akaki Canyon, Cyprus: Implications for the origin of the Troodos ophiolite, *Earth Planet. Sci. Lett., 75*, 369-383, 1985.

Richards, H., J.R. Cann, and J. Jensenius, Mineralogical zonation and metasomatism of the alteration pipes of Cyprus sulfide deposits, *Econ. Geol., 84*, 91-115, 1989.

Robertson, A.H.F., Tectonic evolution of Cyprus, in *Troodos '87: Ophiolites and Oceanic Lithosphere Symposium Volume,* edited by E.M. Moores, pp. 235-250, Cyprus Geological Survey Department, Nicosia, 1990.

Robinson, P.T., W. Melson, O. Hearn and H.-U. Schmincke, Volcanic glass compositions of the Troodos ophiolite, Cyprus, *Geology, 11*, 400-404, 1983.

Schiffman, P., and B.M. Smith, Petrology and oxygen isotope geochemistry of a fossil seawater hydrothermal system within the Solea Graben, northern Troodos ophiolite, Cyprus, *J. Geophys. Res., 93*, 4612-4624, 1988.

Schmincke, H.-U., M. Rautenschlein, P.T. Robinson, and J.M. Mehegan, Troodos extrusive series of Cyprus: A comparison with oceanic crust, *Geology, 11*, 405-409, 1983.

Seyfried, W.E., W.C. Shanks, and W.E. Dibble, Clay mineral formation in DSDP leg 34 basalts, *Earth Planet. Sci. Lett., 41*, 265-276, 1978.

Spooner, E.T.C., H.J. Chapman, and J.D. Smewing, Strontium isotopic contamination and oxidation during ocean floor hydrothermal metamorphism of the ophiolitic rocks of the Troodos Massif, Cyprus, *Geochim. Cosmochim. Acta, 41*, 873-890, 1977.

Stakes, D.S., and K.F. Scheidegger, Temporal variations in secondary minerals from Nazca Plate basalts, in Nazca Plate: Crustal formation and Andean convergence, edited by L.D. Kulm, *Mem. Geol. Soc. Am., 154*, 109-130, 1981.

Staudigel, H., and S.R. Hart, Alteration of basaltic glass: Mechanisms and significance for the oceanic crust-seawater budget, *Geochim. Cosmochim. Acta*, *47*, 377-350, 1983.

Staudigel, H., K. Gillis, and R. Duncan, K/Ar and Rb/Sr ages of celadonites from the Troodos ophiolite, Cyprus, *Geology*, *14*, 72-75, 1986.

Thompson, G., Basalt-seawater interaction, in *Hydrothermal Processes at Seafloor Spreading Centers*, edited by P.A. Rona, K. Bostrom, and E.L. Smith, pp. 225-278, Plenum, New York, 1983.

Thy, P., C.K. Brooks, and J.N. Walsh, Tectonic and petrogenetic implications of major and rare earth element chemistry of Troodos glasses, Cyprus, *Lithos*, *18*, 165-178, 1985.

Tilton, G.R., C.A. Hopson, and J.G. Wright, Uranium-lead isotopic ages of the Samail ophiolite with applications to Tethyan ocean ridge tectonics, *J. Geophys. Res.*, *86*, 2763-2775, 1981.

Varga, R.J., and E.M. Moores, Spreading structure of the Troodos ophiolite, Cyprus, *Geology*, *13*, 846-850, 1985.

Zierenberg, R.A., and W.C. Shanks III, Mineralogy and geochemistry of epigenetic features in metalliferous sediment, Atlantis II Deep, Red Sea, *Econ. Geol.*, *78*, 57-72, 1983.

3

A MINOR AND TRACE ELEMENT SURVEY OF CELADONITES FROM THE TROODOS OPHIOLITE CYPRUS

William E. Gallahan and Robert A. Duncan

Submitted for publication in *Chemical Geology*, December, 1996.

3.1 Abstract

Halide, alkali, and rare earth element concentrations in celadonite, a secondary phyllosilicate associated with low temperature alteration, have been determined for a suite of samples from the Troodos Ophiolite using ICP-MS and electron microprobe techniques. Fluorine concentrations ranged as high as 4.8 wt% and indicated a positive correlation with concentration of a nontronite component. Chlorine concentrations ranged as high as 0.25 wt% and indicated a positive, yet less well defined, correlation with nontronitic composition. These halide concentrations suggest that the elements have markedly different geochemical behaviors in low temperature hydrothermal environments with celadonite acting as a potentially large sink for mobilized F. Alkali element (K, Rb, Cs) concentrations and ratios indicate that celadonite is similar to other smectites and fractionates these elements. The Cs/Rb ratios of the celadonites are significantly different than those produced by simple mixing between Troodos glasses and seawater. Celadonite rare earth element (REE) concentrations and profiles are similar to those of Troodos glasses, except Ce. By modeling REE concentrations produced by mixing of Troodos glasses and seawater, REE celadonite/fluid partition coefficients were calculated using the theoretical composition of hydrothermal fluids. These partition coefficients range from 10 to 500. Thus, celadonite represents a potentially large reservoir for mobilized REE during low temperature alteration of oceanic crust.

3.2 Introduction

Hydrothermal vents at mid-oceanic ridges and heat flow variations within oceanic crust from various tectonic settings provide definitive evidence that

hydrothermal circulation is an intrinsic characteristic of the world ocean basins [e.g. Wolery and Sleep, 1976; Anderson et al., 1977; Stein and Stein, 1994]. In addition, investigations of the chemical composition of vent fluids and of host oceanic crust have shown that significant chemical changes, relative to initial seawater and fresh crustal material, occur during hydrothermal circulation [e.g. Hart, 1970; Alt and Honnorez, 1984; Von Damm and Bischoff, 1987]. These compositional changes provide the basis for a paradigm; that the oceanic crust is a chemical buffer that acts as both sink and source for various components in seawater [e.g. Edmond et al., 1979; Von Damm et al., 1985; Staudigel et al., 1995]. This paradigm, coupled with measurements of fluid composition and flow rates at hydrothermal vents, may be used to balance elemental fluxes within the global ocean if all applicable parameters are understood.

Geochemical modeling in near-axis regions has proven effective in estimating the effects of high temperature water-rock reactions within oceanic crust [e.g. Bowers et al., 1988]. However, geochemical mass-balancing within lower temperature alteration environments has proven harder to constrain for several reasons. First, low temperature hydrothermal circulation is a diffuse process. Visible effluent, which is relatively easy to measure and sample at high temperature vents, is more difficult to discern in low temperature environments. Consequently, fluid compositions must be inferred from mineral compositions, isotopic studies, theoretical fluid/mineral equilibria calculations, and mixing of endmember seawater and host rock compositions.

Second, chemical fluxes must be integrated over appropriate timeframes. Attempts to assess the duration of circulation of low temperature hydrothermal fluids have taken several approaches. These have included correlating geophysical characteristics of oceanic crust (heat flow and seismic velocities) with age [e.g. Houtz and Ewing, 1976; Anderson and Hobart, 1976], studying chemical variations in overlying sediment pore waters [e.g. Mottl and Wheat, 1992], and radiometric dating of

secondary hydrothermal alteration minerals [Hart and Staudigel, 1979; Richardson et al., 1980; Staudigel et al., 1986; Staudigel and Gillis, 1991; Gallahan and Duncan, 1994; Booij et al., 1995]. While each of these methods have provided valuable information at specific locations, the data have been of limited value in constraining a mean timescale for the world ocean. Currently, estimates from various geographic sites range from ~6 m.y. (East Pacific) [Fisher et al., 1994] to ~70 m.y. (Atlantic) [Anderson and Skilbeck, 1981]. The variability in circulation timescales results from many factors such as sedimentation, spreading rates, crustal structure, and permeabilities.

Third, alteration zones within oceanic crust are often superimposed [e.g. Alt and Honnorez, 1984; Gillis and Robinson, 1990] resulting in reactions between low temperature hydrothermal fluids and previously altered material. These reactions are often recorded in cross-cutting relationships of secondary vein minerals. Yet, stratigraphic boundaries between terminal reaction zones in oceanic crust are usually sharp and record distinct conditions in which the fluid-rock chemical exchange has occured.

Despite the difficulties in constraining the extent and duration of water-rock reactions during low temperature alteration, some investigators estimate that lithospheric heat loss and associated chemical reactions within ridge flank environments may account for over 75% of the total chemical and heat budgets of the ocean crust [Morton and Sleep, 1985; Mottl and Wheat, 1992; Stein and Stein, 1994]. Such estimates underscore the significance for further study of geochemical reactions during low temperature alteration within oceanic crust.

In an effort to enhance the known data regarding low temperature geochemical reactions between seawater and oceanic crust, we have focused our analytical efforts on low temperature secondary phyllosilicates (hereafter referred to collectively as celadonite) from various locations within the Troodos ophiolite, Cyprus. The relatively

pristine nature of the massif, with no emplacement-related metamorphic overprint, has preserved secondary alteration zones which are representative of the original submarine environment. In addition, the extensive study of low temperature alteration by Gillis [1987] demonstrated that these subaerially exposed zones correlated well with those mapped in DSDP/ODP cores [Alt et al., 1985].

Within the Troodos massif, celadonite is the most abundant and common product of the palagonitization of igneous glass. It combines with calcite and chalcedony to form the terminal alteration assemblage. While celadonite is known to be more pervasive in Troodos, a likely result of the boninitic composition of the crustal material, than in tholeiitic oceanic crust, it does occur in many DSDP/ODP cores. Consequently, precipitation of celadonite may exert significant control on the concentration of certain elements within altered rocks. In this study, concentrations of rare earth, alkali, and halide (F and Cl) elements, along with major element concentrations, within celadonites from Troodos were determined in order to assess the geochemical effects of celadonite precipitation on these elements during low temperature alteration.

3.3 Elemental Fluxes During Low Temperature Alteration

The most common approach for studying low temperature water-rock chemical exchange is by chemical and isotopic analyses of whole rock and secondary mineral phases from *in situ* oceanic crust and ophiolites [e.g. Staudigel and Hart, 1983; Alt and Honnorez, 1984; Gillis and Robinson, 1990; Bickle and Teagle, 1992; Gillis et al., 1992]. Such studies, combined with the results from experimental work [e.g. Rosenbauer and Bischoff, 1983; Berndt et. al., 1994], have provided valuable insight to the complexity of physicochemical factors associated with "aging" of the oceanic crust

[e.g. Lalou et al., 1990; 1993]. One repeated result has been the relative mobility of alkali, alkaline earth, and rare earth elements (REE) during fluid-rock interaction [e.g. Klinkhammer et al., 1994]. Variations of these elemental concentrations in altered rock yield characteristic signatures of low temperature alteration in oceanic crust. These characteristic signatures, combined with isotopic analyses, provide data required for calculating cumulative elemental fluxes. Specific characteristics of low temperature alteration include water-dominated Sr isotopes (water/rock ratios $\geq$ 50), enrichment of alkali elements, and variable concentrations and patterns of rare earth elements [Hart, 1969; Hart and Staudigel, 1982; Klinkhammer et al., 1994]. In addition, these elements are the most commonly applied indicators in petrologic and geochemical modeling and; thus, their behavior is important in estimating the sinks and sources of elements. Consequently, the study of elemental abundances, partitioning behavior, and chemical reactions within low temperature alteration phases is essential for fully understanding the geochemical effects of low temperature alteration.

The chemical and isotopic characteristics associated with low temperature alteration may be attributed to the precipitation of secondary minerals. Among these minerals, phyllosilicates (micas and/or clays), zeolites, calcite, and quartz (chalcedony) form the predominant replacement phases of igneous glass and minerals, along with filling fractures and voids within crustal material. Of these phases, the phyllosilicates are typically the most abundant, depending on local alteration conditions [Alt and Honnorez, 1984; Alt et al., 1986; Gillis and Robinson, 1990].

The importance of phyllosilicate precipitation on the chemical budget of alkali elements during low temperature water-rock exchange is evident in their compositional makeup. Analyses of phyllosilicates from low temperature alteration zones within Ocean Drilling Program (ODP) cores and the Troodos ophiolite complex indicate mixing between three endmember components: celadonite $KMgFe^{3+}Si_4O_{10}(OH)_2$, nontronite

$(K_x \cdot nH_2O)Fe^{3+}{}_2(Si_{4-x}Al_x)O_{10}(OH)_2$, and saponite $(Na_x \cdot nH_2O)(Fe^{2+},Mg)_3(Si_{4-x}Al_x)O_{10}(OH)_2$ [Bohlke et al., 1980; Alt and Honnorez, 1984; Alt et al., 1986; Peterson et al., 1986; Gillis and Robinson, 1990; Gallahan and Duncan, 1994]. Clearly, precipitation of these phases should have large effects on alkali element concentrations within both the altered crustal material and the circulating fluids. Indeed, results from low temperature (70°C) experimental studies and from flux calculations have indicated that potassium and sodium are depleted in seawater and enriched in crustal material [Rosenbauer and Bischoff, 1983; Gillis, 1986].

Another chemical group that demonstrates large effects from hydrothermal alteration is the rare earth elements (REE) [Humphris, 1984; Ludden and Thompson, 1979; Staudigel and Hart, 1983; Michard, 1989; Klinkhammer et al., 1994]. Because initial seawater contains very low concentrations of REE relative to oceanic crustal material (5-6 orders of magnitude difference), the REE composition of circulating fluids may be solely attributable to rock alteration. Indeed, investigations of REE concentrations of hydrothermal fluids at high temperature vent sites have demonstrated that they are enriched by several orders of magnitude over seawater, they mimic fresh rock profiles [e.g. Michard and Albarede, 1986; Klinkhammer et al., 1994] and, they may be buffered by the plagioclase-to-epidote alteration reaction [Campbell et al., 1988]. Such investigations have provided the basis for modeling REE profiles at most high temperature vents. However, because direct sampling of low temperature fluids has proven problematic, their compositions may be based on mixing of seawater with REE released during the glass-to-palagonite reaction. Gillis et al. [1992] applied such a method to model the REE contents of low temperature fluids responsible for alteration within the Troodos ophiolite. Their results indicated that as little as 10% mobilization of crustal REE would yield a "rock dominated" solution. The 10% mobilization represents a low estimate for the fluid REE concentrations. Other estimates of REE mobilization in

low temperature systems range as high as 60% [Staudigel and Hart, 1983]. A higher percentage of mobilization would result in even higher fluid REE concentrations.

Investigations of altered oceanic crustal material have shown that variations in REE patterns are dependent upon the crystallization history of the crust, degree of alteration, and the particular secondary mineral assemblages [e.g. Humphris et al., 1978; Nystrom, 1984; Gillis et al., 1992]. Rocks altered at high temperatures typically indicate only minor disturbances in REE patterns and abundances [e.g. Menzies et al., 1977; Alt and Emmerman, 1985]. Rocks altered at low temperatures indicate greater variability in REE patterns and abundances [e.g. Frey et al., 1974; Ludden and Thompson, 1979]. Among the secondary alteration phases, the low temperature phyllosilicates and some zeolites, along with high temperature chlorite and epidote have demonstrated the greatest effects on REE patterns [Gillis et al., 1992]. However, the high temperature alteration within the proximal, near-ridge environment is relatively short-lived. Consequently, the precipitation of lower-temperature alteration phases, usually over tens of millions of years may have a much greater cumulative affect on the chemical budget/redistribution of REE during evolution of oceanic crustal material.

The cycling of halide components during hydrothermal alteration of oceanic crust has been the subject of field and experimental studies by many investigators [e.g. Miura et al., 1981; Seyfried et al., 1986; Vanko, 1986; Bowers et al., 1988; Berndt and Seyfried, 1990; Ding and Seyfried, 1992; Butterfield et al., 1994]. However, most of the work has been focused on the high temperature effects on chlorine and fluorine activities and phase partitioning. Within proximal, near-ridge regions, chlorine and fluorine are known to undergo complex changes which affect their relative abundances in host rock and circulating fluids. These include fluid-fluid partitioning during supercritical phase separation, incorporation within hydrous mineral phases, and recycling/enrichment between the magma and chamber cracking fronts [Vanko, 1986;

Smith et al., 1994]. These changes are evident in the variable depletions and enrichments of fluorine and chlorine in hydrothermal vent fluids [Edmond et al., 1979; Von Damm et al., 1985] and the relatively high amounts of fluorine in oceanic basalt/gabbro [Aoki et al., 1981; Smith et al., 1994].

Despite the overwhelming evidence of halide mobilization during high temperature hydrothermal alteration, very little data have been compiled on halide geochemistry during low temperature alteration. This is in spite of the fact that F^- is a likely candidate for exchange with OH^- in hydrous alteration phases. Modeling of this exchange reaction during formation of hydrothermal hydrous minerals has indicated that ideal mixing occurs between F^- (radius=1.05 A) and OH^- (radius=1.00 A) [Shannon, 1976; Zhu and Sverjensky, 1991]. Empirical evidence indicating that halides, particularly fluorine, may be incorporated in low temperature secondary minerals may be found in analyses of pore fluids from sediments. In a study of pore fluids associated with the Galapagos Mounds Hydrothermal Field, Maris et al. [1984] noted that fluorine was depleted relative to seawater. In addition, Mottl and Wheat [1992] noted systematic, increasing depletions of fluorine with depth in vertical profiles of sediments from the Juan de Fuca Ridge. It is possible that hydration of oceanic crust during low temperature alteration may act to fix fluorine in secondary minerals.

3.4 Sample Descriptions

Celadonite occurs as a replacement of interstitial glass in pillows, olivine phenocrysts in lava flows, and pervasive phases within the groundmass/matrix of submarine lavas. In addition, it is the primary fracture, vein, and void-filling phase precipitated from low temperature oxidized fluids. It is commonly turquoise to dark green, massive in appearance, and microscopically acicular.

The samples in this study were collected from two sources, drill cores from the Cyprus Crustal Study Program and from surface outcrop locations within the low temperature alteration zone of the Troodos massif [Gillis and Robinson, 1990]. Drill core samples were typically 1/4 to 1/2 core sections, approximately 5 to 10 centimeters long, containing veins (millimeter-centimeter width) and occasional massive celadonite at flow boundaries. Outcrop samples ranged from veined celadonite (same scale as drill cores) to monomineralic (centimeter size) deposits within fractures and interstitial voids. Sample locations, results of petrographic analyses, and correlations between outcrop lithologies and celadonite occurences are given in Gallahan and Duncan [1994].

3.5 Analytical Methods

We employed electron microanalysis and wet chemical methods to determine elemental concentrations within celadonite. Major and halide element compositions were determined using a Cameca SX-50 electron microprobe at Oregon State University. Beam conditions were set at 30 nA current and 20 keV accelerating voltage. Major elements were counted for 10 s on peak, with F and Cl counted for 20 s. Background counts were taken on each side of the elemental peaks for 1/2 the peak counting time. A partially defocused beam (diameter = 5 mm) was used to minimize volatization of the alkalis Na and K. Data validity was determined by calculating structural formulas based upon the chemical analyses. If the formulas were stoichiometric for the celadonite-nontronite-saponite compositional space, then analyses were considered acceptable. Approximately 10% of the analysis points yielded nonstoichiometric formulas or extremely low oxide totals (<75 wt.%). These points were eliminated from the data set. In addition, the detection limits and reproducibility of halide microprobe analyses precluded any definitive interpretations at elemental concentrations below approximately

0.1 wt.%. Samples included bulk, monomineralic chips mounted in epoxy and polished thin-sections of veins cutting host rock.

The concentrations of REE, cesium and rubidium within celadonites were determined using a VG Instruments quadrupole ICP-MS at Oregon State University. Samples were crushed and sieved to 1-2 mm grain size. Chips of the samples were examined under a binocular microscope, and approximately 300 mg of each sample were hand-picked based upon homogeneity. The samples were then crushed to a powder. Stock solutions for ICP-MS analyses were prepared by bringing ~50 mg splits of each sample into solution using standard HF-HNO_3-HCl dissolution techniques [Jarvis et al., 1992]. An internal spike of 1 ppm each of Be, In, and Bi was added to the stock solutions to generate a calibration curve. Splits of stock solutions were then diluted so that concentrations of the elements of interest would approximate those of the basalt standards BCR-3, W-1, and K1919. Results of the spectral scans over each selected isotope were recast in elemental concentrations, off-line, by the PQ Vision software.

Potassium concentrations were determined by atomic absorption flame spectrophotometry at the University of Oregon. Approximately 250 mg splits were prepared (see above) for analyses. Concurrent analyses of U.S. Geological Survey standards RGM-1, AMH-1, and W-2 reproduced the K concentrations within 1%, relative, of accepted values.

3.6 Results

3.6.1 Halide Elements

The concentrations of F and Cl, along with major element concentrations, were determined at 268 points within 35 different samples of celadonite. Average concentrations were 0.35 and 0.03 wt% for F and Cl, respectively. The highest concentrations of F and Cl were ~4.8 and 0.25 wt%, respectively. Approximately 5% (14 data points) contained fluorine concentrations >1 wt%. The order of magnitude variation in the halide concentrations suggests that variations in celadonite composition and/or structure may control halide partitioning behavior. Comparisons between "high F" celadonite and "low F" celadonite indicated no direct correlations between major element components and F concentrations (Table 3.1). However, structural variations, possibly caused by interlayer mixing of the three components of celadonite [Alt and Honnorez, 1984], are known to correlate with variations in celadonite composition [Gillis and Robinson, 1990; Gallahan and Duncan, 1994]. The pure celadonite component, a dioctahedral mica, typically contains slightly less than 4 octahedrally coordinated cations per formula unit based on 22 oxygen atoms. The incorporation of more Fe^{3+}, the nontronite component, into celadonite increases the octahedrally coordinated cations to 4. Similarly, mixing between the trioctahedral component, saponite, and nontronite decreases the octahedrally coordinated cations. Comprehensive studies of the major element trends, as a function of structural components, are included in Gillis and Robinson [1990] and Gallahan and Duncan [1994]. Thus, we cast our halide concentrations as functions of octahedrally coordinated (VI) cationsbased on the 22 oxygen atom structural formula.

Table 3.1. Representative electron microprobe analyses of high fluorine and low fluorine celadonites.

Sample	F	Na_2O	MgO	Al_2O_3	SiO_2	Cl	K_2O	CaO	TiO_2	MnO	Fe_2O_3	H_2O	Total	F/Cl
High F														
135.45V #10	3.47	0.24	3.93	4.39	49.73	0.06	6.47	0.34	0.16	0.14	20.42	2.19	91.53	57.82
135.45V #10	1.61	0.23	3.93	4.22	49.63	0.06	6.45	0.37	0.13	0.15	20.53	3.06	90.38	28.79
135.45V #10	0.83	0.25	4.07	4.16	48.72	0.04	6.56	0.37	0.17	0.12	19.93	3.38	88.59	20.63
199.60V	0.94	0.18	5.43	3.56	51.26	0.02	8.46	0.14	0.02	0.09	18.73	3.47	92.28	52.11
123.30V #1	2.67	0.17	4.62	3.98	52.87	0.05	7.83	0.29	0.15	0.09	21.95	2.82	97.49	54.53
123.30V #1	1.47	0.13	4.74	3.97	53.56	0.05	7.90	0.27	0.13	0.12	21.98	3.43	97.75	31.34
123.30V #1	1.65	0.16	4.75	3.93	52.63	0.04	7.81	0.27	0.14	0.13	21.49	3.28	96.27	37.41
123.30V Trav	2.25	0.06	4.46	3.92	51.67	0.05	7.10	0.47	0.12	0.12	21.39	2.91	94.53	42.47
123.30V Trav	1.49	0.13	4.98	3.73	52.07	0.04	8.50	0.29	0.13	0.11	20.15	3.29	94.91	36.27
123.30V Trav	4.14	0.29	3.89	4.71	49.70	0.06	6.08	0.86	0.19	0.22	21.19	1.92	93.23	64.75
123.30V Trav	4.79	0.34	3.98	5.40	48.99	0.08	6.49	0.80	0.22	0.20	20.01	1.58	92.86	62.17
123.30V Trav	2.18	0.30	4.27	4.42	50.87	0.07	7.02	0.53	0.11	0.14	20.21	2.89	93.01	32.52
123.30V Trav	1.40	0.30	4.35	3.99	48.11	0.03	7.15	0.32	0.14	0.10	17.80	3.02	86.70	45.10
123.30V Trav	0.84	0.42	4.04	5.10	49.38	0.05	6.79	0.52	0.16	0.08	18.95	3.43	89.76	16.53
123.30V Trav	0.81	0.41	3.73	4.35	46.19	0.04	5.88	0.47	0.19	0.14	18.75	3.20	84.16	23.14
CY-1A 49.9m	1.34	0.05	3.45	8.45	52.26	0.09	4.99	0.24	0.66	0.00	15.24	3.29	90.06	14.89
CY-90-7	1.42	0.05	4.90	6.22	50.09	0.05	6.08	0.14	0.07	0.02	18.21	3.27	90.52	28.40
CY-90-7	1.44	0.00	5.60	5.84	53.66	0.05	6.57	0.14	0.26	0.00	18.62	3.26	95.44	28.80
Low F														
135.45V #9	0.17	0.18	4.56	4.39	51.69	0.04	7.16	0.21	0.17	0.11	20.03	3.89	92.59	3.88
199.60H Trav	0.28	0.69	7.26	5.31	51.33	0.02	5.44	0.54	0.21	0.12	17.46	3.89	92.55	12.82
199.60H Trav	0.30	1.05	7.41	5.78	51.02	0.01	4.16	0.66	0.21	0.09	17.37	3.88	91.94	49.67
199.60H Trav	0.24	0.89	7.42	5.47	51.85	0.01	4.93	0.44	0.18	0.09	17.06	3.93	92.51	48.60
199.60H Trav	0.11	0.59	7.32	4.73	51.25	0.01	6.12	0.44	0.21	0.11	17.84	3.96	92.70	10.60
119.00V #5	0.08	0.36	4.17	3.70	53.49	0.01	6.93	0.37	0.04	0.10	23.72	4.10	97.06	11.86
119.00V #6	0.09	0.32	4.13	3.31	53.48	0.02	7.08	0.34	0.02	0.07	24.22	4.08	97.16	4.38
119.00V #7	0.07	0.29	4.00	3.17	52.74	0.02	7.01	0.36	0.01	0.07	24.30	4.05	96.07	3.82

In figure 3.1, a large increase in F concentration can be seen as the number of VI cations approaches four. This suggests that the nontronite component, and its associated structure, is a dominant control on F concentrations in celadonite. A similar increase in Cl concentrations is seen in Figure 3.2. Several important things are to be noted regarding the data. First, the Cl concentrations of the "high Cl" data points are very low relative to a seawater dominated fluid in low temperature alteration environments. Second, the "high F" data points do not necessarily correspond with the "high Cl" data points. Although both halides demonstrated approximately an order of magnitude variation in concentrations, the F/Cl ratios are not constant. A general increase in the F/Cl is apparent in the "high F" samples. Finally, the Cl data indicate a wider spread and the "high Cl" concentrations appear to be "offset" to lower VI cations from the F apex at ~4 VI cations. This characteristic suggests that the substitution mechanisms for F and Cl are dissimilar.

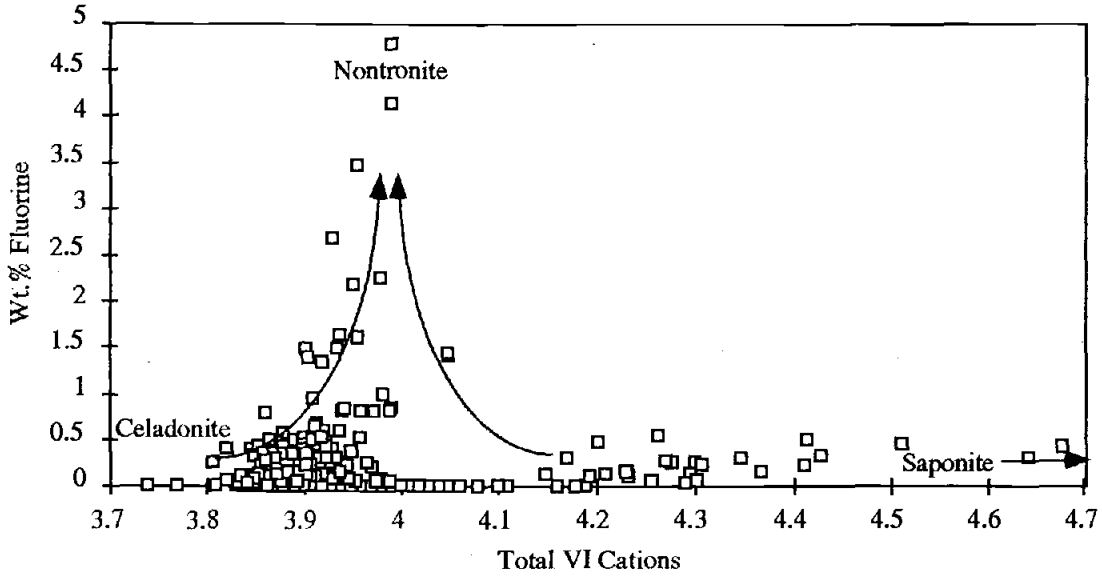

Figure 3.1 Plot of fluorine as a function of octahedrally coordinated cations in Troodos celadonites

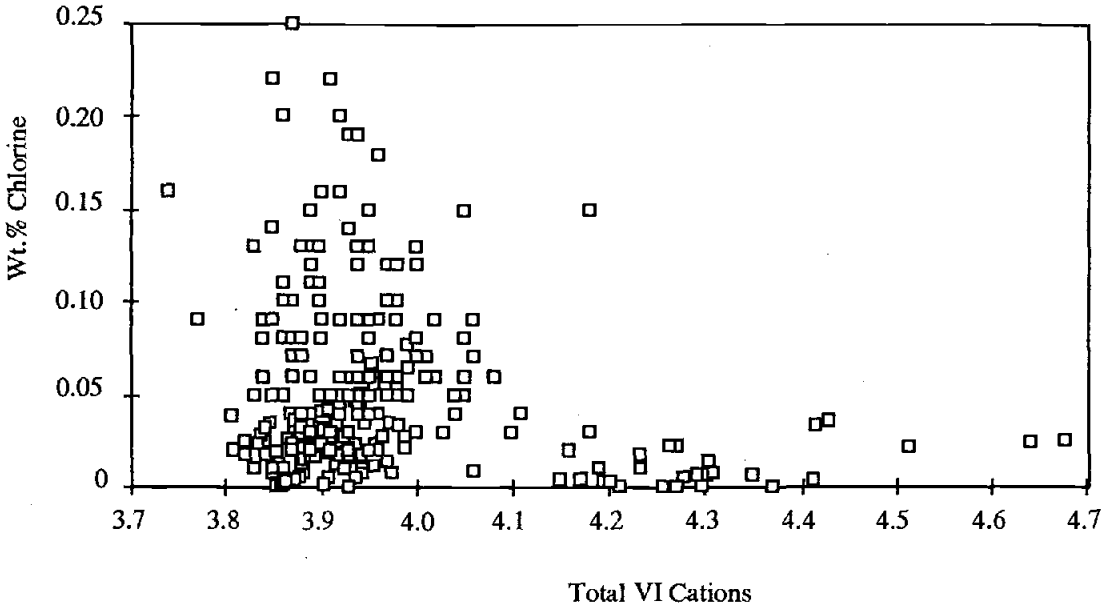

Figure 3.2 Plot of chlorine as a function of octahedrally coordinated cations in Troodos celadonites

3.6.2 Rare Earth Elements

Analytical results from 27 samples of celadonite are shown in Table 3.2. Twenty four of the samples contain relatively consistent REE abundances. These samples show a general flat-to-slightly LREE depleted profile (Fig. 3.3). The profile is similar to the LREE depleted profile defined by Troodos glass compositions (shaded region) [Rautechschlein et al., 1985]. Three samples, however, are in marked contrast to the other 24. These samples (CY-92-35, CY-92-36, CY-92-37) contain approximately one order of magnitude higher REE concentrations. In addition, the REE profiles of the 3 anomalous samples indicate large enrichments in LREE. All of the samples indicate: (1) a small Eu anomaly that may be attributable to the slightly Eu depleted nature of Troodos basalts, (2) a large Ce anomaly that likely results from different fluid/mineral partitioning behavior of Ce in the 4+ oxidation state in seawater, and (3) relatively large scatter at the heavy rare earth (HREE) end of the profiles.

Table 3.2. Rare earth and alkali element concentrations (ppm) of selected celadonites.

Sample	La	Ce	Pr	Nd	Sm	Eu	Gd	Tb	Dy	Ho	Er	Tm	Yb	Lu	K (%)	Rb	Cs
CY-90-4a	0.66	0.37	0.34	1.60	0.49	0.14	0.91	0.05	0.33	0.23	0.24	0.09	0.17	0.09	7.49	258	0.83
CY-90-6	0.46	0.56	0.23	1.13	0.38	0.11	0.63	0.07	0.40	0.17	0.29	0.07	0.21	0.06	7.13	138	0.47
CY-90-8a	0.62	0.43	0.32	1.48	0.49	0.14	0.87	0.06	0.37	0.22	0.26	0.10	0.25	0.10	7.69	246	0.39
CY-90-8b	0.84	0.68	0.47	2.41	0.78	0.24	1.34	0.14	0.90	0.33	0.60	0.13	0.39	0.12	7.61	245	0.81
CY-90-9	0.80	0.60	0.40	1.88	0.60	0.18	1.07	0.09	0.55	0.28	0.39	0.12	0.37	0.11	4.17	125	0.47
CY-90-23	0.61	0.35	0.32	1.51	0.46	0.13	0.86	0.05	0.30	0.21	0.19	0.09	0.05	0.06	4.44	195	2.01
CY-90-29	0.76	0.61	0.41	1.91	0.65	0.19	1.17	0.12	0.87	0.38	0.60	0.21	1.35	0.31	6.36	161	1.00
CY-90-36	0.84	0.90	0.42	2.05	0.65	0.28	1.14	0.10	0.74	0.32	0.60	0.17	0.89	0.20	5.29	196	0.59
CY-90-45	1.47	1.37	0.63	3.13	0.95	0.40	1.56	0.17	1.04	0.39	0.67	0.16	0.53	0.13	4.23	115	0.39
CY-92-35	23.2	10.8	6.51	28.5	7.14	1.66	8.11	1.32	8.01	1.72	4.87	0.74	4.00	0.65	7.11	238	5.36
CY-92-36	23.5	10.3	6.38	28.3	6.96	1.67	8.54	1.41	8.93	1.91	5.74	0.78	4.81	0.71	6.37	200	6.72
CY-92-37	30.6	12.1	7.56	32.1	7.99	1.87	9.05	1.51	9.32	1.96	5.81	0.86	5.22	0.77	6.78	214	3.78
CY-92-38	1.05	0.97	0.47	2.24	0.77	0.23	1.34	0.17	1.21	0.41	1.00	0.23	1.36	0.29	6.08	185	0.77
CY-1A 49.90	0.86	1.02	0.41	1.95	0.69	0.31	1.12	0.18	1.44	0.47	1.52	0.29	2.18	0.42	3.38	90	0.84
CY-1A 50.40	0.80	0.89	0.39	1.91	0.67	0.22	1.15	0.16	1.14	0.41	1.06	0.22	1.26	0.24	3.41	148	0.54
CY-1A 63.10	1.16	1.29	0.60	2.82	0.94	0.30	1.56	0.17	0.98	0.41	0.65	0.16	0.48	0.15	N.A.	96	0.47
CY-1A 132.90	0.61	0.45	0.31	1.50	0.50	0.15	0.92	0.09	0.68	0.30	0.73	0.19	1.09	0.24	6.87	191	0.90
CY-1A 134.70	0.62	0.47	0.33	1.60	0.58	0.19	1.11	0.15	1.11	0.41	1.07	0.23	1.20	0.22	6.53	170	0.54
CY-1A 202.00	2.17	3.64	0.84	3.84	1.35	0.47	2.11	0.35	2.48	0.67	1.89	0.36	2.12	0.42	6.73	168	0.87
CY-2 123.30	0.76	0.50	0.39	1.79	0.58	0.17	1.08	0.10	0.65	0.33	0.67	0.21	1.38	0.32	6.66	215	0.76
CY-2 163.65	0.88	0.79	0.42	2.03	0.63	0.19	1.13	0.09	0.55	0.30	0.46	0.14	0.43	0.15	4.31	123	0.74
CY-2 192.10	0.61	0.32	0.33	1.53	0.49	0.15	0.90	0.07	0.47	0.27	0.47	0.15	0.70	0.19	6.23	175	0.96
CY-2 199.60	1.37	2.14	0.63	3.34	1.12	0.36	1.75	0.27	1.92	0.57	1.87	0.38	2.91	0.57	6.19	136	0.68
CY-2 199.80	0.80	0.82	0.42	2.03	0.70	0.21	1.16	0.12	0.74	0.32	0.60	0.16	0.77	0.17	6.12	161	0.65
CY-1A 66.80	0.64	0.35	0.33	1.57	0.50	0.16	0.94	0.08	0.55	0.27	0.48	0.14	0.58	0.17	7.06	168	0.46
CY-90-33	0.68	0.37	0.36	1.69	0.53	0.15	0.97	0.07	0.41	0.26	0.34	0.11	0.29	0.11	8.07	171	0.67
CY-90-3	1.34	2.28	0.67	3.49	1.35	0.39	2.32	0.44	3.50	1.02	3.33	0.57	3.33	0.57	6.88	120	0.27

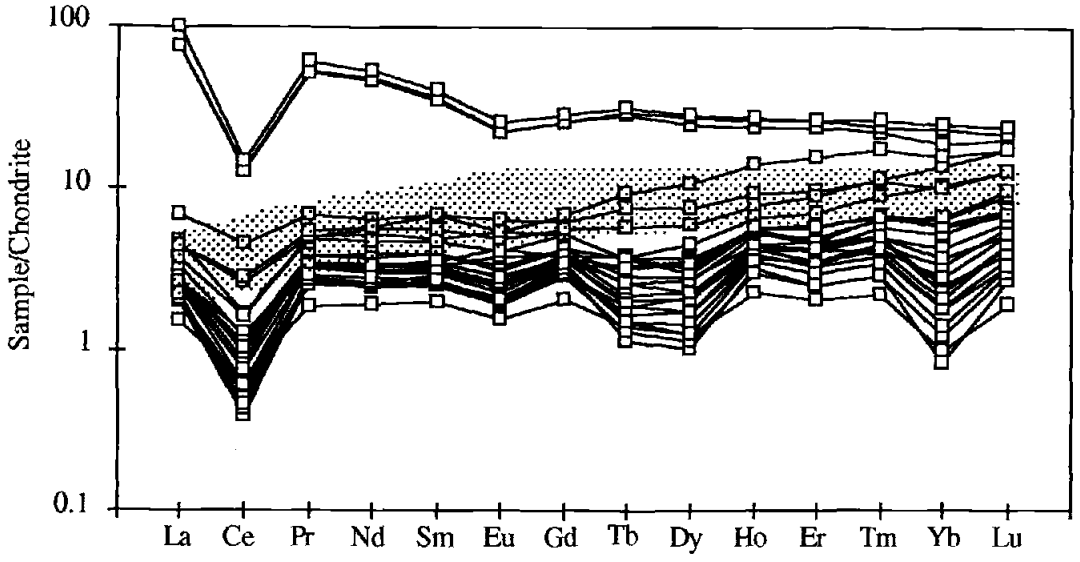

Figure 3.3 Chondrite normalized rare earth element patterns of 26 celadonites from the Troodos ophiolite, Cyprus. Range of Troodos igneous glass patterns is shown in shaded region. Chondrite values from Anders and Ebihara [1982].

3.6.3 Alkali Elements

The abundances of K, Rb, and Cs for the 27 samples above are shown in Table 3.2. These samples indicate relatively consistent K and Rb concentrations. However, the 3 samples that indicated anomalous REE abundances and profiles also contain high concentrations of Cs. Cesium is the most easily mobilized alkali element during water-rock interactions and; thus, it may be an indicator of source rock concentrations, degree of previous alteration of the source rock, or fractionation of the alkali elements during precipitation of the secondary phase [Palmer and Edmond, 1989]. The relative enrichment of Cs within the three anomalous celadonites is best illustrated by plotting Cs/Rb ratios as a function of K or Rb, the less mobile alkali elements. Figures 3.4 and

3.5 indicate that 24 of the 27 samples have Cs/Rb ratios $\leq 11 \times 10^{-3}$. These ratios are similar to those determined from vent fluids in hydrothermal fields along the East Pacific Rise, the Juan de Fuca Ridge, and the Mid-Atlantic Ridge [Palmer and Edmond, 1989]. The three anomalous samples, however, yielded significantly higher Cs/Rb ratios (up to 35×10^{-3}).

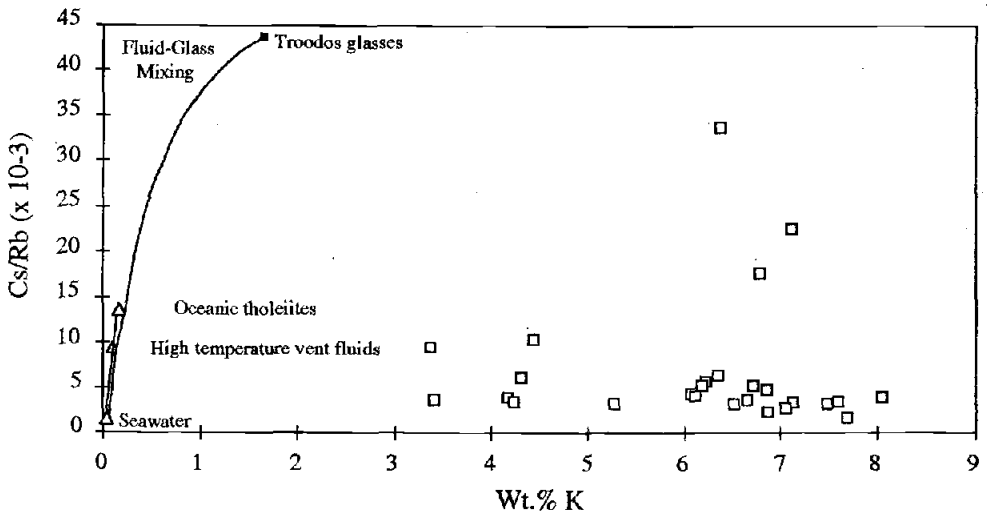

Figure 3.4 Plot of Cs/Rb as a function of potassium concentration in Troodos celadonites. Oceanic tholeiites from Hart [1969]. Hydrothermal vent fluids and seawater from Palmer and Edmond [1989].

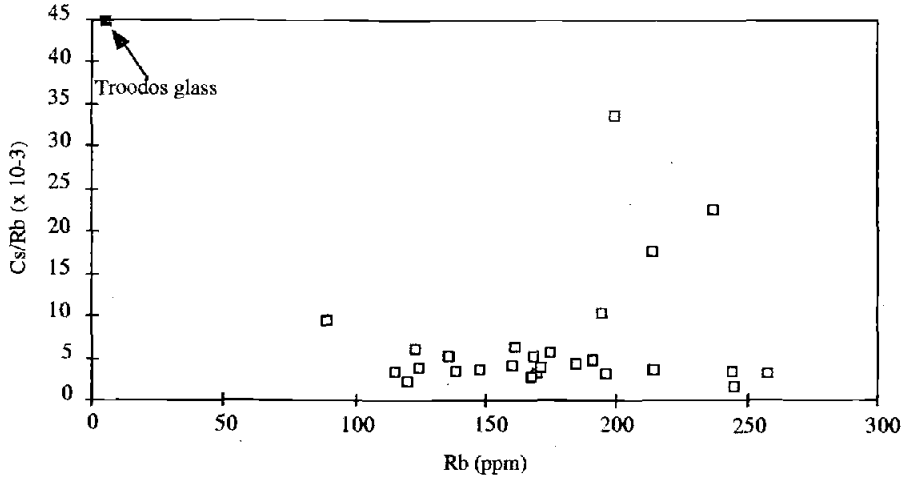

Figure 3.5 Plot of Cs/Rb as a function of rubidium concentration in Troodos celadonites.

3.7 Discussion

3.7.1 Halide Elements

The fluoride and chloride ions commonly substitute for hydroxyl in hydrous igneous and secondary mineral phases [e.g. Deer et al., 1966; Vanko, 1986]. These substitutions may provide valuable tracers for mobilization, transport, and recycling of crustal and seawater components. In particular, halides are important in controling metal transport through aqueous metal-halide complexes [e.g. Ding and Seyfried, 1992] and alteration fluid pH [e.g. Seyfried et al., 1991]. These characteristics have prompted increased interest in the concentration and fluid-mineral partitioning behavior of halides in oceanic hydrothermal systems [e.g. Vanko, 1986; Chu and Sverjensky; 1991].

Perhaps the most important result of recent studies is that F^- and Cl^- behave very differently within hydrothermal systems. They are effectively decoupled by changes in temperature and equilibrium secondary mineral phases. The data from Chu and Sverjensky [1991] predict that Cl^- preferentially partitions into high temperature hydrous mineral phases relative to the fluid phase. This is consistent with the previously noted depletions in axial hydrothermal vent fluids and enrichments of Cl in amphibole and chlorite phases. However, at lower temperatures, the same data predict that Cl^- preferentially partitions into the fluid and F^- partitions into mineral phases [W. Seyfried, 1994 pers. comm.]. This predicted behavior is of added importance when trying to balance the chemical budget of F^-. Theoretical calculations indicate that for a typical oceanic basalt/gabbro, which contains $\geq$ 100 ppm F, the formation of fluorotalc and fluorotremolite components by equilibration with vented hydrothermal fluids cannot account for the observed variable depletions of F^- [W. Seyfried, 1994 pers. comm.].

Therefore, it is possible that formation of another secondary mineral phase plays a predominant role in the fluorine geochemical budget.

Our data suggest that the precipitation of celadonite may play an important, and previously unrecognized, role in the geochemical budget of F during low temperature hydrothermal alteration. Precipitation of a mineral containing up to 5 wt.% F, within the diffuse low temperature alteration environment, will act as a major geochemical sink for fluorine. This sink may account for the noted F-depletions within the pore fluids of the Galapagos Mounds Hydrothermal Field and the Juan de Fuca Ridge sediments [Maris et al., 1984; Mottl and Wheat, 1992].

The role of celadonite in the high temperature geochemical budgets of F is more debatable. Celadonite is typically considered to be a low temperature alteration product. However, K/Ar and Rb/Sr geochronologic studies of celadonite indicate that it may precipitate within a short time after formation of the host rock [Gallahan and Duncan, 1994; Booij et al., 1995]. Such studies suggest that conditions in some locations of near axis environments are appropriate for formation of the mineral. The conditions of low temperature and high water/rock ratios are most probable in the downwelling seawater recharge limb of an axial convection cell. Within this environment, variable depletions of F (along with Mg) within circulating fluids have been ascribed to the formation of magnesium hydroxide sulfate hydrate phases [Janecky and Seyfried, 1983]. Our data, when coupled with geochronologic studies, suggest that celadonite may also play an important role.

3.7.2. Rare Earth Elements

LREE depleted samples. The 24 celadonite samples that demonstrate LREE depleted profiles are similar to the profiles of Troodos glass compositions, except that

the latter does not show a Ce anomaly. However, the absolute abundances of REE vary over a wide range for our data set. We have quantified the variation by calculating the average and standard deviation of the chondrite-normalized abundances for each element. As presented in Table 3.3, one standard deviation ranges from ~40% for the light-to-medium REE (Ce excepted) to as high as 86% for Yb. Such large variations suggest that changes in physical or chemical conditions may affect the absolute abundances of REE in celadonite. This would be consistent with the variable results of studies of low temperature altered basalts, from a variety of oceanic settings, that indicate absolute abundances of REE may be depleted, enriched, or unchanged [e.g. Ludden and Thompson, 1979; Gillis et al., 1992]. These studies have indicated that water/rock ratios play an important part in the absolute abundances and profiles of the altered rock. A corrollary to these results is that water/rock ratios also determine the abundances and profiles of REE mobilized into solution.

Within the extrusive sequence of Troodos, the $^{87}Sr/^{86}Sr$ ratios of whole rock samples range from ~0.7037 (fresh glass) to 0.7071 (90 Ma seawater ~0.7071) [Bickle and Teagle, 1992]. This wide range of values suggests that the extent of water-rock reaction is locally controlled, even at an outcrop scale. The budget for any chemical component mobilized into solution will demonstrate large variations due to local lithologic types, e.g. pillow margins vs. massive flows vs.breccias. Further evidence in support of localized controls of alteration is found in geochronologic studies of celadonites from Troodos [Gallahan and Duncan, 1994; Booij et al., 1995]. These investigations found that celadonites, many samples of which are included in this study, were precipitated over an age range of >30 m.y.

Table 3.3. Chondrite normalized REE abundances of "average celadonite" and modeled hydrothermal solutions.

Sample	La	Ce	Pr	Nd	Sm	Eu	Gd	Tb	Dy	Ho	Er	Tm	Yb	Lu
Celadonites; Mean; (N=24)	2.87	1.14	3.54	3.48	3.56	3.09	4.67	2.98	3.01	5.18	5.03	5.97	4.82	6.93
Celadonites; Standard Deviation; (1σ, N=24)	1.22	0.96	1.15	1.18	1.34	1.32	1.53	2.04	2.32	2.49	2.99	3.43	4.14	4.55
1σ as % of Mean	42.5	84.4	32.6	34.0	37.5	42.8	32.9	68.4	77.0	48.1	59.4	57.5	85.9	65.6
"Seawater"; W/R=50; 60% Mobilization	0.07	0.08	N.D.	0.10	0.11	0.12	0.13	N.D.	0.13	N.D.	0.134	N.D.	0.13	N.D.
"Seawater"; W/R=100; 10% Mobilization	0.01	0.01	N.D.	0.01	0.01	0.01	0.01	N.D.	0.01	N.D.	0.01	N.D.	0.01	N.D.
Range of Hypothetical Partition Coefficients	478-43	189-15	N.D.	435-36	396-31	309-27	424-37	N.D.	273-23	N.D.	458-38	N.D.	438-36	N.D.

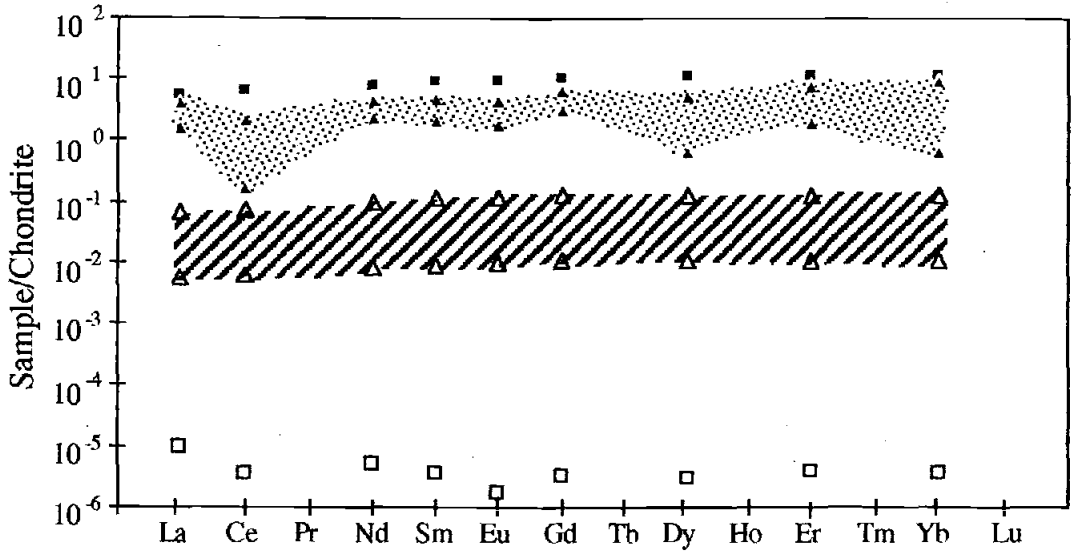

Figure 3.6 Chondrite normalized rare earth element patterns for seawater (open squares [Elderfield and Greaves, 1982]), range of modeled hydrothermal fluids (striped region), range of Troodos celadonites (shaded region), and average Troodos igneous glass [Rautenschlein et al., 1985].

In order to more fully understand the possible controls that water/rock ratios have on chemical mobilization, we have followed the example of Gillis et al. [1992] and modeled the REE concentrations of circulating fluids (Table 3.3; Fig. 3.6). In Figure 3.6, the REE contents of unaltered glass (closed squares), seawater (open squares), the "average" celadonite with 1σ boundaries (stippled region), and the range of "extreme endmember" hypothetical hydrothermal fluids (striped region), are shown. We selected the two "extreme endmember" components of altered seawater based upon minimum and maximum estimations of REE mobilization [Staudigel and Hart, 1983; Gillis et al., 1992]. The first component is formed by 60% mobilization of REE from fresh rock at a water/rock mass ratio of 50. Thus, a large amount of REE at relatively low dilution is mobilized. The other component is formed by 10% mobilization of REE at a water/rock

ratio of 100. This results in low REE concentrations. The important result of the modeling is that the REE fluid concentrations could vary over an order of magnitude. Although such a large variation in the alteration conditions is considered unlikely, it is probable that local alteration conditions may result in REE fluid concentrations that vary over factors of 2-3. If an assumption of constant mineral/fluid partitioning for REE in celadonite is made, then changes in the fluid REE abundances can account for the observed scatter in the REE concentrations in celadonite.

One additional result from the fluid modeling is a set of mineral/fluid partition coefficients (Table 3.3), calculated using REE abundances in the hypothetical fluids and measured REE in the celadonite. We applied the "average celadonite" REE abundances to our calculations and ignored the effects of standard deviation. The measured variability of celadonite REE abundances on the partition coefficients is insignificant when compared to the effects of the modeled fluids. As seen in Table 3.3, the range of hypothetical partition coefficients span an order of magnitude for each element. However, the large values of even the lowest partition coefficients modeled for each element indicate the significance of celadonites as a geochemical sink for aqueous REE. The importance of these modeled partition coefficients to understanding REE behavoir in low temperature water-rock reactions is underscored by a lack of experimental data.

LREE enriched samples. The 3 celadonite samples which yielded anomalously high REE profiles and abundances share a common characteristic in that they all came from the same outcrop. The primary lithology and hydrothermal alteration of this outcrop, near Ayia Marina (see Fig. 2.1), is not as well characterized as that in the Akaki Canyon region [e.g. Gillis and Robinson, 1990]. One observation of possible significance is that the host material, pillow basalt lithology, demonstrated unusually strong alteration. Unlike many pillow basalts in the Troodos massif, no fresh or

partially fresh glass was present. All igneous glass had been palagonitized. In addition, all primary mineralogy was altered to smectites, calcite, and quartz. These characteristics suggest that the location may have experienced anomalously high amounts of hydrothermal circulation (higher temperatures due to possible intrusive events?). Several possible explanations may be invoked to explain the 3 samples.

One possible explanation for the anomalous REE patterns involves changes in the REE profile and abundances of the circulating fluids. This may require an REE source enriched relative to the igneous compositions shown in Figure 3.3. One possible source could be a small alkalic igneous unit. Alkali basalt from oceanic settings typically display REE profiles similar to those of the anomalous celadonites [e.g. Hemond et al., 1993; White et al., 1993]. If a localized alkalic source generated hydrothermal circulation and mobilized its REE, then the fluids would be of appropriate composition to yield the distinctive celadonite signatures. By assuming constant mineral/fluid partitioning, the REE contents of the 3 anomalous celadonites could be reproduced using the partition coefficients and a modeled fluid. Unfortunately, no host or proximal crustal material was collected from the outcrop.

Another possible explanation for the anomalous REE celadonites include the presence of REE-rich trace phases within the celadonites we analyzed. Unusual REE enrichments and LREE-enriched profiles, similar to those observed in this study, have been noted in analyses of extrusive rocks from a variety of igneous provinces [e.g. Roden et al., 1984; Neal and Taylor, 1989; Kuschel and Smith, 1992; Cotten et al., 1995]. Recent studies have found that such REE patterns may result from the presence of microscopic REE-rich phases [Kushel and Smith, 1992; Cotton et al., 1995] These minerals are typically carbonate or phosphate phases such as kimuraite [Nagashima et al., 1986] and rhabdophane [Cotton et al., 1995]. Geochemical evidence of the presence of such minerals is found only in the REE profiles and abundances.

Characteristic REE profiles include LREE-enrichment, extreme (~1 order of magnitude) negative Ce anomalies, and variable Eu anomalies. We refer the reader to Kuschel and Smith [1992] and Cotton et al. [1995] for detailed analyses and profiles. The typical size of these trace phases ranges from ~20 μm diffuse patches within groundmass to 1 μm interspersed veinlets.

Based on the above studies, we reexamined our anomalous celadonite samples for any evidence of trace REE-rich phases. Bulk and chipped splits, along with epoxy mounted microprobe samples, were examined under a reflected light microscope and in the electron microprobe. No evidence was found to suggest the presence of any REE-rich phases by either optical or backscattered electron characteristics.

While the above explanations are speculative, we suggest that an alkalic source for fluid REE is a more likely possibility for the resulting celadonite REE signatures. Our reason is based upon the ubiquitous presence of alkalic seamounts in the eastern Mediterranean. These are evidenced on the island of Cyprus as the separate Mammonia igneous complex [Malpas et al., 1993]. Although the Troodos igneous rocks are considered to be well characterized, it is not impossible that alkalic intrusives have provided localized thermal sources for hydrothermal circulation and REE mobilization. In such a way, this would provide explanation for the celadonite REE signatures and the anomalously intense alteration of the outcrop.

3.7.3 Alkali Elements.

Circulation of hydrothermal fluids and precipitation of secondary minerals have profound effects on the mobilization and recycling of alkali elements within oceanic basalts [e.g. Hart, 1969; Hart and Staudigel, 1982; Bowers et al., 1988; Palmer and Edmond, 1989]. In axial environments, the trace alkalis Cs and Rb are mobilized from

basalt and released within high temperature vent fluids. Absolute abundances and relative ratios indicate that these elements are not significantly fractionated or depleted by uptake of high temperature alteration minerals [Palmer and Edmond, 1989]. The alkali element characteristics of fluids derived from water/rock mass ratios ~0.5 to 1.0 tend to fall between seawater and basalt endmembers. Figure 3.4 illustrates the mixing relationship between seawater and oceanic tholeiites, to yield the typical compositions of high temperature vent fluids.

The behavior of the alkalis during low temperature alteration of oceanic crust is less coherent than in high temperature systems. Many low temperature secondary minerals fractionate the alkalis. For example, Cs and Rb are fractionated by preferential uptake of Cs by smectities and palagonites, and by uptake of Rb by K-feldspar [Hart, 1969; Staudigel and Hart, 1983]. In addition, recycling alkalis from altered crustal material may alter the Cs/Rb in hydrothermal fluids. Palmer and Edmond [1989] found that migration of hydrothermal fluids from altered crustal material to fresh crustal material resulted in a decrease of the measured Cs/Rb in effluents. Consequently, local (outcrop scale) variations in the extent of chemical reactions that a fluid has undergone may drastically effect the Cs/Rb. Thus, modeling of the variations of Cs/Rb in low temperature alteration minerals is problematic.

In Figures 3.4 and 3.5, we have plotted the alkali compositions of 26 celadonites (%K not determined for 1 sample). Figure 3.4 illustrates the compositions relative to seawater and Troodos glasses.

Several observations can be noted from the figures. First, the Troodos glasses have much higher Cs/Rb ratios than oceanic tholeiites and should result in higher initial fluid ratios. Second, 23 of the 26 samples have Cs/Rb $\leq 11 \times 10^{-3}$, with most between 3 and 7. Finally, the 3 anomalously high samples are also the same samples which demonstrated anomalously high REE signatures.

The 23 samples with relatively low Cs/Rb ratios suggest one or two possibly in combination processes. First, celadonite does significantly fractionate Cs from Rb during precipitation, as shown by comparison with a modeled fluid for water/rock ratios of 50 (Cs/Rb = 2.3) and 100 (Cs/Rb = 1.9), commonly associated with celadonite precipitation. Second, the low temperature fluids may have been depleted of Rb, relative to Cs, by precipitation of K-feldspar prior to celadonite precipitation. K-feldspar is an abundant secondary mineral in the Troodos massif. It occurs in the seawater alteration zone (lower temperature than celadonite) and is considered to be derived from the circulating fluids [Gillis, 1986].

The explanation for the 3 samples with high Cs/Rb ratios is speculative. However, we believe that they provide further evidence of a possible nearby source of alkali basalt lavas or intrusive rocks. Palmer and Edmond [1989] demonstrated that recycling of alkalis from crust altered at low temperatures would effectively increase the Cs/Rb of circulating fluids. The introduction of a small thermal source should allow for recycling of Cs-enriched components from previously formed smectites and palagonites into the fluids. In addition, the Cs/Rb ratios may result from an enriched component mobilized from the theorized alkalic source.

3.8 Conclusions.

Hydrothermal circulation within oceanic crust results in the mobilization and cycling of many chemical components. Several of these components, including REE, alkalis, and halides, are utilized as primary indicators of both igneous and secondary processes. Consequently, information regarding their chemical activities during alteration is essential to accurate geochemical modeling. Our data indicate that celadonite, a low temperature alteration mineral common to oceanic basalts, acts as a

sink for many of these elements. Specifically, many celadonites yield fluorine concentrations > 1 wt%, and some as high as 5 wt%. These analyses suggest that the observed F depletions in low temperature pore fluids at sediment-basalt interfaces and within low temperature hydrothermal mounds [Maris et al., 1984; Mottl and Wheat, 1992] may possibly result from precipitation of celadonite within these environments. The REE abundances and patterns from celadonites indicate that they likely do not result in significant fractionation of the elements relative to one another. They tend to mimic the profile of the source and relate in abundance by simple dilution. In addition, hypothetical REE partition coefficients from analyzed samples and modeled fluids indicate that celadonites act as a large geochemical sink for REE mobilized from host rock. Celadonites tend to follow other low temperature smectites and fractionate the trace alkalis Cs and Rb. Consequently, fractionation effects of celadonite precipitation, along with possible recycling of alkalis during alteration, do not allow for accurate modeling of alkali element geochemical budgets.

Acknowledgments. Gracious thanks are extended to C. Xenophontos and A. Panayioutou of the Cyprus Geological Survey Department for their geological and logistical support of our field program. Assistance in the ICP-MS laboratory was provided by Andy Ungerer and in the electron microprobe laboratory by Roger Nielsen. G. Klinkhammer and D. Teagle provided thorough reviews and valuable insight which significantly enhanced this manuscript. This work was supported by Office of Naval Research grant N00014-90-J-1032 to R.A.D.

3.9 References

Alt, J.C. and Emmerman, 1985. Geochemistry of hydrothermally altered basalts: Deep Sea Drilling Project Hole 504B, Leg 83, in: R.N. Anderson, J. Honnorez, K. Becker, et al., eds.: Init. Rep. of the Deep Sea Drilling Project, v. 83, U.S. Gov. Print. Off., Washington, D.C., 249-262.

Alt, J.C. and Honnorez, J., 1984. Alteration of the upper oceanic crust, DSDP site 417: Mineralogy and chemistry. Contrib. Mineral. Petrol., 87: 149-169.

Alt, J.C., Honnorez, J., Laverne, C. and Emmerman, R., 1986. Hydrothermal alteration of a 1 km section through the upper oceanic crust, Deep Sea Drilling Project Hole 504B: Mineralogy, chemistry and evolution of seawater-basalt interactions. J. Geophys. Res., 91: 10,309-10,335.

Anders, E. and Ebihara, M., 1982. Solar-system abundances of the elements. Geochim. Cosmochim. Acta, 46: 2363-2380.

Anderson, R.N. and Hobart, M.A., 1976. The relationship between heat flow, sediment thickness, and age in the eastern Pacific. J. Geophys. Res., 81: 2968-2989.

Anderson, R.N. and Skilbeck, J.N., 1981. Oceanic heatflow, in: C. Emiliani, ed.: The Oceanic Lithosphere, The Sea. Wiley and Sons, New York, 489-524.

Anderson, R.N., Langseth, M.G. and Sclater, J.G., 1977. The mechanism of heat transfer through the floor of the Indian Ocean. J. Geophys. Res., 82: 3391.

Aoki, K., Ishimaka, K. and Kanisasa, S., 1981. Fluorine geochemistry of basaltic rocks from continental and oceanic regions and petrogenetic applications. Contrib. Mineral. Petrol., 76: 53-59.

Berndt, M.E. and Seyfried, W.E. Jr., 1990. Boron, bromine and other trace elements as clues to the fate of chlorine in mid-ocean ridge vent fluids. Geochim. Cosmochim. Acta, 54: 2235-2245.

Bickle, M.J. and Teagle, D.A.H., 1992. Strontium alteration in the Troodos ophiolite: implications for fluid fluxes and geochemical transport in mid-ocean ridge hydrothermal systems. Earth Planet. Sci. Lett., 113: 219-237.

Bohlke, J.K., Honnorez, J. and Honnorez-Guerstein, B.M., 1980. Alteration of basalts from Site 396B DSDP: Petrographic and Mineralogic Studies. Contrib. Mineral. Petrol., 73: 341-369.

Booij, E., Gallahan, W.E. and Staudigel, H., 1995. Ion-exchange experiments and Rb/Sr dating on celadonites from the Troodos ophiolite, Cyprus. Chem. Geol., 126: 155-167.

Bowers, T.S., Campbell, A.C., Measures, C.I., Spivack, A.J. and Edmond, J.M., 1988. Chemical controls on the composition of vent fluids at 13°-11°N and 21°N, East Pacific Rise. J. Geophys. Res., 93: 4522-4536.

Butterfield, D.A., McDuff, R.E., Mottl, M.J., Lilley, M.D., Lupton, J.E. and Massoth, G.J., 1994. Gradients in the composition of hydrothermal fluids from the Endeavor segment vent field: phase separation and brine loss. J. Geophys. Res., 99: 9561-9583.

Campbell, A.C., Palmer, M.R., Klinkhammer, G.P., Bowers, T.S., Edmond, J.M., Lawrence, J.R., Casey, J.R., Thompson, G., Humphris, S., Rona, P. and Karson, J., 1988. Chemistry of hot springs on the Mid-Atlantic Ridge. Nature, 335: 514-519.

Cotton, J., Le Dez, A., Bau, M., Caroff, M., Maury, R.C., Dulski, P., Fourcade, S., Bohn, M. and Brousse, R., 1995. Origin of anomalous rare-earth element and yttrium enrichments in subaerially exposed basalts: Evidence from French Polynesia. Chem. Geol., 119: 115-138.

Deer, W.A., Howie, R.A. and Zussman, J., 1966. An introduction to the rock-forming minerals. Longman, New York, 528 pp.

Ding, K. and Seyfried, W.E. Jr., 1992. Determination of Fe-Cl complexing in the low pressure supercritical (NaCl fluid): Fe solubility constraints on the pH of subseafloor hydrothermal fluids. Geochim. Cosmochim. Acta, 56: 3681-3692.

Edmond, J.M., et al., 1979. Ridge crest hydrothermal activity and the balances of the major and minor elements in the oceans: The Galapagos data. Earth Planet. Sci. Lett., 45: 1-18.

Fisher, K.M., Becker, K. and Narasimhan, T.N., 1994. Off-axis hydrothermal circulation: Parametric tests of a refined model of processes at DSDP/ODP site 504. J. Geophys. Res., 99: 3097-3121.

Frey, F.A., Bryan, W.B. and Thompson, G., 1974. Atlantic ocean floor: Geochemistry and petrology of basalts from Legs 2 and 3 of the Deep Sea Drilling Project. J. Geophys. Res., 79: 5507-5527.

Gallahan, W.E. and Duncan, R.A., 1994. Spatial and temporal variability in crystallization of celadonites within the Troodos ophiolite, Cyprus: Implications for low-temperature alteration of the oceanic crust. J. Geophys. Res., 99: 3147-3161.

Gillis, K.M., 1986. Multistage alteration of the extrusive sequence, Troodos ophiolite, Cyprus. Ph.D thesis, Dalhousie Univ., Halifax, Nova Scotia.

Gillis, K.M. and Robinson, P.T., 1990. Patterns and processes of alteration in the lavas and dykes of the Troodos ophiolite, Cyprus. J. Geophys. Res., 95: 21,523-21,548.

Gillis, K.M., Ludden, J.N. and Smith, A.D., 1992. Mobilization of REE during crustal aging in the Troodos ophiolite, Cyprus. Chem. Geol., 98: 71-86.

Hart, R.A., 1970. Chemical exchange between sea water and deep ocean basalts. Earth Planet. Sci. Lett., 9: 269-279.

Hart, S.R., 1969. K, Rb, Cs contents and K/Rb, K/Cs ratios of fresh and altered submarine basalts. Earth Planet. Sci. Lett., 6: 295-303.

Hart, S.R. and Staudigel, H., 1979. Ocean crust seawater interaction at sites 417 and 418, in: T. Donnely, J. Francheteau et al., eds.: Initial Reports of the Deep Sea Drilling Project, 51, 52, 53: 1169-1176.

Hart, S.R. and Staudigel, H., 1982. The controls of alkalis and uranium in seawater by oceanic crust alteration. Earth Planet. Sci. Lett., 58: 202-212.

Hemond, C., Arndt, N.T., Lichtenstein, U., Hofmann, A.W., Oskarsson, N. and Steinthorsson, S., 1993. The heterogeneous Iceland plume: Nd-Sr-O isotopes and trace element constraints. J. Geophys. Res., 98: 15,833-15,850.

Houtz, R. and Ewing, J., 1976. Upper crustal structure as a function of plate age. J. Geophys. Res., 81: 2490-2498.

Humphris, S.E., 1984. The mobility of the rare earth elements in the crust, in: Henderson, P., ed.: Rare Earth Element Geochemistry, Elsevier, Amsterdam, 317-342.

Humphris, S.E., Morrison, M.A. and Thompson, R.N., 1978. Influence of rock crystallisation history upon subsequent lanthanide mobility during hydrothermal alteration of basalts. Chem. Geol., 23: 125-137.

Jarvis, K.E., Gray, A.L. and Houk, R.S., 1992. Handbook of ICP-MS, Blackie, New York, 380 pp.

Janecky, D.R. and Seyfried, W.E. Jr., 1983. The solubility of magnesium hydroxide sulfate hydrate in seawater at elevated temperatures and pressures. Amer. J. Sci., 283: 831-860.

Klinkhammer, G.P., Elderfield, H., Edmond, J.M. and Mitra, A., 1994. Geochemical implications of rare earth element patterns in hydrothermal fluids from mid-ocean ridges. Geochim. Cosmochim. Acta, 58: 5105-5113.

Kuschel, E. and Smith, I.E.M., 1992. Rare earth mobility in young arc-type volcanic rocks from northern New Zealand. Geochim. Cosmochim. Acta, 56: 3941-3955.

Lalou, C., Reyss, J-L., Brichet, E., Arnold, M., Thompson, G., Fouquet, Y. and Rona, P.A., 1993. New age data for Mid-Atlantic Ridge hydrothermal sites: TAG and Snakepit chronology revisited. J. Geophys. Res., 98: 9705-9713.

Lalou, C., Thompson, G., Arnold, M., Brichet, E., Druffel, E. and Rona, P.A., 1990. Geochronology of TAG and Snakepit hydrothermal fields, Mid-Atlantic Ridge: witness to a long and complex hydrothermal history. Earth Planet. Sci. Lett., 97: 113-128.

Ludden, J.N. and Thompson, G., 1979. An evaluation of the behavior of the rare earth elements during weathering of seafloor basalt. Earth Planet. Sci. Lett., 43: 85-92.

Malpas, J., Calon, T. and Squires, G., 1993. The development of a late Cretaceous microplate suture zone in SW Cyprus, in: H.M. Prichard, T. Alabaster, N.B.W. Harris, C.R. Neary, eds.: Magmatic Processess and Plate Tectonics. Alden Press, Oxford, 177-197.

Maris, C.R., Bender, M.L., Froelich, P.N., Barnes, R. and Luedtke, N.A., 1984. Chemical evidence for advection of hydrothermal solutions in the sediments of the Galapagos Mounds hydrothermal field. Geochim. Cosmochim. Acta, 48: 2167-2404.

Menzies, M., Blanchard, D. and Jacobs, J., 1977. Rare earth and trace element geochemistry of metabasalts from the Point Sal Ophiolite, California. Earth Planet. Sci. Lett., 37: 203-215.

Michard, A., 1989. Rare earth element systematics in hydrothermal fluids. Geochim. Cosmochim. Acta, 53: 745-750.

Michard, A. and Albarede, R., 1986. The REE content of some hydrothermal fluids. Chem. Geol., 55: 51-60.

Miura, Y., Rucklidge, J. and Nord, G.L., 1981. The occurrence of chlorine in serpentine minerals. Contrib. Mineral. Petrol., 76: 17-23.

Morton, J.L. and Sleep, N.H., 1985. A mid-ocean ridge thermal model: Constraints on the volume of axial hydrothermal heat flux. J. Geophys. Res., 90: 11,345-11,353.

Mottl, M.J. and Wheat, G.C., 1992. Hydrothermal circulation through mid-ocean ridge flanks: Heat and chemical fluxes. V.M. Goldschmidt Conference, Reston, Va.: A72-A73.

Nagashima, K., Miyawaki, R., Takase, J., Nakai, I., Sakurai, K., Matsubara, S., Kato, A. and Iwano, S., 1986. Kimuraite, $CaY_2(CO_3)_4 \cdot 6H_2O$, a new mineral from fissures in an alkali olivine basalt from Saga Prefecture, Japan, and new data on lokkaite. Amer. Mineral., 71: 1028-1033.

Neal, C.R. and Taylor, L.A., 1989. A negative Ce anomaly in a peridotite xenolith: evidence for crustal recycling into the mantle or mantle metasomatism? Geochim. Cosmochim. Acta, 53: 1035-1040.

Nystrom, J.O., 1984. Rare earth element mobility in vesicular lava during low-grade metamorphism. Contrib. Mineral. Petrol., 88: 328-331.

Palmer, M.R. and Edmond, J.M., 1989. Cesium and rubidium in submarine hydrothermal fluids: evidence for recycling of alkali elements. Earth Planet. Sci. Lett., 95: 8-14.

Peterson, C., Duncan, R. and Scheidegger, K.F., 1986. Sequence and longevity of basalt alteration at Deep Sea Drilling Project site 597, in: Initial Rep. Deep Sea Drill. Proj., 92: 505-515.

Rautenschlein, M., Jenner, G., Hertozen, J., Hofman, A.H., Kerrich, R., Schmincke, H.-U. and White, W.M., 1985. Isotopic and trace element composition of volcanic glass from the Akaki Canyon, Cyprus: Implications for the origins of the Troodos Ophiolite. Earth Planet. Sci. Lett., 75: 369-383.

Richardson, S.H., Hart, S.R. and Staudigel, H., 1980. Vein mineral ages of old oceanic crust. J. Geophys. Res., 85: 7195-7200.

Roden, M.F., Frey, F.A. and Clague, D.A., 1984. Geochemistry of tholeiitic and alkalic lavas from the Koolau Range Oahu, Hawaii: Implications for Hawaiian volcanism. Earth Planet. Sci. Lett., 69: 141-158.

Rosenbauer, R.J. and Bischoff, J.L., 1983. Uptake and transport of heavy metals by heated seawater: A summary of the experimental results, in: Rona, P.A., Bostrom, K., Laubier, L. and Smith Jr., K.L., eds.: Hydrothermal processes at seafloor spreading centers. Plenum, New York, 177-197.

Seyfried, W.E. Jr., Berndt, M.E. and Janecky, D.R., 1986. Chloride depletions and enrichments in seafloor hydrothermal fluids: Constraints from experimental basalt alteration studies. Geochim. Cosmochim. Acta, 50: 469-475.

Seyfried, W.E. Jr., Ding, D. and Berndt, M.E., 1991. Phase equilibria constraints on the chemistry of hot spring fluids at mid-ocean ridges. Geochim. Cosmochim. Acta, 55: 3559-3580.

Shannon, R.D., 1976. Revised effective ionic radii and systematic studies of interatomic distances in halides and chalcogenides. Acta Crystal., 32: 751-767

Smith, M.C., Perfit, M.R. and Jonasson, I.R., 1994. Petrology and geochemistry of basalts from the southern Juan de Fuca Ridge: Controls on the spatial and temporal evolution of mid-ocean ridge basalt. J. Geophys. Res., 99: 4787-4812.

Staudigel, H. and Gillis, K., 1991. The timing of hydrothermal alteration in the Troodos ophiolite, in: J. Malpas, E. Moores, A. Panayiotou and C. Xenophontos, eds.: "Troodos 87" symposium volume: 665-672.

Staudigel, H., and Hart, S.R., 1983. Alteration of basaltic glass: Mechanisms and significance for the oceanic crust-seawater budget. Geochim. Cosmochim. Acta, 47: 337-350.

Staudigel, H., Davies, G.R., Hart, S.R., Marchant, K.M. and Smith, B.M., 1995. Large scale isotopic Sr, Nd and O isotopic anatomy of altered oceanic crust: DSDP/ODP sites 417/418. Earth Planet. Sci. Lett., 130: 169-185.

Staudigel, H., Gillis, K. and Duncan, R., 1986. K/Ar and Rb/Sr ages of celadonites from the Troodos ophiolite, Cyprus. Geology, 14: 72-75.

Stein, C.A. and Stein, S., 1994. Constraints on hydrothermal heatflux through the oceanic lithosphere from global heat flow. J. Geophys. Res., 99: 3081-3095.

Vanko, D.A., 1986. High-chlorine amphiboles from oceanic rocks: product of highly saline hydrothermal fluids. Amer. J. Sci., 71: 51-59.

Von Damm, K.L. and Bischoff, J.L., 1987. Chemistry of hydrothermal solutions from the southern Juan De Fuca Ridge. J. Geophys. Res., 92: 11,334-11,346.

Von Damm, K.L., Edmond, J.L., Grant, B., Measures, C.I., Walden, B. and Weiss, R.F., 1985. Chemistry of submarine hydrothermal solutions at 21°N, East Pacific Rise. Geochim. Cosmochim. Acta, 49: 2221-2237.

White, W.M., McBirney, A.R. and Duncan, R.A., 1993. Petrology and geochemistry of the Galapagos Islands: Portrait of a pathological mantle plume. J. Geophys. Res., 98: 19,533-19,563.

Wolery, T.J. and Sleep, N.H., 1976. Hydrothermal circulation and geochemical flux at mid-ocean ridges. J. Geol., 84: 249-275.

Zhu, C. and Sverjensky, D.A., 1991. Partitioning of F-Cl-OH between minerals and hydrothermal fluids. Geochim. Cosmochim. Acta, 55: 1837-1858.

4

DISCUSSION & CONCLUSIONS

4.1 Comparison with Previous Studies

4.1.1 Introduction

Alteration studies of the Troodos ophiolite have, historically, focused on geochemistry and metallogenesis within the volcanogenic massive sulfide deposits (VMS) [e.g. Wilson, 1959; Gass, 1960; Constantinou and Govett, 1972; 1973]. The significance of these deposits to the Cypriot economy dates from the Roman era to modern times. It was this significance that provided much of the impetus of early scientific research in Troodos. However, serendipitous results of these early studies yielded much broader reaching implications. Comparisons of data from the Troodos VMS deposits with those from geochemical studies of *in situ* oceanic hydrothermal sites established correlations between metallogenic zones associated with contemporary "black smoker" hydrothermal vents and VMS deposits in Troodos. These studies established some of the initial analogues between contemporary oceanic hydrothermal processes and those, as evidenced by ore deposits, that occurred within the Troodos crust. Within the past 15-20 years, an increased emphasis has been placed on studying Troodos as an analogue for a variety of oceanic crustal processes. This interest culminated in the deep drilling of the entire oceanic crustal section of Troodos by the Cyprus Crustal Study Program in 1982. Subsequent extensive investigations into the stratigraphic, structural, geophysical, and geochemical characteristics of the Troodos drill cores and field relationships yielded additional correlations with data from DSDP/ODP sites.

One of the most important results from these new studies of the Troodos ophiolite is the correlation between low temperature alteration/geochemistry of the extrusive units and that observed in drill cores from DSDP/ODP sites [Gillis and Robinson, 1990]. This correlation has added significance due to the subaerial exposure of large cross-sections of the extrusive units. Thus, a three dimensional model of low temperature alteration zones and processes could be developed and extrapolated to *in situ* oceanic crust. Within this context, the results of this thesis may be compared and contrasted with those of other investigations.

4.1.2 Location

The celadonite samples in this study were collected from volcanic units of pillow, massive, and breccia lithologies, representative of those commonly found in DSPD/ODP drill cores (See Appendix A for sample locations and descriptions). Sample locations were chosen in order to cover the entire stratigraphic alteration range of celadonite and to encompass the region characterized by Gillis and Robinson [1990]. Thus, the results of this thesis may be extrapolated to those of Gillis and Robinson [1990] and investigations of DSDP/ODP low temperature alteration.

4.1.3 K/Ar Dates

The 40 m.y. range of radiometric ages of the celadonites, relative to the age of the host material, in this study represents a 100% increase over those previously determined from Troodos or from DSDP/ODP sites. Several factors may account for this result. First, the sample population within this study represents the largest number and most comprehensive sampling of celadonites from a coherent section of ocean crust ever radiometrically dated. Prior studies have typically focused on alteration mineral

assemblages, thus sampling only two or three celadonites from a relatively small region of the host material. The results of this study indicate that sampling from small areas in a single unit may yield consistent ages. By focusing on a single phase, this study allowed for inclusion of the many variables affecting low temperature circulation and mineral precipitation discussed in chapter 2.

Second, this study included celadonite samples from a variety of lithologic units. These units yielded celadonite K/Ar ages that are fairly consistent within a common lithology, but varied between distinct lithologies. As outlined in chapter 2, units with high primary permeabilities contained celadonites with distinctly younger ages, while celadonites from more massive units yielded older ages. High permeability lithologic types typically yield very low recovery percentages in DSDP/ODP cores. Consequently, the massive lithologic types most commonly recovered in DSDP/ODP cores are the same types that yield older celadonite ages. Thus, the limited number of celadonite geochronologic age determinations from *in situ* crust may be skewed by a bias in sample recovery by rotary drilling.

Third, "typical" oceanic crust contains little celadonite as a secondary phyllosilicate phase and more Mg saponite relative to Troodos crustal material. This result is a consequence of the depleted nature of tholeiitic oceanic crust (low in alkali elements and silica) relative to the arc tholeiite to boninitic trends of Troodos material. The dissolution of tholeiitic glass yields much lower concentrations of the chemical components required to precipitate celadonite. Consequently, celadonite recovered from DSDP/ODP drill cores is commonly identified as a minor vein/vug filling phase in the millimeter to micron size range. These DSDP/ODP samples, save for a few exceptions noted in chapter 2, are of inadequate size or purity to perform radiometric age determinations. Consequently, the size constraints of working on DSDP/ODP samples has severely limited the available radiometric data base. While this has limited the

knowledge of celadonite geochronology from *in situ* oceanic crust it does not lessen the importance of celadonite as a tracer for low temperature fluid circulation. The major element compositions of celadonites from the Troodos ophiolite are consistent with those from DSDP/ODP sites. Thus, they may still be considered accurate tracers for mobilized chemical components.

4.1.4 Celadonite Ages versus Stratigraphic Position

Previous studies of celadonite precipitation as a function of stratigraphic position have been limited by the sampling difficulties outlined above. However, a single geochronologic study of three celadonites from two adjacent DSDP/ODP drill holes found that two celadonites in stratigraphically lower positions yielded K/Ar dates older than the overlying sample [Duncan et al., 1984]. Peterson et al. [1986] combined this limited data with a conceptual model of thermally driven convection cells [Fehn and Cathles, 1979; 1986] to suggest that low temperature hydrothermal circulation decreases upward by progressive sealing with secondary alteration minerals with age of the oceanic crust. However, the results of the study of the Troodos section indicate no progressive upward sealing. Indeed, this study is the first to yield definitive three dimensional relationships of celadonite radiometric ages with stratigraphic position.

The geochronologic data in this study indicate that celadonite precipitation within the Troodos ophiolite was dependent on localized, outcrop-scale alteration conditions and independent of stratigraphic position. These results are consistent with several characteristics noted from previous studies of the Troodos ophiolite. First, the intensity of low temperature alteration within the extrusive units of Troodos is extremely variable [Gillis and Robinson, 1990]. The presence of fresh volcanic glass throughout the

extrusive sequence indicates that alteration facies and mineral assemblages are not stratigraphically controlled [Robinson et al., 1983].

Second, Gillis [1987] noted an order of low temperature alterature intensity, from high to low, by the sequence of breccia units to pillow basalt rims and interstices to massive lava flow boundaries to interior lava flows. This intensity of alteration positively correlates with the primary permeability of the unit. Radiometric ages of celadonites within this study indicate a correlation between young ages with high primary permeabilities. The permeability of the flow unit appears to a primary control on low temperature fluid circulation and secondary mineral precipitation.

Third, Gillis [1987] was able to define five variables which affect the movement of solutions and concommitant precipitation of alteration minerals throughout oceanic crust, including Troodos. These variables include permeability, cooling rate of the thermal source, temperature, hydrothermal reaction rate, and sedimentation rate. Four of the variables are dependent on the others, with only sedimentation rate being independent. For instance, the cooling rate of the host crustal material is affected by the permeability and the sedimentation rate. Reaction rates are determined by temperature, which is affected by cooling rates, which is affected by permeability, and so on. Clearly, the variability of these factors on an outcrop scale may cause nonuniform, time-dependent flow of circulating fluids and resulting precipitation of secondary minerals. This heterogeneous circulation and precipitation is manifested in the relatively variable distribution of celadonite K/Ar dates throughout the extrusive sequence.

4.1.5 Celadonite Ages versus Heat Flow and Seismic Measurements

During the 1970's, geophysical measurements along mid-oceanic ridges and ridge flanks indicated anomalously low seismic velocities and heat flow [e.g.

Christensen and Salisbury, 1972; Anderson and Hobart, 1976]. In proximal regions of oceanic ridges, the anomalies could easily be explained by the presence of magma bodies and convection of high temperature fluids at the ridges. However, the occurrence of these anomalies in more distal ridge flank zones was more problematic. How could the heat flow and seismic velocities be depressed in regions up to 1000 km off axis? Such anomalies lead to the idea, based upon several considerations, that low temperature fluid circulation through the crustal material was responsible. First, advecting water is the most effective means of removing the latent heat of formation of the basement material [Anderson et al., 1977; Lister, 1982]. Two, the presence of water-filled fractures and voids would cause the prerequisite attenuation of the seismic velocities [Christensen and Salisbury, 1972]. Three, the magnitude of both geophysical anomalies decreased with increasing age of the crustal material, to the point where they disappeared together [Houtz and Ewing, 1976]. Thus, they appeared to be linked by a common process. The most likely process was low temperature fluid circulation through the crustal material. The decrease of anomalies with crustal age could be attributed to progressive filling of fluid pathways by secondary mineral precipitation. However, studies of secondary alteration phases found no minerals with formation ages that spanned the timeframe of the anomalies.

It is now generally accepted that heat flow anomalies, resulting from low temperature hydrothermal circulation, may occur over long spans of time. The timeframes range from 6 m.y. to 60 m.y. [Becker, 1985; Stein and Stein, 1994]. Such timeframes, determined by *in situ* geophysical measurements and theoretical modeling, have been, prior to this study, contrasted by the relatively short timeframes of secondary mineral precipitation determined by geochronologic studies [e.g. Duncan et al., 1984; Staudigel et al., 1986; Staudigel and Gillis, 1991]. It is obvious that there was a discrepancy that needed resolving.

The 40 m.y. range of celadonite K/Ar dates in this thesis provides the first definitive evidence that low temperature mineral phases are precipitating in oceanic crust for >20 m.y. and appears to resolve the aforementioned discrepancy between geophysical measurements and geochronologic dates.

4.1.6 Celadonite Precipitation Mechanisms

Various precipitation mechanisms for low temperature, fracture-filling phyllosilicates in oceanic crust have been proposed to explain variation in their chemical compositions. The models of Donnelly et al. [1979] and Stakes and Scheidegger [1981] suggest that preexisting high temperature phases which formed in proximal, near-ridge environments undergo dissolution and reprecipitation of lower temperature phases during crustal aging. This mechanism has been used to explain the lack of vein mineral zonation. Other models [e.g. Alt and Honnorez, 1984; Alt et al., 1986] suggest sequential precipitation of different phases in response to changing alteration conditions. This mechanism has been used to explain phase zoning in veins.

The lack of physical and chemical zoning of the celadonites in this study suggest that partial to complete reequilibration of a preexisting phase is the predominant mechanism in Troodos celadonites. This interpretation is supported by the results of microprobe traverses across two veins as noted in Chapter 2. The lack of structural heterogeneity within either vein suggests that each is relatively unzoned. Also, the repeat geochronology experiments on multiple splits of sample CY-90-14 and the experiments on the outer and inner regions of sample CY-90-6 further support the interpretation that celadonites within this study were relatively homogeneous. Such homogeneity could only be achieved either through direct precipitation of celadonite or

reequilibration of an existing phase. In addition, the data suggest that celadonite precipitation occurs on a rapid timescale under relatively restricted conditions.

4.1.7 Celadonite Geochemistry

The major element, Rb, and Cs contents of the celadonites in this study are comparable to those from other studies of Troodos and various DSDP/ODP sites [Bohlke et al., 1980; Alt and Honnorez, 1984; Alt et al., 1986; Peterson et al., 1986; Staudigel et al., 1986; Gillis, 1987; Gillis and Robinson, 1990]. These chemical similarities are important in that they allow for direct extrapolation of the results of this study to contemporary *in situ* oceanic crust. However, comparison of celadonite halide and rare earth element concentrations with other studies is difficult due to the paucity of data. Prior to this study, halide contents of low temperature secondary phyllosilicates from oceanic crust had not been reported. The previous total data base on rare earth element concentrations is limited to one celadonite sample from Troodos [Gillis, 1992]. Consequently, interstudy comparisons are difficult. However, the rare earth element concentrations and patterns within this study encompass those determined by Gillis [1992]. In addition, the interstudy similarities of celadonite major element compositions adds validity to extrapolations of the trace element chemistry in this study.

4.1.8 Chemical Fluxes, Low Temperature Alteration versus High Temperature

The significance of the K/Ar dates determined in this study are underscored by past attempts at modeling geochemical budgets within the oceans [e.g. Wolery and Sleep, 1976]. Such models have assumed fixation of mobile alkali elements and magnesium, terrigenously derived, during high temperature hydrothermal alteration of primary igneous phases in black smoker vents. Historically, the effects of low

temperature alteration had been considered minor for two reasons. First, by having no visible effluent, the location and measurement of low temperature vent fluid compositions were problematic. Consequently, there was no direct way of determining what components were being exchanged between basalt and seawater during low temperature alteration. However, several studies of bulk rock compositional changes indicated that alkalis and other elements were fixed during low temperature alteration [e.g. Hart, 1970]. Further investigations of low temperature alteration phases were required in order to constrain these effects.

Second, limited geochronologic studies had suggested that low temperature mineral precipitation, and concommitant elemental fixation, occurred over a relatively short timeframe after crustal formation. Such studies further advanced the belief that low temperature alteration played a minor role in overall elemental budgets.

In the past 15 years, greater focus has been placed on the processes, and importance, of secondary mineral precipitation during low temperature alteration of oceanic crust [e.g. Hart and Staudigel, 1982; Alt, 1984; Alt et al., 1985; Mottl and Wheat, 1992; Staudigel et al., 1995]. Methods including electrical resistivity, bulk porosity, permeability, heat flow, and stable isotope and pore fluid geochemistry have been applied to help better understand low temperature processes. In a landmark study, Mottl and Wheat [1992] combined elemental depletions within pore fluids with heat flow measurements to estimate that up to 75% of total heat loss from oceanic crust may occur by advection of low temperature fluids in ridge flank environments. This estimate agrees with the heat flow modeling of Morton and Sleep [1985].

Combining the recent results on studies of heat flow and pore fluids with the K/Ar dates in this thesis yields compelling evidence that low temperature alteration is the predominant chemical and heat exchange mechanism within oceanic crust. Indeed, recent heat flow modeling by Stein and Stein [1994] estimated a worldwide average

duration of heat flow anomalies of 60 m.y. The 40 m.y. range of celadonite formation in ocean crust found in this study supports the latest modeling.

The chemical composition of celadonites adds significance to the 40 m.y. duration of precipitation in Troodos. The fixation of Mg within celadonite is of particular importance, considering that many geochemical mass balance models assume that all Mg is fixed during high temperature alteration at mid-oceanic ridges. The precipitation of even small amounts of celadonite, including the endmember component Mg-saponite, will have profound effects on that element's geochemical budget when integrated over such long timeframes.

The rare earth element patterns of celadonite appear to mimic the whole rock patterns. However, based on the analyzed REE concentrations and theoretical calculations of fluid compositions it is clear that rare earth elements have mineral/fluid partition coefficients in the range of 10 to 500. Consequently, precipitation of even small amounts of celadonite within relatively fresh crustal material may drastically affect the REE signatures of the bulk material. In addition, the anomalously high REE contents of three samples in this study suggest that they may record fluid signatures derived from non-hostal sources.

The results of the fluorine analyses in this study are significant for several reasons. First, fluorine has long been neglected from analyses of low temperature alteration phases in oceanic crust. The geochemical budget of F in seawater has been assumed to be dominated by precipitation and dissolution of magnesium hydroxy sulfate hydrate at temperatures above 150°C (Janecky and Seyfried, 1983). The analyses in this thesis are the first known indication that low temperature phases may play a vital role in seawater fluorine budgets. The apparent contemporaneous precipitation of some celadonite immediately after crustal formation suggests that there may be some coupling between low temperature and high temperature hydrothermal systems. If so, then the

geochemical budgets of fluorine, and all other hydrothermally mobile elements, may not be attributed solely to either low temperature or high temperature processes and phases.

4.2 Summary of Conclusions

It is apparent from this study of celadonite in the Troodos ophiolite that low temperature alteration occurred in this ancient "oceanic" crust for at least 40 m.y. after crustal formation. The low temperature alteration processes were heterogeneous in the extrusive sequence and depended upon variables such as permeability, water/rock ratios, temperature, and reaction rates. There is no systematic variation of these controling factors and they are apparently independent of time and space. Integration of these heterogeneities over the entire extrusive sequence yields a progressive (time-dependent) sealing of the upper oceanic crust to hydrothermal circulation.

The chemical composition of celadonite, when combined with the estimated timescale for precipitation, underscores its importance in geochemical mass balance calculations. Adequate geochemical modeling of magnesium fluxes and uptake must include celadonite as a sink. In addition, the importance of celadonite in explaining fluorine signatures in low temperature, and possibly high temperature, hydrothermal processes should not be ignored.

Finally, celadonite acts as a large sink for rare earth elements in low temperature solutions. It does not fractionate the rare earth elements from one another, and the REE's tend to mimic the signature of the fluid. Under certain circumstances, where the fluid REE signature does not mimic the matrix signature, the contamination of relatively fresh petrologic samples by small amounts of celadonite may yield erroneous data.

BIBLIOGRAPHY

Allerton, S., and Vine, F.J., 1987. Spreading structure of the Troodos ophiolite Cyprus: Some paleomagnetic constraints. Geology, 15: 593-597.

Alt, J.C. and Emmerman, 1985. Geochemistry of hydrothermally altered basalts: Deep Sea Drilling Project Hole 504B, Leg 83, in: R.N. Anderson, J. Honnorez, K. Becker, et al., eds.: Init. Rep. of the Deep Sea Drilling Project, v. 83, U.S. Gov. Print. Off., Washington, D.C., 249-262.

Alt, J.C., and Honnorez, J., 1984. Alteration of the upper oceanic crust, DSDP site 417: Mineralogy and chemistry. Contrib. Mineral. Petrol., 87: 149-169.

Alt, J.C., Honnorez, J., Laverne, C. and Emmerman, R., 1986. Hydrothermal alteration of a 1 km section through the upper oceanic crust, Deep Sea Drilling Project Hole 504B: Mineralogy, chemistry and evolution of seawater-basalt interactions. J. Geophys. Res., 91: 10,309-10,335.

Alt, J.C., Muehlenbachs, K., and Honnorez, J., 1986. An oxygen profile through the upper kilometer of the oceanic crust, Deep Sea Drilling Project hole 504B, J. Geophys. Res., 91: 10,309-10,335.

Anders, E. and Ebihara, M., 1982. Solar-system abundances of the elements. Geochim. Cosmochim. Acta, 46: 2363-2380.

Anderson, R.N. and Hobart, M.A., 1976. The relationship between heat flow, sediment thickness, and age in the eastern Pacific, J. Geophys. Res., 81: 2968-2989.

Anderson, R.N., Langseth, M.G., and Sclater, J.G., 1977. The mechanism of heat transfer through the floor of the Indian Ocean, J. Geophys. Res., 82: 3391-3409.

Anderson, R.N. and Skilbeck, J.N., 1981. Oceanic heatflow, in: C. Emiliani, ed.: The Oceanic Lithosphere, The Sea. Wiley and Sons, New York, 489-524.

Andrews, A.J., 1977. Low temperature fluid alteration of oceanic layer 2 basalts, DSDP leg 37, Can. J. Earth Sci., 14: 911-926.

Andrews, A.J., 1980. Saponite and celadonite in layer 2 basalts, DSDP leg 37, Contrib. Mineral. Petrol., 73: 323-340.

Aoki, K., Ishimaka, K. and Kanisasa, S., 1981. Fluorine geochemistry of basaltic rocks from continental and oceanic regions and petrogenetic applications. Contrib. Mineral. Petrol., 76: 53-59.

Bednarz, U., and Schmincke, H.-U., 1987. Volcanology in the Pediaeos, Onouphrios, Kokkinovrysi and Mazovounos river system, in Troodos '87: Ophiolites and Oceanic Lithosphere Symposium Field Excursion Guidebook, pp. 260-285, Cyprus Geological Survey Department, Nicosia.

Berndt, M.E. and Seyfried, W.E. Jr., 1990. Boron, bromine and other trace elements as clues to the fate of chlorine in mid-ocean ridge vent fluids. Geochim. Cosmochim. Acta, 54: 2235-2245.

Bickle, M.J., and Teagle, D.A.H., 1992. Strontium alteration in the Troodos ophiolite: implications for fluid fluxes and geochemical transport in mid-ocean ridge hydrothermal systems, Earth Planet. Sci Lett., 113: 219-237.

Blome, C.D., and Irwin, W.P., 1985. Equivalent radiolarian ages from ophiolitic terranes of Cyprus and Oman, Geology, 13: 401-404.

Bohlke, J.K., Honnorez, J., and Honnorez-Guerstein, M.B., 1980. Alteration of basalts from site 396B, DSDP: Petrographic and mineralogic studies, Contrib. Mineral. Petrol., 73: 341-364.

Booij, E., Gallahan, W.E. and Staudigel, H., 1995. Ion-exchange experiments and Rb/Sr dating on celadonites from the Troodos ophiolite, Cyprus. Chem. Geol., 126: 155-167.

Bott, M.H.P., 1971.The Interior of the Earth, St. Martin's, New York.

Bowers, T.S., Campbell, A.C., Measures, C.I., Spivack, A.J. and Edmond, J.M., 1988. Chemical controls on the composition of vent fluids at 13°-11°N and 21°N, East Pacific Rise. J. Geophys. Res., 93: 4522-4536.

Buatier, J., Honnorez, J., and Ehret, G., 1989. Fe-smectite-glauconite transition in the hydrothermal green clays from the Galapagos Spreading Center, Clays Clay Miner., 37: 532-541.

Butterfield, D.A., McDuff, R.E., Mottl, M.J., Lilley, M.D., Lupton, J.E. and Massoth, G.J., 1994. Gradients in the composition of hydrothermal fluids from the Endeavor segment vent field: phase separation and brine loss. J. Geophys. Res., 99: 9561-9583.

Cameron, W.E., 1985. Petrology and origin of primitive lavas from the Troodos ophiolite, Cyprus, Contrib. Mineral. Petrol., 89: 239-255.

Campbell, A.C., Palmer, M.R., Klinkhammer, G.P., Bowers, T.S., Edmond, J.M., Lawrence, J.R., Casey, J.R., Thompson, G., Humphris, S., Rona, P. and Karson, J., 1988. Chemistry of hot springs on the Mid-Atlantic Ridge. Nature, 335: 514-519.

Chapman, H.J., and Spooner, E.T.C., 1977. ^{87}Sr enrichment of ophiolitic sulphide deposits in Cyprus confirms ore formation by circulating seawater, Earth Planet. Sci. Lett., 35: 71-78.

Christensen, N.I., and Salisbury, M.H., 1972. Sea floor spreading, progressive alteration of layer 2 basalts, and associated changes in seismic velocities, Earth Planet. Sci. Lett., 15: 367-375.

Constantinou, G., 1980. Metallogenesis associated with the Troodos ophiolite, in Ophiolites, Proceedings, International Ophiolite Symposium, Cyprus 1979,

edited by A. Panayiotou, pp. 663-673 Cyprus Geological Survey Department, Nicosia.

Corliss, J.B., et al., 1979. Submarine thermal springs on the Galapagos Rift, Science, 203: 1073-1083.

Cotton, J., Le Dez, A., Bau, M., Caroff, M., Maury, R.C., Dulski, P., Fourcade, S., Bohn, M. and Brousse, R., 1995. Origin of anomalous rare-earth element and yttrium enrichments in subaerially exposed basalts: Evidence from French Polynesia. Chem. Geol., 119: 115-138.

Dalrymple, G.B., and Lanphere, M.A., 1969. Potassium-Argon Dating, W.H. Freeman, New York.

Deer, W.A., Howie, R.A. and Zussman, J., 1966. An introduction to the rock-forming minerals. Longman, New York, 528 pp.

Ding, K. and Seyfried, W.E. Jr., 1992. Determination of Fe-Cl complexing in the low pressure supercritical (NaCl fluid): Fe solubility constraints on the pH of subseafloor hydrothermal fluids. Geochim. Cosmochim. Acta, 56: 3681-3692.

Donnelly, T.W., Thompson, G., and Robinson, P.T., 1979. Very-low-temperature hydrothermal alteration of the oceanic crust and the problem of fluxes of potassium and magnesium, in Deep Sea Drilling Results in the Atlantic Ocean: Ocean Crust, edited by M. Talwani, C.G. Harrison, and D.E. Hayes, AGU, pp. 369-382, Washington, D. C.

Duncan, R.A., Peterson, C., and Scheidegger, K.F., 1984. The duration of hydrothermal circulation in crust from age determinations on celadonite, Eos Trans. AGU, 65: 1126.

Edmond, J.M., et al., 1979. Ridge crest hydrothermal activitiy and the balances of the major and minor elements in the oceans: The Galapagos data, Earth Planet. Sci. Lett., 45: 1-18.

Fehn, U., and Cathles, L., 1979. Hydrothermal convection at slow-spreading midocean ridges, Tectonophysics, 55: 239-260.

Fehn, U., and Cathles, L., 1986. The influence of plate movement on the evolution of hydrothermal convection cells in the oceanic crust, Tectonophysics, 125: 289-312.

Fisher, A.T., Becker, K., Narasimhan, T.N., Langseth, M.G., and Mottl, M.J., 1990. Passive, off-axis convection through the southern flank of the Costa Rica Rift, J. Geophys. Res., 95: 9343-9370.

Fisher, K.M., Becker, K. and Narasimhan, T.N., 1994. Off-axis hydrothermal circulation: Parametric tests of a refined model of processes at DSDP/ODP site 504. J. Geophys. Res., 99: 3097-3121.

Frey, F.A., Bryan, W.B. and Thompson, G., 1974. Atlantic ocean floor: Geochemistry and petrology of basalts from Legs 2 and 3 of the Deep Sea Drilling Project. J. Geophys. Res., 79: 5507-5527.

Gallahan, W.E. and Duncan, R.A., 1994. Spatial and temporal variability in crystallization of celadonites within the Troodos ophiolite, Cyprus: Implications for low-temperature alteration of the oceanic crust. J. Geophys. Res., 99: 3147-3161.

Gass, I.G., and Masson-Smith, D., 1963. The geology and gravity anomalies of the Troodos Massif, Cyprus, Philos. Trans. R. Soc. London, Ser. A, 255: 417-467.

Gillis, K.M., 1987. Multistage alteration of the extrusive sequence, Troodos ophiolite, Cyprus, Ph.D. thesis, Dalhousie Univ., Halifax, Nova Scotia.

Gillis, K.M., and Robinson, P.T., 1988. Distribution of alteration zones in the upper oceanic crust, Geology, 16: 262-266.

Gillis, K.M., and Robinson, P.T., 1990. Patterns and processes of alteration in the lavas and dykes of the Troodos ophiolite, Cyprus, J. Geophys. Res., 95: 21,523-21,548.

Gillis, K.M., Ludden, J.N. and Smith, A.D., 1992. Mobilization of REE during crustal aging in the Troodos ophiolite, Cyprus. Chem. Geol., 98: 71-86.

Hart, R.A., 1970. Chemical exchange between sea water and deep ocean basalts, Earth Planet. Sci. Lett., 9: 269-279.

Hart, S.R., 1969. K, Rb, Cs contents and K/Rb, K/Cs ratios of fresh and altered submarine basalts. Earth Planet. Sci. Lett., 6: 295-303,

Hart, S.R. and Staudigel, H., 1979. Ocean crust seawater interaction at sites 417 and 418, in: T. Donnely, J. Francheteau et al., eds.: Initial Reports of the Deep Sea Drilling Project, 51, 52, 53: 1169-1176.

Hart, S.R. and Staudigel, H., 1982. The controls of alkalis and uranium in seawater by oceanic crust alteration. Earth Planet. Sci. Lett., 58: 202-212.

Hemond, C., Arndt, N.T., Lichtenstein, U., Hofmann, A.W., Oskarsson, N. and Steinthorsson, S., 1993. The heterogeneous Iceland plume: Nd-Sr-O isotopes and trace element constraints. J. Geophys. Res., 98: 15,833-15,850.

Honnorez, J., 1981. The aging of the oceanic crust at low-temperatures, in The Sea, vol.7, The Oceanic Lithosphere, edited by E. Emiliani, pp. 525-588, Wiley-Interscience, New York.

Horbie, Y., Kim, K.-R., and Craig, H., 1986. Hydrothermal methane plumes in the Marianas back-arc spreading center, Nature, 324: 131.

Houtz, R., and Ewing, J., 1976. Upper crustal structure as a function of plate age, J. Geophys. Res., 81: 2490-2498.

Humphris, S.E., 1984. The mobility of the rare earth elements in the crust, in: Henderson, P., ed.: Rare Earth Element Geochemistry, Elsevier, Amsterdam, 317-342.

Humphris, S., Melson, W.G., and Thompson, R.N., 1981. Basalt weathering on the East Pacific Rise and Galapagos Spreading Center, DSDP Leg 54, Initial. Rep. Deep Sea Drill. Proj., 54: 773-787.

Humphris, S.E., Morrison, M.A. and Thompson, R.N., 1978. Influence of rock crystallisation history upon subsequent lanthanide mobility during hydrothermal alteration of basalts. Chem. Geol., 23: 125-137.

Janecky, D.R. and Seyfried, W.E. Jr., 1983. The solubility of magnesium hydroxide sulfate hydrate in seawater at elevated temperatures and pressures. Amer. J. Sci., 283: 831-860.

Jarvis, K.E., Gray, A.L. and Houk, R.S., 1992. Handbook of ICP-MS, Blackie, New York, 380 pp.

Klinkhammer, G.P., Elderfield, H., Edmond, J.M. and Mitra, A., 1994. Geochemical implications of rare earth element patterns in hydrothermal fluids from mid-ocean ridges. Geochim. Cosmochim. Acta, 58: 5105-5113.

Kuschel, E. and Smith, I.E.M., 1992. Rare earth mobility in young arc-type volcanic rocks from northern New Zealand. Geochim. Cosmochim. Acta, 56: 3941-3955.

Lalou, C., Reyss, J-L., Brichet, E., Arnold, M., Thompson, G., Fouquet, Y. and Rona, P.A., 1993. New age data for Mid-Atlantic Ridge hydrothermal sites: TAG and Snakepit chronology revisited. J. Geophys. Res., 98: 9705-9713.

Lalou, C., Thompson, G., Arnold, M., Brichet, E., Druffel, E. and Rona, P.A., 1990. Geochronology of TAG and Snakepit hydrothermal fields, Mid-Atlantic Ridge: witness to a long and complex hydrothermal history. Earth Planet. Sci. Lett., 97: 113-128.

Lister, C.R.B., 1972. On the thermal balance of a mid ocean ridge, Geophys. J. R. Astro. Soc., 26: 515-535.

Ludden, J.N. and Thompson, G., 1979. An evaluation of the behavior of the rare earth elements during weathering of seafloor basalt. Earth Planet. Sci. Lett., 43: 85-92.

Makris, J., et al., 1983. Seismic refraction profiles between Cyprus and Israel, Geophys. J. R. Astron. Soc., 75: 575-591.

Malahoff, A., McMurtry, G.M., Wiltshire, J.C., and Yeh, H.-W., 1982. Geology and chemistry of hydrothermal deposits from active submarine volcano Loihi, Hawaii, Nature, 298: 234-239.

Malpas, J., Calon, T. and Squires, G., 1993. The development of a late Cretaceous microplate suture zone in SW Cyprus, in: H.M. Prichard, T. Alabaster, N.B.W. Harris, C.R. Neary, eds.: Magmatic Processess and Plate Tectonics. Alden Press, Oxford, 177-197.

Malpas, J.G., Calon, T., and Xenophontos, C., 1987. Plutonic rocks of the Troodos ophiolite, in *Troodos '87: Ophiolites and Oceanic Lithosphere Symposium Field Excursion Guidebook*, pp. 158-181, Cyprus Geological Survey Department, Nicosia.

Maris, C.R., Bender, M.L., Froelich, P.N., Barnes, R. and Luedtke, N.A., 1984. Chemical evidence for advection of hydrothermal solutions in the sediments of the Galapagos Mounds hydrothermal field. Geochim. Cosmochim. Acta, 48: 2167-2404.

McCallum, J.E., and Robertson, A.H.F., 1990. Pulsed uplift of the Troodos massif-Evidence from the Plio-Pleistocene Mesaoria basin, in Troodos '87: Ophiolites and Oceanic Lithosphere Symposium Volume, edited by E.M. Moores, pp. 217-229, Cyprus Geological Survey Department, Nicosia.

Mehegan, J.M., 1988. Temporal, spatial, and chemical evolution of the Troodos ophiolite lavas, Cyprus: Supra-subduction zone volcanism in the Tethys Sea, Ph.D. thesis, Dalhousie Univ., Halifax, Nova Scotia.

Menzies, M., Blanchard, D. and Jacobs, J., 1977. Rare earth and trace element geochemistry of metabasalts from the Point Sal Ophiolite, California. Earth Planet. Sci. Lett., 37: 203-215.

Michard, A., 1989. Rare earth element systematics in hydrothermal fluids. Geochim. Cosmochim. Acta, 53: 745-750.

Michard, A. and Albarede, R., 1986. The REE content of some hydrothermal fluids. Chem. Geol., 55: 51-60.

Miura, Y., Rucklidge, J. and Nord, G.L., 1981. The occurrence of chlorine in serpentine minerals. Contrib. Mineral. Petrol., 76: 17-23.

Miyashiro, A., 1973. The Troodos ophiolite was probably formed in an island arc, Earth Planet. Sci. Lett., 19: 218-224.

Moores, E.M., and Vine, F.J., 1971. The Troodos massif, Cyprus and other ophiolites as oceanic crust: Evaluation and implications, Philos. Trans. R. Soc. London, Ser. A, 268: 443-466.

Moores, E.M., Robinson, P.T., Malpas, J., and Xenophontos, C., 1984. A model for the origin of the Troodos Massif, Cyprus and other mid-east ophiolites, Geology, 12: 500-503.

Morton, J.L. and Sleep, N.H., 1985. A mid-ocean ridge thermal model: Constraints on the volume of axial hydrothermal heat flux. J. Geophys. Res., 90: 11,345-11,353.

Mottl, M.J. and Wheat, G.C., 1992. Hydrothermal circulation through mid-ocean ridge flanks: Heat and chemical fluxes. V.M. Goldschmidt Conference, Reston, Va.: A72-A73.

Mukasa, S.B., and Ludden, J.L., 1987. Uranium-lead isotopic ages of plagiogranites from the Troodos ophiolite, Cyprus, and their tectonic significance, Geology, 15: 825-828.

Nagashima, K., Miyawaki, R., Takase, J., Nakai, I., Sakurai, K., Matsubara, S., Kato, A. and Iwano, S., 1986. Kimuraite, $CaY_2(CO_3)_4 \cdot 6H_2O$, a new mineral from fissures in an alkali olivine basalt from Saga Prefecture, Japan, and new data on lokkaite. Amer. Mineral., 71: 1028-1033.

Neal, C.R. and Taylor, L.A., 1989. A negative Ce anomaly in a peridotite xenolith: evidence for crustal recycling into the mantle or mantle metasomatism? Geochim. Cosmochim. Acta, 53: 1035-1040.

Nystrom, J.O., 1984. Rare earth element mobility in vesicular lava during low-grade metamorphism. Contrib. Mineral. Petrol., 88: 328-331.

Palmer, M.R. and Edmond, J.M., 1989. Cesium and rubidium in submarine hydrothermal fluids: evidence for recycling of alkali elements. Earth Planet. Sci. Lett., 95: 8-14.

Peterson, C., Duncan, R., and Scheidegger, K.F., 1986. Sequence and longevity of basalt alteration at Deep Sea Drilling Project site 597, Initial Rep. Deep Sea Drill. Proj., 92: 505-515.

Rautenschlein, M., Jenner, G., Hertozen, J., Hofman, A.H., Kerrich, R., Schmincke, H.-U. and White, W.M., 1985. Isotopic and trace element composition of volcanic glass from the Akaki Canyon, Cyprus: Implications for the origins of the Troodos Ophiolite. Earth Planet. Sci. Lett., 75: 369-383.

Richards, H., Cann, J.R., and Jensenius, J., 1989. Mineralogical zonation and metasomatism of the alteration pipes of Cyprus sulfide deposits, Econ. Geol., 84: 91-115.

Richardson, S.H., Hart, S.R. and Staudigel, H., 1980. Vein mineral ages of old oceanic crust. J. Geophys. Res., 85: 7195-7200.

Robertson, A.H.F., 1990. Tectonic evolution of Cyprus, in Troodos '87: Ophiolites and Oceanic Lithosphere Symposium Volume, edited by E.M. Moores, pp. 235-250, Cyprus Geological Survey Department, Nicosia.

Robinson, P.T., Melson, W., Hearn O., and Schmincke, H.-U., 1983. Volcanic glass compositions of the Troodos ophiolite, Cyprus, Geology, 11: 400-404.

Roden, M.F., Frey, F.A. and Clague, D.A., 1984. Geochemistry of tholeiitic and alkalic lavas from the Koolau Range Oahu, Hawaii: Implications for Hawaiian volcanism. Earth Planet. Sci. Lett., 69: 141-158.

Rosenbauer, R.J. and Bischoff, J.L., 1983. Uptake and transport of heavy metals by heated seawater: A summary of the experimental results, in: Rona, P.A., Bostrom, K., Laubier, L. and Smith Jr., K.L., eds.: Hydrothermal processes at seafloor spreading centers. Plenum, New York, 177-197.

Schiffman, P., and Smith, B.M., 1988. Petrology and oxygen isotope geochemistry of a fossil seawater hydrothermal system within the Solea Graben, northern Troodos ophiolite, Cyprus, J. Geophys. Res., 93: 4612-4624.

Schmincke, H.-U., Rautenschlein, M., Robinson, P.T., and Mehegan, J.M., 1983. Troodos extrusive series of Cyprus: A comparison with oceanic crust, Geology, 11: 405-409.

Seyfried, W.E. Jr., Berndt, M.E. and Janecky, D.R., 1986. Chloride depletions and enrichments in seafloor hydrothermal fluids: Constraints from experimental basalt alteration studies. Geochim. Cosmochim. Acta, 50: 469-475.

Seyfried, W.E. Jr., Ding, D. and Berndt, M.E., 1991. Phase equilibria constraints on the chemistry of hot spring fluids at mid-ocean ridges. Geochim. Cosmochim. Acta, 55: 3559-3580.

Seyfried, W.E., Shanks, W.C., and Dibble, W.E., 1978. Clay mineral formation in DSDP leg 34 basalts, Earth Planet. Sci. Lett., 41: 265-276.

Shannon, R.D., 1976. Revised effective ionic radii and systematic studies of interatomic distances in halides and chalcogenides. Acta Crystal., 32: 751-767

Smith, M.C., Perfit, M.R. and Jonasson, I.R., 1994. Petrology and geochemistry of basalts from the southern Juan de Fuca Ridge: Controls on the spatial and temporal evolution of mid-ocean ridge basalt. J. Geophys. Res., 99: 4787-4812.

Spooner, E.T.C., Chapman, H.J., and Smewing, J.D., 1977. Strontium isotopic contamination and oxidation during ocean floor hydrothermal metamorphism of the ophiolitic rocks of the Troodos Massif, Cyprus, Geochim. Cosmochim. Acta, 41: 873-890.

Stakes, D.S., and Scheidegger, K.F., 1981. Temporal variations in secondary minerals from Nazca Plate basalts, in Nazca Plate: Crustal formation and Andean convergence, edited by L.D. Kulm, Mem. Geol. Soc. Am., 154: 109-130.

Staudigel, H., Davies, G.R., Hart, S.R., Marchant, K.M. and Smith, B.M., 1995. Large scale isotopic Sr, Nd and O isotopic anatomy of altered oceanic crust: DSDP/ODP sites 417/418. Earth Planet. Sci. Lett., 130: 169-185.

Staudigel, H. and Gillis, K., 1991. The timing of hydrothermal alteration in the Troodos ophiolite, in: J. Malpas, E. Moores, A. Panayiotou and C. Xenophontos, eds.: "Troodos 87" symposium volume: 665-672.

Staudigel, H., Gillis, K. and Duncan, R., 1986. K/Ar and Rb/Sr ages of celadonites from the Troodos ophiolite, Cyprus. Geology, 14: 72-75.

Staudigel, H., and Hart, S.R., 1983. Alteration of basaltic glass: Mechanisms and significance for the oceanic crust-seawater budget. Geochim. Cosmochim. Acta, 47: 337-350.

Stein, C.A. and Stein, S., 1994. Constraints on hydrothermal heatflux through the oceanic lithosphere from global heat flow. J. Geophys. Res., 99: 3081-3095.

Thompson, G., 1983. Basalt-seawater interaction, in Hydrothermal Processes at Seafloor Spreading Centers, edited by P.A. Rona, K. Bostrom, and E.L. Smith, pp. 225-278, Plenum, New York.

Thy, P., Brooks, C.K., and Walsh, J.N., 1985. Tectonic and petrogenetic implications of major and rare earth element chemistry of Troodos glasses, Cyprus, Lithos, 18: 165-178.

Tilton, G.R., Hopson, C.A., and Wright, J.G., 1981. Uranium-lead isotopic ages of the Samail ophiolite with applications to Tethyan ocean ridge tectonics, J. Geophys. Res., 86: 2763-2775.

Vanko, D.A., 1986. High-chlorine amphiboles from oceanic rocks: product of highly saline hydrothermal fluids. Amer. J. Sci., 71: 51-59.

Varga, R.J., and Moores, E.M., 1985. Spreading structure of the Troodos ophiolite, Cyprus, Geology, 13: 846-850.

Von Damm, K.L. and Bischoff, J.L., 1987. Chemistry of hydrothermal solutions from the southern Juan De Fuca Ridge. J. Geophys. Res., 92: 11,334-11,346.

Von Damm, K.L., Edmond, J.L., Grant, B., Measures, C.I., Walden, B. and Weiss, R.F., 1985. Chemistry of submarine hydrothermal solutions at 21°N, East Pacific Rise. Geochim. Cosmochim. Acta, 49: 2221-2237.

White, W.M., McBirney, A.R. and Duncan, R.A., 1993. Petrology and geochemistry of the Galapagos Islands: Portrait of a pathological mantle plume. J. Geophys. Res., 98: 19,533-19,563.

Wolery, T.J. and Sleep, N.H., 1976. Hydrothermal circulation and geochemical flux at mid-ocean ridges. J. Geol., 84: 249-275.

Zhu, C. and Sverjensky, D.A., 1991. Partitioning of F-Cl-OH between minerals and hydrothermal fluids. Geochim. Cosmochim. Acta, 55: 1837-1858.

Zierenberg, R.A., and Shanks, W.C., III, 1983. Mineralogy and geochemistry of epigenetic features in metalliferous sediment, Atlantis II Deep, Red Sea, Econ. Geol., 78: 57-72.

APPENDICES

APPENDIX A

Sample Field Locations and Descriptions

CY-90-1a Celadonite veins within volcanic basal breccia, underlying pillows adjacent to a feeder dike. South facing road cut 2 km W. of Leiya at the east end of the Arakapas transform zone. 34°50'10"N/33°10'10"W.

CY-90-2 Celadonite veins within pillows. Road cut at east entrance into the town of Arakapas. 34°50'00"N/33°07'30"W.

CY-90-3 Celadonite veins in basal breccia,underlying thin sheet flows of the third volcanic series (Ghastraes volcano) [Bednarz and Schmincke, 1987], in the lower Pediaeos River. Location is approximately 2 km S.W. of Kambia.

CY-90-4a Celadonite lenses in thin sheet flows approximately 100 m. S.W. of sample CY-90-3 location. 35°02'00"N/33°15'10"W.

CY-90-5 Celadonite veins in thick (> 0.5 m.) sheet flows approximately 70 m. W. of sample CY-90-4 location. 35°02'00"N/33°15'10"W.

CY-90-6 Celadonite lenses in pillows of west-facing road cut, 1.2 km S. of Kambia. 35°01'30"N/33°14'30"W.

CY-90-7 Celadonite veins in volcanic breccia, north-facing road cut, at end of Kambia mine road. 35°02'20"N/33°16'20"W.

CY-90-8a Celadonite lenses in pillows adjacent to vertical dikes at Kambia mine. 35°02'20"N/33°16'20"W.

CY-90-8b Celadonite veins in sheet flows adjacent to vertical dikes at Kambia mine. 35°02'20"N/33°16'20"W.

CY-90-9C Celadonite lenses in sheet flows of Akaki Canyon unit C [Schmincke and Rautenschlein, 1987], approximately 100m S.W. of old Malounda bridge.

CY-90-10E Celadonite lenses in at interface of Akaki Canyon units D & E [Schmincke and Rautenschlein, 1987].

CY-90-11L Celadonite veins in Akaki Canyon unit L [Schmincke and Rautenschlein, 1987], 50 m. W. of Klirou bridge.

CY-90-12 Celadonite filled vesicles in sheet flows of Akaki Canyon unit K [Schmincke and Rautenschlein, 1987].

CY-90-14 Celadonite veins in pillows of road cut approximately 0.5 km. W. of Sha. 34°51'20"N/33°22'30"W.

CY-90-15 Very small and thin (0.1 mm) veins of celadonite and calcite in road cut approximately half the distance between Sha and Lythrodonda. 34°53'10"N/33°20'50"W.

CY-90-16a Celadonite filled vesicles in chill margin of small dike cutting through pillows. Road cut located 1 km. S. of Anatoliondas. 34°51'20"N/33°18'10"W.

CY-90-16b Celadonite filled veins in glassy pillows at same location of CY-90-16a. 34°51'20"N/33°18'10"W.

CY-90-17 Celadonite filled veins in small pillow margins. Road cut located 0.5 km. E. of Pyrga. 34°53'20"N/33°27'20"W.

CY-90-18 Thin celadonite veins in glassy pillow rinds. Road cut located 1 km. N. of Parekklisia. 34°53'50"N/33°12'20"W.

CY-90-19 Thin celadonite veins in pillows. Road cut entering the east side of Ephtagonia. 34°52'30"N/33°09'20"W.

CY-90-20 Celadonite(?) lenses in pillows. Road cut located 1 km west of Arakapas. 34°52'20"N/33°08'00"W.

CY-90-21 Celadonite(?) lenses in pillows. Road cut in village of Ayios Mamas. 34°50'00"N/32°55'00"W.

CY-90-22 Celadonite lenses in pillows 2 km. S. of Troulli. 35°03'20"N/33°36'20"W.

CY-90-23 Celadonite lenses in pillows 3 km. S. of Troulli. 35°03'10"N/33°36'20"W.

CY-90-24 Celadonite veins in pillows 1 km. S. of Skouritissa mine on the mine access road. 35°05'20"N/32°54'10"W.

CY-90-25 Celadonite veins in pillows 1.5 km. S. of Skouritissa mine on the mine access road. 35°05'10"N/32°54'10"W.

CY-90-26 Celadonite veins in breccia base of thin sheet flows; (Gyri volcano) [Bednarz and Schmincke, 1987], in the lower Pediaeos River. Approximately 2.5 km S.W. of Kambia.

CY-90-27 Celadonite veins at intersection of sheet flow margins with dike. Location is 20 m. upstream in Kokkinovrusis River Canyon from intersection with Pediaeos River Canyon [Bednarz and Schmincke, 1987].

CY-90-28 Celadonite veins in volcanic breccia 200 m. upstream in Kouphou River Canyon from intersection with Pediaeos River Canyon [Bednarz and Schmincke, 1987].

CY-90-29 Celadonite veins in pillows approximately 10 m. upstream from location of CY-90-28 [Bednarz and Schmincke, 1987].

CY-90-30 Celadonite filled vesicles in sheet flows approximately 100m upstream from location of CY-90-29 [Bednarz and Schmincke, 1987].

CY-90-31 Celadonite veins in pillows 100 m. upstream in Mazovounos River Canyon from intersection with Pediaeos River Canyon [Bednarz and Schmincke, 1987].

CY-90-32 Celadonite veins in pillows 50 m. upstream in Kokkinovrusis River Canyon from intersection with Kouphou River Canyon [Bednarz and Schmincke, 1987].

CY-90-33 Celadonite lenses in glassy pillow margins 250 m. upstream from location of CY-90-32 [Bednarz and Schmincke, 1987].

CY-90-34L Celadonite veins in pillows at base of Akaki Canyon unit L [Schmincke and Rautenschlein, 1987], 150 m. S. W. of Klirou bridge.

CY-90-35L Celadonite veins in pillows at top of Akaki Canyon unit L [Schmincke and Rautenschlein, 1987], 30 m. N. W. of Klirou bridge.

CY-90-36L Celadonite veins in sheet flows at dike intersection. Location is the base of Akaki Canyon unit L [Schmincke and Rautenschlein, 1987], 20 m. E. of Klirou bridge.

CY-90-37K Celadonite and chalcedony veins in sheet flows of Akaki Canyon unit K [Schmincke and Rautenschlein, 1987], 150 m. N. E. of Klirou bridge.

CY-90-38K Small celadonite veins in sheet flows of Akaki Canyon unit K [Schmincke and Rautenschlein, 1987], 600 m. N. E. of Klirou bridge.

CY-90-39K Small celadonite veins in sheet flows of Akaki Canyon unit K [Schmincke and Rautenschlein, 1987], 50 m. N. E. of CY-90-38 location.

CY-90-40K Massive large celadonite lense in sheet flows of Akaki Canyon unit K [Schmincke and Rautenschlein, 1987], 100 m. N.E. of CY-90-39 location.

CY-90-41K Massive large celadonite lense in sheet flows adjacent to dike intersection. Location is in Akaki Canyon unit K [Schmincke and Rautenschlein, 1987], 100 m. N. E. of CY-90-40 location.

CY-90-42I Small, thin celadonite veins in sheet flows of Akaki Canyon unit I [Schmincke and Rautenschlein, 1987], 30 m. N. E. of unit I-unit J interface.

CY-90-43I Massive, large celadonite veins in sheet flows of Akaki Canyon unit I [Schmincke and Rautenschlein, 1987], 60 m. N. E. of CY-90-42 location.

CY-90-44K Pervasive small celadonite veins in sheet flows of Akaki Canyon unit K [Schmincke and Rautenschlein, 1987], 50 m. N. E. of CY-90-43 location.

CY-90-45G Celadonite veins in sheet flow immediately adjacent to dike intersection ofAkaki Canyon unit G [Schmincke and Rautenschlein, 1987], 50 m. N. E. of unit G-unit H interface.

CY-92-1G Celadonite lenses in Akaki Canyon unit G [Schmincke and Rautenschlein, 1987], adjacent to unit F-unit G interface.

CY-92-2 Celadonite lenses in large pillows in south facing wall of Kambia mine. 35°02'20"N/33°16'20"W.

CY-92-3 Celadonite lenses interfingered with fresh glass of pillow units; south facing wall of Kambia mine. 35°02'20"N/33°16'20"W.

CY-92-10L Celadonite filled vesicle/vug in Akaki Canyon unit L [Schmincke and Rautenschlein, 1987],150 S. W. of Klirou bridge.

CY-92-13L Celadonite veins cutting through pillows of Akaki Canyon unit L [Schmincke and Rautenschlein, 1987], 50 m. S. W. of CY-92-10L location.

CY-92-14 Celadonite lenses in pillows of west-facing road cut, 1.2 km S. of Kambia. 35°01'30"N/33°14'30"W.

CY-92-15 Celadonite lenses in pillows of west-facing road cut, 1.2 km S. of Kambia. 35°01'30"N/33°14'30"W.

CY-92-35 Large, massive celadonite veins cross-cutting highly altered pillows near quarry approximately 1 km N. of Ayia Marina. 35°03'30"N/33°03'30"W.

CY-92-36 Large, massive celadonite veins cross-cutting highly altered pillows near quarry approximately 1 km N. of Ayia Marina. 35°03'30"N/33°03'30"W.

CY-92-37 Large, massive celadonite veins cross-cutting highly altered pillows near quarry approximately 1 km N. of Ayia Marina. 35°03'30"N/33°03'30"W.

CY-92-38 Large, massive celadonite veins cross-cutting highly altered pillows near quarry approximately 1 km N. of Ayia Marina. 35°03'30"N/33°03'30"W.

CY-92-43 Small celadonite veins in road cut 2.7 km. N. after turning onto Linou/Skouritissa Road. 35°05'10"N/32°54'10"W.

CY-92-44 Small celadonite veins in road cut 1.6 km. N. after turning onto Linou/Skouritissa Road. 35°05'00"N/32°54'10"W.

CY-92-45 Small celadonite veins in road cut 50 m. N. of CY-92-44 location. 35°05'10"N/32°54'10"W.

CY-92-46a Celadonite veins in road cut 3.1 km. N. after turning onto Linou/Skouritissa Road.

CY-92-47 Celadonite veins in road cut 10 m. N. of CY-92-46a location. 35°05'10"N/32°54'10"W.

CY-92-48 Celadonite lenses in road cut 2.1 km. E. of road intersection in Kataliondas. 35°00'20"N/33°19'10"W.

APPENDIX B

Electron Microprobe Results (in wt.%) of All Analyzed Celadonites

Sample	F	Na_2O	MgO	Al_2O_3	SiO_2	Cl	K_2O	CaO	TiO_2	MnO	Fe_2O_3	H_2O	Total
135.45V #1	0.27	0.27	4.33	4.67	49.26	0.02	7.21	0.12	0.12	0.10	17.88	3.65	87.89
135.45V #1	0.31	0.30	4.18	4.83	49.62	0.03	6.93	0.15	0.15	0.11	18.30	3.66	88.57
135.45V #1	0.49	0.29	4.25	4.59	49.82	0.04	7.00	0.13	0.16	0.11	19.11	3.60	89.57
135.45V #1	0.26	0.33	4.10	4.38	47.89	0.02	6.73	0.13	0.11	0.07	18.12	3.55	85.68
135.45V #1	0.13	0.21	4.16	4.25	48.36	0.01	7.10	0.10	0.14	0.09	17.89	3.64	86.06
135.45V #2	0.47	0.21	4.30	4.08	47.52	0.02	7.03	0.12	0.11	0.09	16.80	3.39	84.14
135.45V #2	0.34	0.20	4.25	3.81	46.28	0.03	6.94	0.13	0.13	0.05	16.22	3.35	81.70
135.45V #2	0.40	0.19	4.25	4.13	47.95	0.03	7.02	0.12	0.13	0.11	17.58	3.47	85.37
135.45V #2	0.38	0.21	4.09	4.11	46.99	0.03	6.74	0.14	0.12	0.15	17.22	3.40	83.57
135.45V #2	0.67	0.22	4.13	3.90	45.56	0.04	6.65	0.13	0.08	0.15	17.01	3.17	81.70
135.45V #3	0.59	0.23	3.96	4.51	47.55	0.01	6.44	0.10	0.12	0.12	18.04	3.37	85.04
135.45V #3	0.45	0.23	3.89	4.28	46.68	0.02	6.45	0.08	0.10	0.07	17.80	3.37	83.42
135.45V #3	0.45	0.23	3.81	4.35	46.76	0.03	6.60	0.11	0.12	0.11	17.91	3.38	83.85
135.45V #4	0.52	0.22	4.59	4.71	52.98	0.03	7.52	0.19	0.11	0.02	19.47	3.80	94.13
135.45V #4	0.34	0.30	4.20	4.45	48.67	0.03	6.96	0.12	0.13	0.12	17.78	3.56	86.64
135.45V #4	0.32	0.27	4.30	5.64	52.50	0.04	7.04	0.24	0.10	0.16	18.58	3.86	93.05
135.45V #4	0.45	0.20	4.58	4.39	50.59	0.03	7.40	0.21	0.12	0.09	17.95	3.64	89.63
135.45V #4	0.24	0.20	4.04	4.89	47.86	0.01	6.75	0.15	0.12	0.08	17.62	3.57	85.54
135.45V #4	0.33	0.25	4.17	4.71	48.28	0.02	7.08	0.19	0.12	0.12	18.36	3.58	87.19
135.45V #5	0.29	0.24	4.62	4.51	49.22	0.03	7.63	0.18	0.14	0.12	18.38	3.66	89.01
135.45V #5	0.35	0.25	4.38	4.55	48.40	0.03	7.04	0.16	0.11	0.12	17.98	3.56	86.91
135.45V #5	0.42	0.26	4.36	4.65	48.54	0.02	7.19	0.19	0.11	0.14	18.18	3.55	87.61
135.45V #5	0.48	0.27	4.47	4.58	48.77	0.03	7.27	0.17	0.11	0.18	18.11	3.53	87.96
135.45V #5	0.10	0.20	4.52	4.52	49.17	0.03	7.47	0.17	0.14	0.13	18.16	3.74	88.33
135.45V #6	0.49	0.19	4.24	4.72	49.12	0.03	6.95	0.21	0.14	0.12	17.82	3.53	87.54
135.45V #6	0.11	0.16	4.34	4.71	50.20	0.02	7.03	0.19	0.14	0.10	18.31	3.79	89.07
135.45V #6	0.25	0.21	4.52	4.91	50.03	0.02	7.10	0.18	0.13	0.16	18.29	3.73	89.52
135.45V #7	0.40	0.19	4.16	4.63	49.96	0.01	6.76	0.23	0.10	0.13	18.92	3.64	89.12

135.45V #8	0.30	0.21	4.15	4.85	51.48	0.02	6.92	0.26	0.14	0.13	20.01	3.82	92.28
135.45V #9	0.17	0.18	4.56	4.39	51.69	0.04	7.16	0.21	0.17	0.11	20.03	3.89	92.59
135.45V #10	3.47	0.24	3.93	4.39	49.73	0.06	6.47	0.34	0.16	0.14	20.42	2.19	91.53
135.45V #10	1.61	0.23	3.93	4.22	49.63	0.06	6.45	0.37	0.13	0.15	20.53	3.06	90.38
135.45V #10	0.83	0.25	4.07	4.16	48.72	0.04	6.56	0.37	0.17	0.12	19.93	3.38	88.59
123.30V #1	2.67	0.17	4.62	3.98	52.87	0.05	7.83	0.29	0.15	0.09	21.95	2.82	97.49
123.30V #1	1.47	0.13	4.74	3.97	53.56	0.05	7.90	0.27	0.13	0.12	21.98	3.43	97.75
123.30V #1	1.65	0.16	4.75	3.93	52.63	0.04	7.81	0.27	0.14	0.13	21.49	3.28	96.27
123.30V #2	0.63	0.30	4.39	3.77	48.38	0.03	7.45	0.27	0.14	0.13	19.30	3.44	88.24
123.30V #2	0.60	0.32	4.10	3.61	45.12	0.02	6.81	0.25	0.12	0.10	18.79	3.23	83.07
123.30V #2	0.29	0.23	4.20	3.53	46.01	0.04	6.91	0.23	0.14	0.08	17.69	3.39	82.73
123.30V #2	0.39	0.24	4.41	3.60	47.94	0.03	7.47	0.24	0.15	0.08	18.75	3.50	86.79
123.30V Trav	2.25	0.06	4.46	3.92	51.67	0.05	7.10	0.47	0.12	0.12	21.39	2.91	94.53
123.30V Trav	1.49	0.13	4.98	3.73	52.07	0.04	8.50	0.29	0.13	0.11	20.15	3.29	94.91
123.30V Trav	0.40	0.10	5.00	3.01	51.38	0.02	8.89	0.14	0.16	0.05	18.64	3.70	91.47
123.30V Trav	1.40	0.30	4.35	3.99	48.11	0.03	7.15	0.32	0.14	0.10	17.80	3.02	86.70
123.30V Trav	0.84	0.42	4.04	5.10	49.38	0.05	6.79	0.52	0.16	0.08	18.95	3.43	89.76
123.30V Trav	0.34	0.14	4.63	3.22	46.10	0.03	7.78	0.15	0.17	0.07	16.91	3.36	82.89
123.30V Trav	0.34	0.21	4.26	3.48	45.79	0.04	7.27	0.22	0.16	0.06	16.69	3.33	81.83
123.30V Trav	0.49	0.21	4.90	2.99	48.17	0.03	8.06	0.16	0.14	0.07	18.62	3.46	87.30
123.30V Trav	0.81	0.41	3.73	4.35	46.19	0.04	5.88	0.47	0.19	0.14	18.75	3.20	84.16
123.30V Trav	0.40	0.27	4.74	3.02	49.25	0.04	8.08	0.17	0.16	0.07	18.43	3.55	88.16
123.30V Trav	0.24	0.13	4.85	2.79	50.39	0.04	8.51	0.10	0.20	0.04	17.93	3.67	88.87
123.30V Trav	0.33	0.10	4.52	2.86	45.76	0.05	7.79	0.10	0.18	0.07	16.87	3.32	81.95
123.30V Trav	0.58	0.21	5.14	3.39	51.95	0.03	8.61	0.18	0.20	0.13	19.72	3.70	93.83
123.30V Trav	0.42	0.28	3.89	3.85	42.88	0.03	6.23	0.22	0.13	0.06	16.17	3.10	77.25
123.30V Trav	0.83	0.27	3.61	4.73	42.90	0.03	5.24	0.33	0.15	0.13	15.65	2.91	76.76
123.30V Trav	0.50	0.25	3.88	3.63	43.42	0.04	6.28	0.24	0.14	0.08	16.21	3.08	77.74
123.30V Trav	0.48	0.18	4.49	3.08	47.50	0.04	7.78	0.16	0.13	0.08	18.57	3.41	85.89
123.30V Trav	0.52	0.26	4.00	3.86	43.12	0.04	6.40	0.21	0.18	0.07	15.91	3.07	77.64
123.30V Trav	0.98	0.42	3.53	4.94	42.73	0.03	5.12	0.49	0.15	0.14	15.94	2.85	77.33
123.30V Trav	4.14	0.29	3.89	4.71	49.70	0.06	6.08	0.86	0.19	0.22	21.19	1.92	93.23
123.30V Trav	0.50	0.22	4.20	3.41	45.87	0.03	7.14	0.18	0.10	0.09	16.76	3.25	81.75
123.30V Trav	0.42	0.16	4.44	3.56	47.25	0.03	7.56	0.21	0.15	0.11	17.36	3.41	84.67
123.30V Trav	0.51	0.43	3.92	4.56	48.81	0.02	6.47	0.47	0.11	0.10	20.15	3.56	89.12

123.30V Trav	4.79	0.34	3.98	5.40	48.99	0.08	6.49	0.80	0.22	0.20	20.01	1.58	92.86
123.30V Trav	2.18	0.30	4.27	4.42	50.87	0.07	7.02	0.53	0.11	0.14	20.21	2.89	93.01
199.60H Trav	0.41	1.03	8.08	5.30	47.71	0.03	2.47	2.13	0.19	0.16	17.68	3.67	88.85
199.60H Trav	0.45	0.93	8.59	5.28	49.67	0.02	3.67	0.55	0.18	0.11	17.85	3.76	91.06
199.60H Trav	0.29	1.16	8.80	5.67	47.88	0.02	2.59	0.80	0.22	0.12	17.85	3.76	89.13
199.60H Trav	0.32	0.94	8.57	5.06	50.17	0.04	4.87	0.52	0.23	0.11	17.93	3.86	92.61
199.60H Trav	0.50	0.78	8.53	4.73	49.66	0.03	5.29	0.40	0.26	0.12	18.35	3.74	92.39
199.60H Trav	0.28	0.69	7.26	5.31	51.33	0.02	5.44	0.54	0.21	0.12	17.46	3.89	92.55
199.60H Trav	0.30	1.05	7.41	5.78	51.02	0.01	4.16	0.66	0.21	0.09	17.37	3.88	91.94
199.60H Trav	0.24	0.89	7.42	5.47	51.85	0.01	4.93	0.44	0.18	0.09	17.06	3.93	92.51
199.60H Trav	0.11	0.59	7.32	4.73	51.25	0.01	6.12	0.44	0.21	0.11	17.84	3.96	92.70
199.60H Trav	0.22	0.97	7.14	5.55	48.47	0.00	3.85	0.63	0.45	0.22	18.67	3.81	89.96
199.60H Trav	0.14	0.99	7.22	5.46	50.64	0.00	4.64	0.59	0.23	0.09	17.09	3.91	90.98
199.60H Trav	0.25	0.87	6.90	6.09	51.69	0.01	4.25	0.75	0.16	0.15	16.62	3.91	91.63
199.60H Trav	0.06	0.60	7.75	5.14	51.61	0.01	5.80	0.59	0.23	0.11	17.74	4.04	93.67
199.60H Trav	0.06	0.60	5.79	6.18	49.81	0.00	4.48	0.76	0.23	0.12	17.85	3.90	89.75
199.60H Trav	0.15	0.65	7.45	5.57	50.36	0.00	4.83	0.77	0.30	0.14	17.60	3.92	91.75
199.60H Trav	0.02	0.58	7.58	5.37	52.44	0.01	5.64	0.63	0.21	0.13	17.65	4.10	94.35
199.60H Trav	0.11	0.40	7.27	4.47	52.31	0.00	6.99	0.46	0.23	0.11	18.96	4.05	95.36
199.60H Trav	0.14	0.51	7.57	4.73	53.00	0.00	6.67	0.46	0.22	0.12	17.97	4.07	95.46
199.60H Trav	0.12	0.37	7.25	4.20	52.16	0.00	7.51	0.40	0.25	0.11	18.58	4.02	94.97
199.60H Trav	0.26	0.52	7.55	4.90	51.75	0.00	6.08	0.63	0.20	0.10	17.80	3.94	93.73
199.60H Trav	0.23	0.44	7.43	5.16	51.28	0.01	5.49	0.71	0.17	0.11	17.10	3.90	92.03
199.60H Trav	0.55	0.51	7.65	4.70	51.42	0.02	6.37	0.62	0.24	0.10	17.66	3.77	93.61
199.60H Trav	0.30	0.55	7.22	4.70	52.93	0.00	6.72	0.51	0.22	0.09	17.86	3.97	95.07
199.60H Trav	0.48	1.30	6.96	5.77	51.86	0.00	4.80	0.29	0.21	0.06	17.07	3.82	92.61
199.60H Trav	0.16	0.73	7.64	4.68	51.89	0.02	6.33	0.34	0.21	0.06	18.47	4.00	94.53
199.60V dkgn	0.22	0.04	6.11	2.31	53.13	0.01	9.72	0.04	0.03	0.11	19.09	3.91	94.70
199.60V dkgn	0.36	0.00	6.04	2.34	51.10	0.01	9.30	0.00	0.05	0.12	18.05	3.69	91.07
199.60V dkgn	0.06	0.00	6.18	2.25	52.07	0.01	9.67	0.01	0.05	0.09	18.91	3.92	93.22
199.60V dkgn	0.41	0.00	5.86	2.39	50.85	0.00	9.49	0.00	0.01	0.08	18.07	3.65	90.82
199.60V dkgn	0.14	0.02	6.03	2.41	51.20	0.02	9.43	0.02	0.05	0.07	18.61	3.83	91.81
199.60V dkgn	0.24	0.01	6.02	2.27	51.82	0.01	9.49	0.01	0.03	0.09	18.11	3.79	91.89
199.60V dkgn	0.34	0.00	5.76	2.23	49.52	0.00	9.19	0.00	0.02	0.08	17.58	3.58	88.30
199.60V dkgn	0.13	0.00	6.10	2.23	52.59	0.00	9.67	0.01	0.06	0.13	19.27	3.93	94.11

199.60V ltgn	0.94	0.18	5.43	3.56	51.26	0.02	8.46	0.14	0.02	0.09	18.73	3.47	92.28
199.60V ltgn	0.30	0.10	5.08	3.12	46.57	0.02	8.04	0.06	0.02	0.05	15.78	3.38	82.52
199.60V ltgn	0.23	0.11	5.18	3.05	46.13	0.01	7.65	0.08	0.04	0.05	15.84	3.39	81.76
199.60V ltgn	0.36	0.07	5.20	3.02	46.16	0.00	7.75	0.07	0.02	0.06	15.63	3.33	81.66
199.60V ltgn	0.28	0.04	5.26	2.65	46.93	0.00	8.25	0.02	0.03	0.05	15.93	3.40	82.86
199.60V ltgn	0.35	0.06	5.22	2.97	45.66	0.02	8.03	0.04	0.01	0.06	15.51	3.30	81.23
199.60V ltgn	0.23	0.11	5.14	3.00	46.86	0.02	7.74	0.07	0.03	0.08	16.32	3.44	83.05
119.00V vug	0.21	0.23	5.69	3.04	50.20	0.01	8.52	0.09	0.17	0.12	19.81	3.79	91.87
119.00V vug	0.20	0.20	5.93	3.21	50.68	0.01	8.63	0.10	0.17	0.08	20.07	3.84	93.12
119.00V vug	0.00	0.26	6.11	2.91	46.38	0.01	7.42	0.11	0.12	0.06	18.07	3.62	85.07
119.00V vug	0.05	0.22	5.70	3.22	48.50	0.01	8.06	0.05	0.10	0.11	18.67	3.73	88.42
119.00V vug	0.25	0.27	5.82	2.98	49.81	0.03	8.35	0.07	0.17	0.13	19.73	3.74	91.35
119.00V vug	0.31	0.25	5.67	2.99	50.81	0.03	8.69	0.07	0.19	0.12	19.93	3.78	92.84
119.00V #2	0.05	0.35	3.49	3.22	53.05	0.01	6.27	0.37	0.03	0.11	26.34	4.10	97.39
119.00V #2	0.05	0.33	3.73	3.35	52.28	0.02	6.45	0.43	0.01	0.10	26.29	4.08	97.11
119.00V #3	0.09	0.18	4.68	2.78	55.24	0.02	8.78	0.15	0.00	0.08	23.38	4.17	99.54
119.00V #3	0.10	0.18	4.69	2.73	55.13	0.03	8.82	0.18	0.00	0.02	23.42	4.16	99.44
119.00V #3	0.05	0.17	4.63	2.78	55.19	0.03	8.68	0.16	0.00	0.08	23.02	4.17	98.96
119.00V #3	0.00	0.19	4.72	2.87	55.14	0.00	8.72	0.16	0.00	0.09	23.77	4.23	99.89
119.00V #3	0.03	0.16	4.73	2.83	55.18	0.01	8.81	0.16	0.01	0.07	23.30	4.20	99.48
119.00V #3	0.12	0.20	4.70	2.83	54.80	0.02	8.68	0.16	0.01	0.10	23.29	4.13	99.03
119.00V #3	0.07	0.18	4.73	2.81	55.39	0.01	8.78	0.17	0.00	0.08	23.32	4.19	99.72
119.00V #3	0.03	0.17	4.60	2.81	55.50	0.01	8.66	0.14	0.00	0.06	22.99	4.20	99.18
119.00V #3	0.05	0.18	4.63	2.74	55.40	0.03	8.82	0.18	0.00	0.07	22.67	4.17	98.92
119.00V #3	0.10	0.18	4.59	2.72	55.16	0.02	8.47	0.16	0.00	0.05	22.80	4.13	98.38
119.00V #4	0.12	0.33	4.17	3.61	54.04	0.01	7.04	0.35	0.00	0.06	23.54	4.10	97.35
119.00V #5	0.08	0.36	4.17	3.70	53.49	0.01	6.93	0.37	0.04	0.10	23.72	4.10	97.06
119.00V #6	0.09	0.32	4.13	3.31	53.48	0.02	7.08	0.34	0.02	0.07	24.22	4.08	97.16
119.00V #7	0.07	0.29	4.00	3.17	52.74	0.02	7.01	0.36	0.01	0.07	24.30	4.05	96.07
119.00V #8	0.03	0.26	3.94	3.05	56.39	0.03	7.22	0.28	0.01	0.07	23.19	4.22	98.68
119.00V #8	0.08	0.29	4.09	3.41	52.80	0.04	7.26	0.31	0.02	0.09	25.05	4.08	97.49
119.00V #8	0.15	0.28	4.10	3.46	53.17	0.01	7.39	0.33	0.00	0.06	25.00	4.08	98.01
119.00V #8	0.05	0.24	4.11	3.33	54.44	0.02	7.42	0.31	0.02	0.03	23.84	4.15	97.96
CY-1A 63.1m	0.00	0.19	7.58	5.25	50.70	0.01	7.72	0.14	0.09	0.03	18.24	N.D.	89.95
CY-1A 63.1m	0.00	0.00	5.80	5.48	53.93	0.01	9.92	0.02	0.11	0.00	17.05	N.D.	92.32

CY-1A 63.1m	0.00	0.00	6.49	5.33	52.31	0.03	8.99	0.08	0.10	0.00	17.25	N.D.	90.58
CY-1A 63.1m	0.00	0.00	7.55	5.22	51.68	0.02	7.99	0.18	0.10	0.00	18.01	N.D.	90.75
CY-1A 63.1m	0.00	0.00	5.95	5.48	52.46	0.02	9.33	0.05	0.10	0.00	16.16	N.D.	89.55
CY-1A 49.9m	1.34	0.05	3.45	8.45	52.26	0.09	4.99	0.24	0.66	0.00	15.24	N.D.	86.77
CY-1A 49.9m	0.00	0.07	3.74	8.31	48.27	0.12	4.58	0.37	0.70	0.00	12.84	N.D.	79.00
CY-1A 134.7m	0.00	0.02	5.17	7.30	49.32	0.09	7.40	0.04	0.07	0.04	12.40	N.D.	81.85
CY-1A 134.7m	0.37	0.00	5.03	7.52	49.41	0.05	7.42	0.07	0.06	0.00	12.73	N.D.	82.66
CY-1A 134.7m	0.00	0.00	4.67	7.06	44.36	0.19	6.76	0.12	0.06	0.00	10.07	N.D.	73.29
CY-1A 134.7m	0.00	0.00	4.25	6.13	41.59	0.19	6.17	0.12	0.05	0.00	10.46	N.D.	68.96
CY-1A 134.7m	0.00	0.00	5.19	7.35	50.44	0.06	7.59	0.05	0.08	0.03	12.99	N.D.	83.78
CY-1A 132.9m	0.00	0.02	4.50	5.00	50.30	0.05	8.48	0.11	0.01	0.02	20.90	N.D.	89.39
CY-1A 132.9m	0.00	0.00	4.38	4.92	48.55	0.06	8.13	0.09	0.03	0.00	20.55	N.D.	86.71
CY-1A 132.9m	0.00	0.00	4.75	5.18	51.42	0.06	8.43	0.11	0.01	0.00	20.47	N.D.	90.43
CY-1A 132.9m	0.00	0.00	4.95	5.44	52.35	0.05	8.60	0.09	0.01	0.00	20.24	N.D.	91.73
CY-1A 132.9m	0.00	0.00	4.99	5.31	51.85	0.05	8.43	0.06	0.01	0.00	20.19	N.D.	90.89
CY-1A 92.9m	0.00	0.03	5.68	5.22	49.98	0.09	7.58	0.04	0.05	0.07	13.42	N.D.	82.16
CY-1A 92.9m	0.00	0.00	5.23	4.82	43.52	0.15	6.99	0.04	0.07	0.00	11.55	N.D.	72.37
CY-1A 92.9m	0.00	0.00	5.41	5.76	53.98	0.05	8.38	0.09	0.06	0.01	16.66	N.D.	90.40
CY-2 192.1m	0.00	0.04	4.82	4.49	52.47	0.07	6.12	0.05	0.05	0.06	18.32	N.D.	86.49
CY-2 192.1m	0.00	0.00	4.98	2.96	50.27	0.06	8.85	0.02	0.07	0.03	18.78	N.D.	86.02
CY-2 192.1m	0.00	0.00	5.21	3.78	51.20	0.07	7.98	0.16	0.08	0.02	17.38	N.D.	85.88
CY-2 192.1m	0.00	0.00	5.12	3.86	51.39	0.07	8.09	0.03	0.04	0.00	17.89	N.D.	86.49
CY-2 192.1m	0.00	0.13	5.28	6.77	55.28	0.07	5.90	0.41	0.08	0.05	17.10	N.D.	91.07
CY-2 123.3m	0.00	0.04	5.00	3.76	52.92	0.05	8.82	0.09	0.16	0.08	18.95	N.D.	89.87
CY-2 123.3m	0.00	0.00	4.69	3.94	51.69	0.08	8.06	0.07	0.15	0.00	18.93	N.D.	87.61
CY-2 123.3m	0.00	0.00	3.91	4.34	49.28	0.09	6.42	0.15	0.11	0.03	19.52	N.D.	83.85
CY-2 123.3m	0.00	0.00	4.54	3.67	48.36	0.14	7.76	0.06	0.17	0.00	17.32	N.D.	82.02
CY-2 123.3m	0.00	0.00	4.24	4.18	47.85	0.13	6.64	0.17	0.12	0.07	16.99	N.D.	80.39
CY-2 117.85m	0.00	0.04	4.27	3.35	45.16	0.13	8.01	0.01	0.12	0.05	16.24	N.D.	77.38
CY-2 117.85m	0.00	0.00	4.14	4.08	50.53	0.09	8.01	0.10	0.10	0.02	17.20	N.D.	84.27
CY-2 117.85m	0.78	0.00	4.40	4.63	49.98	0.05	7.74	0.05	0.06	0.00	17.76	N.D.	85.45
CY-1A 202.0m	0.00	0.07	3.92	10.51	51.62	0.04	8.22	0.08	0.03	0.05	14.32	N.D.	88.86
CY-1A 202.0m	0.00	0.00	4.58	11.28	55.85	0.06	8.29	0.09	0.05	0.00	15.26	N.D.	95.46
CY-1A 202.0m	0.00	0.00	4.32	10.44	54.50	0.04	8.75	0.14	0.03	0.00	14.90	N.D.	93.12
CY-1A 202.0m	0.00	0.01	5.17	11.63	57.87	0.05	8.66	0.06	0.04	0.00	14.75	N.D.	98.24

CY-1A 202.0m	0.00	0.00	4.49	10.97	53.12	0.04	8.47	0.07	0.04	0.00	14.88	N.D.	92.08
CY-2 196.3m	0.00	0.00	6.43	3.53	45.58	0.15	6.91	0.12	0.08	0.00	13.24	N.D.	76.04
CY-2 196.3m	0.00	0.02	5.25	4.30	49.69	0.11	7.60	0.21	0.05	0.04	15.76	N.D.	83.03
CY-2 195.8m	0.00	0.06	5.56	3.52	52.32	0.03	8.24	0.15	0.02	0.11	19.07	N.D.	89.08
CY-2 195.8m	0.00	0.00	5.07	4.46	50.81	0.05	6.36	0.39	0.04	0.00	17.32	N.D.	84.50
CY-2 195.8m	0.00	0.00	5.87	3.08	53.66	0.02	9.19	0.14	0.02	0.05	19.63	N.D.	91.66
CY-2 195.8m	0.00	0.00	3.81	4.28	47.16	0.06	6.18	0.24	0.10	0.00	20.39	N.D.	82.22
CY-2 195.8m	0.00	0.00	5.38	3.50	50.21	0.02	8.39	0.08	0.05	0.04	20.16	N.D.	87.83
CY-2 212.2m	0.00	0.26	3.60	5.54	50.83	0.04	6.48	0.94	0.08	0.06	22.65	N.D.	90.48
CY-2 212.2m	0.00	0.00	3.65	5.91	51.46	0.05	6.45	0.84	0.05	0.03	22.99	N.D.	91.43
CY-2 212.2m	0.00	0.03	4.33	6.07	52.65	0.05	7.11	0.48	0.08	0.00	20.27	N.D.	91.07
CY-2 212.2m	0.00	0.00	4.33	6.05	52.65	0.05	7.34	0.50	0.07	0.00	19.71	N.D.	90.70
CY-2 212.2m	0.00	0.00	4.36	6.18	52.14	0.05	7.36	0.48	0.08	0.00	19.75	N.D.	90.40
CY-2 199.6m	0.00	0.13	4.61	3.94	46.22	0.13	5.58	0.27	0.06	0.10	15.17	N.D.	76.21
CY-2 199.6m	0.00	0.00	4.76	3.47	46.27	0.09	6.26	0.10	0.12	0.04	15.90	N.D.	77.01
CY-2 199.6m	0.07	0.00	4.60	4.16	46.60	0.09	5.94	0.14	0.05	0.00	16.53	N.D.	78.18
CY-2 199.6m	0.00	0.00	5.63	4.63	52.94	0.05	7.18	0.11	0.07	0.00	18.03	N.D.	88.64
CY-2 199.6m	0.00	0.00	6.10	2.90	50.98	0.07	8.48	0.02	0.09	0.00	17.93	N.D.	86.57
CY-90-6	0.00	0.00	4.99	1.96	41.52	0.12	7.08	0.09	0.07	0.00	14.24	N.D.	70.07
CY-90-6	0.00	0.00	4.98	2.46	45.91	0.08	7.87	0.04	0.07	0.00	16.70	N.D.	78.11
CY-90-6	0.00	0.00	4.65	4.38	51.60	0.04	7.41	0.12	0.05	0.00	20.95	N.D.	89.20
CY-90-6	0.00	0.00	5.05	4.56	53.01	0.09	7.24	0.07	0.08	0.00	19.38	N.D.	89.48
CY-90-5b	0.00	0.00	5.89	4.47	49.13	0.06	7.54	0.03	0.06	0.00	14.81	N.D.	81.99
CY-90-5b	0.85	0.00	5.83	4.83	50.02	0.05	7.60	0.06	0.06	0.00	15.42	N.D.	84.72
CY-90-5b	0.00	0.00	3.38	2.60	29.76	0.02	7.84	0.06	0.03	0.00	13.24	N.D.	56.93
CY-90-5b	0.00	0.00	5.90	5.28	49.03	0.06	7.37	0.06	0.09	0.00	14.61	N.D.	82.40
CY-90-5b	0.00	0.00	5.54	5.14	47.07	0.06	7.09	0.05	0.03	0.00	13.33	N.D.	78.31
CY-90-5a	0.00	0.00	5.19	2.28	43.95	0.15	7.40	0.10	0.01	0.00	15.24	N.D.	74.32
CY-90-5a	0.00	0.00	4.85	2.33	42.52	0.16	6.69	0.14	0.01	0.00	15.16	N.D.	71.86
CY-90-5a	0.00	0.00	4.80	2.92	47.91	0.12	6.06	0.27	0.01	0.00	20.29	N.D.	82.38
CY-90-5a	0.00	0.00	4.84	2.76	44.60	0.18	6.14	0.25	0.00	0.00	16.28	N.D.	75.05
CY-90-5a	0.00	0.00	4.54	2.13	39.55	0.10	6.83	0.08	0.01	0.00	13.12	N.D.	66.36
CY-90-3	0.00	0.01	4.76	2.20	40.10	0.20	6.53	0.08	0.00	0.03	13.35	N.D.	67.26
CY-90-3	0.00	0.00	4.86	2.23	40.61	0.22	6.64	0.13	0.00	0.00	13.71	N.D.	68.40
CY-90-12	0.00	0.03	5.04	6.01	49.87	0.08	8.98	0.02	0.01	0.05	14.34	N.D.	84.43

CY-90-12	0.00	0.00	4.96	5.75	47.29	0.08	8.53	0.05	0.03	0.00	14.21	N.D.	80.90
CY-90-12	0.00	0.00	4.52	6.77	48.04	0.09	8.06	0.10	0.00	0.00	12.76	N.D.	80.34
CY-90-12	0.00	0.00	4.42	6.82	47.78	0.10	7.39	0.08	0.00	0.00	12.50	N.D.	79.09
CY-90-12	0.00	0.00	4.09	6.35	44.53	0.10	6.96	0.07	0.02	0.00	11.84	N.D.	73.96
CY-90-10	0.00	0.04	2.68	2.19	27.85	0.16	5.29	0.10	0.12	0.07	9.02	N.D.	47.52
CY-90-7	1.42	0.05	4.90	6.22	50.09	0.05	6.08	0.14	0.07	0.02	18.21	N.D.	87.25
CY-90-7	1.44	0.00	5.60	5.84	53.66	0.05	6.57	0.14	0.26	0.00	18.62	N.D.	92.18
CY-90-7	0.00	0.00	4.47	1.70	36.17	0.14	6.11	0.07	0.06	0.00	12.57	N.D.	61.29
CY-90-7	0.00	0.02	5.78	2.61	49.41	0.05	8.21	0.10	0.13	0.04	17.66	N.D.	84.01
CY-90-26	0.00	0.13	5.38	3.99	48.51	0.06	6.33	0.21	0.01	0.05	18.82	N.D.	83.49
CY-90-26	0.00	0.00	5.15	3.84	46.74	0.08	6.24	0.20	0.03	0.00	18.44	N.D.	80.72
CY-90-26	0.00	0.03	4.81	3.77	46.21	0.07	5.55	0.26	0.04	0.00	18.60	N.D.	79.34
CY-90-26	0.00	0.10	4.51	3.32	43.28	0.05	5.52	0.24	0.05	0.00	18.07	N.D.	75.14
CY-90-26	0.00	0.00	4.95	3.73	44.74	0.06	5.52	0.23	0.05	0.02	17.70	N.D.	77.00
CY-90-20	0.00	0.46	5.45	7.37	54.39	0.03	7.43	0.07	0.01	0.06	20.16	N.D.	95.43
CY-90-20	0.00	0.00	6.34	6.99	53.55	0.04	7.71	0.07	0.01	0.00	18.85	N.D.	93.56
CY-90-20	0.00	0.08	5.93	6.43	53.13	0.04	7.97	0.08	0.00	0.00	18.73	N.D.	92.39
CY-90-20	0.00	0.13	7.37	6.29	53.63	0.03	7.50	0.08	0.01	0.00	18.60	N.D.	93.64
CY-90-20	0.00	0.09	6.64	6.38	54.02	0.03	7.94	0.07	0.02	0.00	19.03	N.D.	94.22
CY-90-29	0.00	0.14	5.09	4.22	50.78	0.08	7.35	0.50	0.05	0.06	17.68	N.D.	85.95
CY-90-29	0.00	0.00	5.36	3.71	48.42	0.08	7.85	0.20	0.06	0.00	16.14	N.D.	81.82
CY-90-29	0.00	0.00	5.51	5.57	51.27	0.07	6.56	0.21	0.09	0.01	15.52	N.D.	84.81
CY-90-29	0.00	0.00	4.91	5.09	49.56	0.06	6.87	0.20	0.07	0.00	16.64	N.D.	83.40
CY-90-29	0.82	0.08	4.11	4.74	48.04	0.09	6.35	0.25	0.04	0.04	19.10	N.D.	83.66
CY-90-28	0.00	0.04	6.30	5.34	51.26	0.06	7.93	0.18	0.12	0.07	14.37	N.D.	85.67
CY-90-28	0.00	0.00	6.64	5.31	52.27	0.05	8.10	0.21	0.13	0.00	14.71	N.D.	87.42
CY-90-28	0.00	0.00	6.79	5.35	49.72	0.09	6.69	0.75	0.13	0.03	14.07	N.D.	83.62
CY-90-28	0.00	0.00	6.04	4.61	49.05	0.12	8.13	0.09	0.09	0.01	13.89	N.D.	82.03
CY-90-28	0.00	0.00	5.51	4.50	46.73	0.11	7.71	0.10	0.08	0.03	12.79	N.D.	77.56
CY-90-41	0.00	0.03	4.55	1.88	40.43	0.20	6.99	0.10	0.00	0.01	14.79	N.D.	68.98
CY-90-41	0.00	0.00	4.67	2.37	43.56	0.13	6.67	0.24	0.01	0.00	17.42	N.D.	75.07
CY-90-41	0.00	0.00	4.62	1.79	40.79	0.22	7.22	0.06	0.01	0.00	14.47	N.D.	69.18
CY-90-41	0.00	0.00	4.11	1.58	36.42	0.25	6.17	0.10	0.00	0.00	13.03	N.D.	61.66
CY-90-41	0.00	0.00	5.95	2.89	51.11	0.06	8.89	0.10	0.00	0.00	16.97	N.D.	85.97
CY-90-40	0.00	0.00	5.18	4.51	46.57	0.13	7.39	0.24	0.10	0.00	13.50	N.D.	77.62

CY-90-40	0.00	0.00	5.13	4.21	45.12	0.13	7.52	0.13	0.06	0.00	12.93	N.D.	75.23
CY-90-40	0.00	0.00	5.25	4.41	46.66	0.10	7.53	0.19	0.10	0.00	13.66	N.D.	77.90
CY-90-40	0.00	0.00	5.21	4.70	47.95	0.08	7.66	0.23	0.08	0.00	14.73	N.D.	80.64
CY-90-40	0.00	0.00	4.82	4.26	47.26	0.11	7.52	0.24	0.09	0.00	15.12	N.D.	79.42
CY-90-33	0.00	0.04	6.53	2.24	54.36	0.03	9.53	0.15	0.04	0.09	20.27	N.D.	93.28
CY-90-33	0.00	0.00	6.54	2.32	55.41	0.02	9.56	0.08	0.02	0.02	20.50	N.D.	94.47
CY-90-33	0.00	0.00	6.60	2.28	55.31	0.00	8.98	0.14	0.01	0.00	20.76	N.D.	94.08
CY-90-33	0.00	0.00	6.85	2.36	56.55	0.02	9.25	0.09	0.03	0.00	20.37	N.D.	95.52
CY-90-33	0.00	0.00	6.71	2.41	54.80	0.02	9.22	0.07	0.01	0.03	20.62	N.D.	93.89
CY-90-32	0.00	0.04	5.10	3.42	52.63	0.03	8.01	0.19	0.07	0.05	22.08	N.D.	91.62
CY-90-32	0.00	0.00	5.05	3.48	52.32	0.04	7.83	0.20	0.06	0.00	22.05	N.D.	91.03
CY-90-32	0.00	0.00	5.20	3.31	51.10	0.04	7.87	0.15	0.07	0.00	20.40	N.D.	88.14
CY-90-32	0.00	0.00	5.20	3.54	53.05	0.04	7.99	0.23	0.09	0.00	21.92	N.D.	92.06
CY-90-32	0.00	0.00	5.03	3.40	52.09	0.05	7.96	0.25	0.07	0.00	22.16	N.D.	91.01
CY-92-36	0.00	0.00	6.68	2.01	52.80	0.06	8.27	0.21	0.05	0.03	18.16	N.D.	88.27
CY-92-36	0.00	0.00	6.14	2.13	49.32	0.07	7.43	0.41	0.03	0.00	17.38	N.D.	82.91
CY-92-36	0.00	0.00	6.67	2.33	52.46	0.05	7.84	0.30	0.04	0.00	17.54	N.D.	87.23
CY-92-35	0.00	0.02	6.60	2.99	49.86	0.07	8.26	0.15	0.06	0.01	15.89	N.D.	83.91
CY-92-35	0.00	0.00	7.28	3.41	52.91	0.05	8.83	0.26	0.05	0.00	15.86	N.D.	88.65
CY-92-35	0.00	0.00	6.64	3.62	50.58	0.06	7.61	0.33	0.07	0.00	16.02	N.D.	84.93
CY-92-35	0.00	0.00	6.42	3.88	50.43	0.09	6.94	0.16	0.07	0.00	15.18	N.D.	83.17
CY-92-2	0.00	0.03	4.32	5.38	41.61	0.13	5.34	0.46	0.10	0.04	13.82	N.D.	71.23
CY-92-2	0.00	0.00	4.69	6.46	46.84	0.12	5.52	0.53	0.16	0.00	13.16	N.D.	77.48
CY-92-2	0.00	0.00	5.61	3.89	47.29	0.09	8.40	0.07	0.15	0.01	12.97	N.D.	78.48
CY-92-2	0.00	0.00	4.38	5.88	47.08	0.16	5.97	0.49	0.15	0.00	13.50	N.D.	77.61
CY-92-38	0.00	0.00	6.21	5.86	52.51	0.06	9.04	0.12	0.02	0.00	13.07	N.D.	86.89
CY-92-37	0.00	0.03	4.95	3.55	40.65	0.15	5.42	0.24	0.07	0.04	18.65	N.D.	73.75
CY-92-37	0.00	0.00	5.88	2.63	45.19	0.10	7.03	0.47	0.02	0.00	15.86	N.D.	77.18
CY-92-37	0.00	0.00	5.71	3.05	46.78	0.08	6.90	0.58	0.03	0.00	15.99	N.D.	79.12
CY-92-37	0.00	0.00	5.85	2.80	45.17	0.10	6.88	0.62	0.01	0.00	15.36	N.D.	76.79
CY-92-37	0.00	0.00	6.13	2.95	47.61	0.08	7.10	0.47	0.06	0.01	16.92	N.D.	81.33

APPENDIX C

ICP-MS Results (in ppm) of All Analyzed Celadonites

Sample	Li Sm	B Eu	Sc Gd	Rb Tb	Sr Dy	Y Ho	Cs Er	Ba Tm	La Yb	Ce Lu	Pr	Nd
CY-90-4a	25 0.49	41 0.14	4.5 0.91	258 0.05	2.67 0.33	0.08 0.23	0.83 0.24	1.03 0.09	0.66 0.18	0.37 0.09	0.34	1.60
CY-90-6	17 0.38	14 0.11	4.1 0.63	138 0.07	4.53 0.40	2.03 0.17	0.47 0.29	1.16 0.07	0.46 0.21	0.56 0.06	0.23	1.13
CY-90-8a	23 0.49	31 0.14	2.5 0.87	246 0.06	5.24 0.37	0.68 0.22	0.39 0.26	1.76 0.10	0.62 0.25	0.43 0.10	0.32	1.48
CY-90-8b	4 0.78	8 0.24	8.3 1.34	245 0.14	6.81 0.90	4.47 0.33	0.81 0.60	3.50 0.13	0.84 0.39	0.68 0.12	0.47	2.41
CY-90-9	11 0.60	38 0.18	12.3 1.07	125 0.09	25.5 0.55	1.76 0.28	0.46 0.39	4.89 0.12	0.79 0.37	0.60 0.11	0.40	1.88
CY-90-23	15 0.46	49 0.14	1.13 0.86	195 0.05	16.8 0.30	0.04 0.21	2.01 0.19	4.64 0.09	0.61 0.05	0.35 0.06	0.32	1.51
CY-90-29	42 0.65	91 0.19	9.00 1.17	161 0.12	12.1 0.87	6.59 0.38	1.00 0.80	3.08 0.21	0.75 1.35	0.61 0.31	0.41	1.91
CY-90-36	14 0.65	28 0.28	15.5 1.14	196 0.10	64.3 0.74	3.55 0.32	0.59 0.60	7.80 0.17	0.84 0.88	0.90 0.20	0.42	2.05
CY-90-45	11 0.95	14 0.40	21.5 1.56	115 0.17	320 1.04	41 0.39	0.39 0.67	47.4 0.16	1.47 0.53	1.37 0.13	0.63	3.13

CY-92-35	34 7.14	53 1.66	8.74 8.11	238 1.32	28.4 8.01	54 1.72	5.36 4.87	12.5 0.74	23.2 4.00	10.9 0.65	6.51	28.5
CY-92-36	23 6.96	74 1.67	6.38 8.54	200 1.40	48.1 8.93	66 1.91	6.72 5.74	11.7 0.78	23.45 4.81	10.3 0.71	6.38	28.3
CY-92-37	29 7.99	36 1.87	5.70 9.05	214 1.51	28.8 9.32	67 1.96	3.78 5.80	7.40 0.86	30.64 5.22	12.06 0.77	7.56	32.1
CY-92-38	9.7 0.77	14 0.23	19.1 1.34	185 0.17	19.9 1.21	9.4 0.41	0.77 1.00	6.21 0.22	1.05 1.36	0.97 0.29	0.47	2.24
CY-1A 49.90	12 0.69	68 0.31	18.5 1.12	90 0.18	94.1 1.44	11.6 0.47	0.84 1.52	23.3 0.29	0.86 2.18	1.02 0.42	0.41	1.95
CY-1A 50.40	7.7 0.67	23 0.22	41.0 1.15	148 0.16	55.7 1.14	10.2 0.41	0.54 1.06	8.0 0.22	0.80 1.25	0.89 0.24	0.39	1.91
CY-1A 63.10	3.0 0.94	20 0.30	29.3 1.56	96 0.17	74.3 0.98	3.93 0.41	0.47 0.65	9.34 0.16	1.16 0.48	1.29 0.15	0.59	2.82
CY-1A 132.90	5.4 0.50	183 0.15	13.3 0.92	190 0.09	5.75 0.68	3.77 0.30	0.90 0.73	2.26 0.19	0.61 1.09	0.45 0.24	0.31	1.50
CY-1A 134.70	11.5 0.58	67 0.19	9.90 1.11	170 0.15	6.79 1.11	9.45 0.41	0.54 1.07	2.18 0.23	0.62 1.20	0.47 0.22	0.33	1.60
CY-1A 202.00	4.4 1.35	72 0.47	16.7 2.11	168 0.35	11.3 2.48	16.0 0.67	0.87 1.89	18.6 0.36	2.17 2.12	3.64 0.42	0.84	3.84
CY-2 123.30	6.3 0.58	29 0.17	34.0 1.08	214 0.06	7.59 0.65	3.46 0.33	0.76 0.67	1.61 0.21	0.76 1.38	0.50 0.32	0.39	1.79
CY-2 163.65	3.0 0.63	16 0.19	15.0 1.13	123 0.05	25.6 0.55	2.43 0.30	0.74 0.46	13.4 0.14	0.88 0.43	0.79 0.15	0.42	2.03

CY-2 192.10	8.4 0.49	19 0.15	8.7 0.90	175 0.07	16.8 0.47	2.20 0.27	0.96 0.47	0.93 0.15	0.61 0.70	0.32 0.18	0.33	1.53
CY-2 199.60	18.0 1.12	26 0.36	18.0 1.75	136 0.27	31.1 1.92	13.7 0.57	0.68 1.87	3.96 0.38	1.37 2.91	2.14 0.57	0.63	3.34
CY-2 199.80	13.1 0.70	23 0.21	15.4 1.16	161 0.12	24.1 0.74	4.11 0.32	0.65 0.60	4.45 0.16	0.80 0.77	0.82 0.17	0.41	2.03
CY-1A 66.80	11.0 0.50	61 0.16	31.4 0.94	168 0.08	3.1 0.55	2.21 0.27	0.46 0.48	1.06 0.14	0.64 0.58	0.35 0.17	0.33	1.57
CY-90-33	8.9 0.52	7.6 0.15	5.1 0.97	171 0.07	2.0 0.41	0.89 0.26	0.67 0.34	1.87 0.11	0.68 0.29	0.37 0.11	0.36	1.69
CY-90-3	22.0 1.35	39 0.39	2.5 2.32	120 0.44	10.7 3.50	29.8 1.02	0.26 .33	3.37 0.57	1.38 3.33	2.28 0.57	0.67	3.49